UNIVERSITY OF OKLAHOMA

GRADUATE COLLEGE

THE INTERSECTION OF RADAR AND COMMUNICATIONS: A STUDY ON SPECTRUM MANAGEMENT FOR ADDRESSING RF INTERFERENCE

A THESIS

SUBMITTED TO THE GRADUATE FACULTY

in partial fulfillment of the requirements for the

Degree of

MASTER OF SCIENCE

By

JACOB PRICE
Norman, Oklahoma
2023

THE INTERSECTION OF RADAR AND COMMUNICATIONS: A STUDY ON SPECTRUM MANAGEMENT FOR ADDRESSING RF INTERFERENCE

A THESIS APPROVED FOR THE
SCHOOL OF ELECTRICAL AND COMPUTER ENGINEERING

BY THE COMMITTEE CONSISTING OF

Dr. Justin G. Metcalf, Chair

Dr. Mark A. Raymond

Dr. Joao R. Cruz

Acknowledgments

I would like to express my gratitude to my thesis committee, Dr. Metcalf, Dr. Raymond, and Dr. Cruz, for their invaluable insight and guidance. I would also like to thank my friends and family for their unwavering support.

Table of Contents

List of Tables

List of Figures

Abstract

The radio frequency (RF) spectrum is a fruitful yet competitive frontier that enables technologies like 5G, Wi-Fi, Bluetooth, GPS, long-range telescopes, microwave ovens, radar, and more. With finite supply and increasing demand, the RF spectrum is highly contested for both government and private use. Industry innovators need an increasing stake in the spectrum to keep up with modern data consumption needs, yet governments around the world require the same spectrum for important issues like national defense. This duality in demand often results in highly congested bands of frequency that host both stakeholders in dense configuration, increasing interference and difficulties in managing the spectrum. Interference of radar signals by communication waveforms, like *orthogonal frequency division multiplexing* (OFDM), is on the rise and can greatly impact system performance. This thesis introduces a novel interference mitigation algorithm that leverages the known structure of OFDM waveforms to estimate and subtract interference from a pulse-Doppler radar system. The proposed technique can significantly improve radar performance in the face of OFDM interference and quantify interference metrics to inform new regulations pertaining to spectrum management.

Chapter 1

Introduction

1.1 Overview

This project aims to contextualize OFDM interference on pulse-Doppler radar systems within the confines of spectrum management. *Spectrum management* is a broad term that refers to the oversight and organization of the radio frequency spectrum to promote a net societal benefit. The world of spectrum management is often difficult to navigate, as regulations are embedded in vast volumes of federal documents from many different sources. This thesis seeks to facilitate an effective understanding of the complex regulatory landscape of spectrum management.

Spectrum management plays a central role in mitigating interference between multiple radio systems. This thesis will focus on addressing the recurring problem of interference between communication systems and legacy radar systems. *Pulse-Doppler radar* is a widely used radar technology in many critical applications, such as missile defense, weather forecasting, and air collision avoidance. They are, however, particularly vulnerable to interference. Relatively recent regulations require many radar systems to share frequency bands with communication devices in the *Unlicensed National Information Infrastructure* (U-NII) and *Citizens Broadband Radio Service* (CBRS) bands. Moreover, many communication system operators in these new bands either uninten-

tionally or deliberately violate regulations, causing harmful interference to legacy radar systems equipped with outdated technology.

A common modulation scheme used in communication systems is OFDM, and an increasing number of radar systems report interference from communication systems employing this technology [3]. This thesis proposes a solution to address such interference and inform the development of new transmission regulations in the problematic bands.

1.2 Contributions

The following contributions are made in this thesis:

- Proposal of a novel interference mitigation algorithm to remove OFDM interference from pulse-Doppler radar *in-phase* and *quadrature* (IQ) data.
- Analysis of the effect of lost samples on the OFDM demodulation process and bit-error-rate of recovered data.
- Exploration of a potential approach to constellation reconstruction using the DBSCAN clustering algorithm.
- Recommendation of new regulations based on performance results of the interference mitigation algorithm.

1.3 Thesis Outline

Chapter 2 will discuss spectrum management from a technical and regulatory perspective. **Chapter 3** will discuss the fundamentals of OFDM in communications systems, such as error correction techniques, the importance of the cyclic prefix, multipath

fading channels, and equalization. **Chapter 4** will discuss pulse-Doppler radar fundamentals, such as range resolution, matched filtering, the ambiguity function, and the Doppler effect. **Chapter 5** will frame the problem of radar interference of OFDM waveforms. **Chapter 6** will explain how the aforementioned novel OFDM interference removal algorithm works in practice, analyze simulation results of the algorithm, and inform potential new regulations on these results. **Chapter 7** will provide concluding remarks and potential avenues for future research.

Chapter 2

An Overview of Spectrum Management: Common Practices and Emerging Markets

2.1 Introduction

The radio frequency spectrum is one of the most sought-after, yet scarce, global resources. Many governments, industries, and consumers utilize the spectrum for wireless communication, radiolocation, media broadcasting, and even combustion-free cooking. This widespread utility, however, elicits more demand than supply. Moreover, demand inherently increases as society advances technologically. Modern society is more digitally linked than ever before, and many visions for the future involve even more interconnectedness. The *Internet of Things* (IoT) is a somewhat prophetic vision of forward societal progression where historically "dumb" devices, such as washing machines and refrigerators, are wirelessly linked to increase the daily efficiency of individuals. For instance, one's alarm clock might signal to their TV to turn on the morning news after their first morning alarm occurs. These wireless connections, though, occupy finite bands of frequency. A single household could harbor dozens — or possibly hundreds — of these connections, which is not something that current wireless infrastructure could support on a large scale due to spectrum efficiency issues. The current 5th generation mobile broadband network (5G) is working to remedy this problem, but

significant improvements must be made on the frontier of spectrum management. Spectrum management, which involves key actors such as national regulators, international organizations, and industry stakeholders, refers to the regulation of RF transmission to increase spectrum efficiency and eliminate harmful interference. From a technical standpoint, it has been both historically and presently done through the management of transmission space, time, and frequency. More recent methods also employ oversight of things like signal orthogonality and signal polarization. Despite modern-day spectrum management following the same basic outline, it has evolved considerably in the last few decades and will likely continue to evolve in the coming decades. As researchers and engineers work to advance this area of focus, the importance of rigorizing metrics of spectrum efficiency for every niche outlet of signal generation is indeed apparent, but so too is the proportionate workload of accomplishing this.

2.2 The Radio Frequency Spectrum

The radio frequency spectrum is defined loosely as the electromagnetic field (EMF) propagation ranging from 0 to 300 GHz of frequency. At 300 GHz, EMF propagation starts to become infrared light [4]. Among the RF community frequencies below 6 GHz are considered "beachfront" spectrum, meaning that most entities find spectrum in this range most valuable to their operations (due to ideal propagation characteristics). This boundary is certainly subject to the technological capability of present society. Modern innovations are beginning to utilize higher transmission frequencies and are obscuring previous limitations. For instance, 5G NR Release 17 specifies plans for utilizing frequencies as high as 71 GHz, where signal wavelengths are expressed in millimeters ("mmWave") [5]. By comparison, 4G LTE only occupies frequencies as high as 5.9 GHz (though usually much lower) [6].

2.2.1 Allocations, Allotments, and Assignments

The frequency spectrum is divided into *allocations*, *allotments*, and *assignments*, which is a system used globally. Allocations are granted to specific radio services [7]. These services include radionavigation, maritime mobile, radiolocation, and so on. The *National Telecommunications and Information Administration* (NTIA) periodically releases a chart that positions each U.S. frequency allocation from 0 GHz to 300 GHz on a horizontal scale [8]. It serves as a simple way to determine which services are in which bands, as opposed to sifting through archives of federal regulatory code [9]. Allotments confine certain services to geographical regions or countries, while assignments specify authorizations given by a radio frequency authority to operate at specific discrete frequencies [7, 10].

2.2.2 Frequency Designations

The RF spectrum is also divided into *frequency designations*. As specified by the *International Telecommunications Union Radiocommunication Sector* (ITU-R), the frequency range from 3 to 30 kHz is designated as *very low frequency* (VLF); 30 to 300 kHz is *low frequency* (LF); 300 to 3000 kHz is *medium frequency* (MF); 3 to 30 MHz is *high frequency* (HF); 30 to 300 MHz is *very high frequency* (VHF); 300 to 3000 MHz is *ultra high frequency* (UHF); 3 to 30 GHz is *super high frequency* (SHF); 30 to 300 GHz is *extremely high frequency* (EHF) [11]. Notice that each adjacent designation is separated by one numerical decade. It is important to note that perceptible bandwidth occupancy is subject to logarithmic scaling depending on where the frequencies are located on the frequency axis. For instance, AM broadcasting ranges from 540 kHz to 1700 kHz, or about 1.16 MHz of occupied bandwidth. This same bandwidth at, say, 30 GHz, would be insignificant for wide-scale broadcasting. Excluding the discus-

sion of the propagation characteristics of different frequency ranges, this phenomenon is a primary result of the inverse correlation between signal generation and reception sensitivity and frequency of transmission.

2.2.3 Physical Propagation Characteristics

In addition to frequency boundaries specified by policy, there are also frequency boundaries specified by physics. Frequency ranges can be broken into characteristics based on how signals propagate through various environments. For instance, signals under 2 MHz abide by the principle of ground-wave propagation and can travel along Earth's surface around the horizon. It works most effectively across bodies of water, thus ground-wave frequencies are good for maritime communication. Similarly, signals in the HF band can optimally refract off the Earth's ionosphere or troposphere, making this band of frequencies a suitable selection for long-range communication. These properties exist for many variables, such as humidity, temperature, precipitation, foliage, man-made physical structures, like buildings, and so on. Picking the right frequency is important to the function of a system. Unfortunately, however, the complex world of spectrum issuance has established a legacy system of first come, first served assignment, meaning that many systems are utilizing frequencies that are not optimized for their service. Moreover, legacy allocations are often at gridlock because entities are unwilling to give up their spectrum despite more effective applications existing, so redistributing the spectrum is difficult [4].

2.3 Categories of Service

There are many services that occupy bands of the radio frequency spectrum. According to [7], these services fall within three categories: *radiodetermination*, *radio-*

communication, and *radio astronomy*.

2.3.1 Radiodetermination

Radiodetermination is the process of utilizing radio waves to determine aspects of an object pertaining to its position or velocity. Within radiodetermination are *radionavigation* and *radiolocation* (or radar). Generally, what separates these two technologies is the context of their use, rather than the methods in which they operate. Both work by transmitting a waveform and then interpreting the changes incurred by that waveform upon reception to describe the nearby environment. Radionavigation uses these techniques for the purposes of maneuvering a vehicle or craft from one location to another. There are many types of radionavigation depending on the medium of travel; maritime radionavigation is used by ships; aeronautical radionavigation is used by airplanes; satellites are equipped with radionavigation-satellite service. Radiolocation is defined (rather circularly) by the ITU-R as "radiodetermination used for purposes other than those of radionavigation." These "other purposes" include the missile defense systems created and used by the Department of Defense (DoD), Doppler radar systems used by meteorologists, and much more [12].

2.3.2 Radiocommunication

According to [7], Radiocommunication is the broadest category of RF service. It includes mobile and fixed communications, broadcasting, telemetry, and amateur (ham) radio. A *mobile service*, according to the ITU-R, is "a radiocommunication service between mobile and land stations, or between mobile stations." Maritime mobile pertains to mobile communication links between ships or between ships and base stations. Unsurprisingly, aeronautical mobile, mobile-satellite service, and land mobile all abide

by similar relationships but with aircraft and aircraft stations, space stations and earth stations, and mobile stations on land and base stations, respectively. A *fixed communication service*, by contrast, operates between fixed locations. An RF broadcasting service provides direct media to the general public. The form of media is usually either sound (FM and AM radio) or television. Radiotelemetry is a process by which statistical data or measurements are remotely transmitted from the collection site to another location for processing. It is used in a wide variety of applications, from monitoring animal populations to surveilling patient vitals in a medical context [13, 14]. Amateur radio is the final subcategory of radiocommunication. It provides a resource in which individuals can operate radiocommunication systems for nonpecuniary purposes [7].

2.3.3 Radio Astronomy

Radio astronomy is the final category of radio frequency service [7]. According to [15], until the 1930s, astronomy was limited to the visible spectrum. After several discoveries made by radio engineers like Karl Jansky and Grote Reber, it was concluded that, along with the visible spectrum, there was also extraterrestrial radiation in the radio spectrum. In fact, by observing the radio spectrum, astronomers can peer much deeper into the universe than by observing the visible spectrum due to the relatively low propagative attenuation experienced by radio waves. Also, since the universe is constantly expanding, most extraterrestrial objects are moving away from the Earth at considerable velocities (up to 90% of the speed of light for distant quasars). The *Doppler effect* — which describes a shift in the perceived radiated frequency of an object that is moving relative to an observer — can severely shift the visible radiation of objects into the infrared and radio spectrums. Radio astronomy allows astronomers to view these otherwise invisible objects.

2.4 The Evolution of Spectrum Management

2.4.1 The Emergence of International Spectrum Management

In the early 1900s, when wireless communication was in its infancy, the first widely-adopted application of RF technology was maritime communications. Guglielmo Marconi was the first to demonstrate the long-range wireless telegraph. His ingenuity, though, was fueled by shrewd business operations. He started the Marconi Wireless Telegraph Company and quickly established himself as the leading service provider. His company set up an extensive network of shore stations that refused to handle telegraph signals that were emitted with equipment manufactured by his competitors. Several nations congregated in protest when Marconi stations refused to handle their messages, despite many of them pertaining to maritime safety. It was quickly decided among many nations that every station must handle telegraphs from any seafaring vessel. This sequence of affairs kickstarted the desire for widespread coordination and assembly of government to organize and manage issues pertaining to radiocommunications. Today's ITU-R was born from this incident [4].

2.4.2 The Emergence of Spectrum Management in the United States

During the rise of wireless communication and broadcasting in the early 20th century, it was quickly understood that signal interference was a big problem [16]. The *Radio Act of 1912* bolstered itself as "an act to regulate radio communication," but did not specify any apparatus or guidelines for spectrum organization, so its efforts were futile [17]. In 1922, however, the *Interdepartment Radio Advisory Council* (IRAC) was formed from several U.S. government agencies that utilized RF transmission, marking the first coordinated attempt at assigning and distributing frequency licenses [18].

Though the IRAC only sought to organize government use of the spectrum, it still played a pivotal role in establishing modern spectrum management practices [18]. The *Federal Communications Commission* (FCC) was established through the Communications Act of 1934, which sought to make both wire and radio communications as fair and equitable as possible [19]. It repeatedly cites "the public interest, convenience, and necessity" as motivations for its judgment. The Act did not allocate specific frequency bands through statute, but granted the newly formed FCC to establish non-governmental frequency allocations through its own procedures and discretion.

The NTIA, much like the FCC, was created to oversee radio spectrum usage [20]. It was established in 1978 by Executive Order 12046 [21]. While the FCC serves as a regulatory body for non-governmental radio communications and broadcasting, the NTIA serves to regulate governmental use of the spectrum [22, 20]. As such, the NTIA is advised by the IRAC [23]. Together, the FCC and NTIA manage the RF spectrum in the United States, often collaborating to coordinate frequency allocations and spectrum usage [24].

2.4.3 The United States Doctrine of Spectrum Scarcity

Beginning in 1933, the Supreme Court of the United States (SCOTUS) adopted a *doctrine of spectrum scarcity* [25]. The doctrine, which was later rigorously outlined in 1943 during National Broadcasting Co. v. the United States, recognized the RF spectrum as a limited resource and granted the FCC control over not just the "technical aspects of radio communication" but also "the public interest" [26, p. 190]. This marked a (temporary) formal recognition by the United States that the public owns the spectrum and not corporate America. This doctrine was later extended in 1969 during Red Lion Broadcasting Co. v. Federal Communications Commission to include FCC

oversight of broadcasting content to ensure ample expression of opposing viewpoints [27]. In 2005, the FCC argued that technological advancements had made broadcasting much more accessible and that "The Scarcity Rationale no longer serves as a valid justification for the government's intrusive regulation of traditional broadcasting" [28, p. 8]. Notably, these three variables — spectrum demand, spectrum regulation based on perceived public interest, and spectrum efficiency technology — seem to be in constant fluctuation with one another. That is, when demand surpasses technology, the community favors tight regulation. However, when technology surpasses demand, the community favors deregulation. In this way, spectrum management is at the mercy of market dynamics.

2.5 The Interconnected Roles of the NTIA, FCC, ITU-R, and Industry in Spectrum Management

2.5.1 Multilateralism in the ITU-R

Multilateralism is the concept of three or more countries collaborating to establish shared governing policies within a specific domain [29, 30]. The ITU-R is an excellent example of this due it it being a collection nation states convening to sort out international spectrum management policies. Together, the ITU-R organizes the World Radiocommunication Conference (WRC) where they discuss numerous topics like allocation of frequency bands to various services, coordination of satellites, and the creation of cohesive regulations for global telecommunications infrastructure [31].

2.5.2 Multistakeholder Governance Between the NTIA, FCC, ITU-R, and Industry

Multistakeholder governance (or *multistakeholderism*) is a type of governance model in which entities from various actor classes collaborate to establish policies for a specific public domain [30]. In the context of spectrum management, multistakeholder governance exists between the NTIA, FCC, ITU-R, and various industry players, each seeking to safeguard their respective interests while offering diverse perspectives to the issues at hand in the United States.

The NTIA aims to protect critical government systems, such as missile defense warning systems, weather monitoring systems, and air traffic control systems. The FCC is responsible for promoting the effective use of spectrum and addressing the needs of consumers and the broader public. The ITU-R strives to globalize spectrum policy, facilitating cohesive radio frequency usage and telecommunications infrastructure across national boundaries. This is essential given the disregard of electromagnetic waves for geopolitical borders. Industry stakeholders seek to impose the interests of the economy and serve as a grounding force to emphasize the practical implications of technological developments and policy. Together, these diverse viewpoints foster balanced decision making in the realm of spectrum management.

2.6 Spectrum Management Techniques

Spectrum management has been historically (and is presently) done through the regulation of *transmission space*, *time*, and *frequency*. Within each of these domains, though, exists significant innovation. What separates modern methods of spectrum management from past methods is the reigning technologies of that period. As technol-

ogy progresses, researchers have discovered increasingly efficient ways to accomplish the same tasks. These innovations are the reason that the global infrastructure can support as many services and allocations as it does.

2.6.1 Regulation of Transmission Space

Isolating a signal in space is commonly achieved by controlling *transmission power* and *spatial directivity*. This is particularly important for frequency reuse applications and in cases of shared spectrum allocation between government and non-government users. The 5 GHz band, for instance, features shared frequencies between U-NII devices and federal radar systems like the *Terminal Doppler Weather Radars* (TDWRs) of the *Federal Aviation Administration* (FAA) [32]. In this case, TDWRs operate with primary status over the shared spectrum and U-NII devices operate with secondary status [32]. Secondary status users must typically accept any unwanted interference, while immediately correcting their own interference inflicted on other devices [32, 4].

The U-NII devices are unlicensed radiators typically used for wireless communications systems such as Wi-Fi. If U-NII devices transmit too much power at a shared frequency, then a TDWR might receive interference, which could corrupt weather forecasting results [32]. Moreover, distance limitations must be implemented as well. Federal radar systems must be segregated from densely-populated U-NII device use. Research has shown that even small amounts of transmission power can interfere with radars "at distances of tens of kilometers" [32]. Resulting corruption is generally a function of how much interference is received, thus U-NII devices must take careful precautions to limit their transmission power to stay under the TDWR interference threshold [32]. These transmission guidelines are rigidly defined by the FCC and enforced upon device manufacturers [33].

The elements of spatial separation include *geographical separation*, *altitudinal separation*, use of *directional antennas*, such as parabolic dish antennas and phased arrays, and utilizing *higher transmission frequencies* to reduce signal propagation distance. Geographical and altitudinal separation involve separating transmission regions and elevations, respectively. They embody the concept of incorporating distance between competing radio systems to reduce interference. They are considered elementary concepts and were among the first spectrum management practices performed by the radio community. Directional antennas spatially separate signals by intentionally transmitting only in relevant directions, which reduces harmful interference and allows for more devices to operate within the same area and frequency band. Parabolic antennas are concave in shape and rely on the reflection of the passive disk material to focus RF radiation. They are highly directive and used for things like home satellite television, Wi-Fi, and simple radar systems. However, they must be mechanically steered, making them unsuitable for highly dynamic systems like target tracking radar. Phased array antennas utilize an array of fixed antennas and variations in signal phase between each antenna to create and steer a concentrated beam of transmission in a specific direction [34]. The beam can be directed electronically, making phased array systems highly adaptive [34]. They are commonly used for modern radar systems and communications systems like 5G [34, 35]. Finally, transmission frequency is an important consideration for spatially segregating signals. The frequency of transmission and the distance of propagation are inversely correlated. Systems that require frequency reuse between areas of close proximity are better suited for higher frequency transmission.

2.6.2 Regulation of Transmission Time

Separating RF transmissions in time is an intuitive concept for humans to understand. Similar to how people take turns talking to each other to prevent speech interference, radio systems separate their transmissions in time to prevent RF interference. A simple example of this is in the U-NII system regulatory guidelines [32]. The FCC requires *dynamic frequency selection* (DFS) in 5.25-5.35 GHz and 5.470-5.725 GHz U-NII 2A and 2C bands, where the device must monitor the channel for radar waveforms before transmitting [36]. If a radar signal is detected, the device must not transmit on the channel for a specified period, often referred to as a "non-occupancy period" [32]. This technological advancement, whereby real-time frequency allocation of secondary users is based on the occupied channels of primary users, is a key aspect of DFS [32]. Coordinating the transmission timing of multiple radio devices, in general, is an extremely frequent practice in spectrum management. Other aspects of spectrum management in time involve transmitting multiple data streams at the same time using *time-division multiplexing* (TDM). TDM works by alternating samples of each signal (at least twice per period per signal, as per the Nyquist theorem), lowpass filtering the resultant signal, transmitting, sampling, and separating the received signal back into pulse signals, then lowpass filtering each constituent pulse signal to get the original signals back [37]. It can be used to transmit multiple inefficient signals (in terms of bit rate) at the same time and frequency.

2.6.3 Regulation of Transmission Frequency

Spectrum management in frequency is indeed the embodiment of why RF transmission is so valuable. To isolate a signal, devices are equipped with filtering capacities, either analog or digital, allowing them to segregate desired frequency bands. This al-

lows many services and users to use the radio frequency spectrum without interfering with one another, as with the other variables of spectrum management. As previously discussed, the RF spectrum is organized into allocations, allotments, and assignments. Moreover, individual services can subdivide their issued frequency band to accomplish more granular tasks. In *cellular networks*, for instance, users operating within the coverage of the same base station (cell) are assigned different adjacent frequencies within that station's band and sent together on a combined transmission. The mobile device can then filter the signal to extract its respective communication. This concept is known as *frequency-division multiplexing* (FDM). Additionally, each adjacent base station utilizes different frequency bands to prevent interference among neighboring cell areas. Another practice related to the concept of spectrum management in frequency is narrowbanding. *Narrowbanding* is a *spectrum refarming* method that involves transforming wide bandwidth channels into multiple narrowband channels [4].

2.6.4 Signal Polarization

Signal polarization is another important dimension of spectrum management. It is generally determined by the orientation and configuration of the transmitting antenna. For example, a vertically oriented dipole antenna will emit a vertically polarized signal [38]. To optimally receive the transmitted signal, the receiver antenna should be matched in configuration to the transmitting antenna [38]. If the receiver antenna is polarized orthogonally to the transmitting antenna or falls out of orientation, then significant signal loss can occur [38]. This can be a problem in mobile systems that are highly dynamic in signal polarization [38]. Recent research has prioritized designing dynamic polarization control (DPC) systems utilizing phased array technology [38]. Such a system can adaptively optimize signal polarization for the best possible

reception. Conversely, system designers can utilize orthogonal signal polarization to distinguishably send and receive two different signals at the same frequency, time, and location [4]. In practice, this is challenging to do because of multipath.

2.6.5 Signal Orthogonality

Orthogonality is an important concept in the world of spectrum. In fact, the Fourier transform — the operation that converts a signal from the *time domain* (TD) to the *frequency domain* (FD) — is predicated on the orthogonality of sine waves at different frequencies. Two signals are said to be orthogonal if their inner product evaluates to zero. RF engineers often use orthogonality to multiplex signals and make better use of the available spectrum. *Code-division multiple access* (CDMA) was one of the first widespread uses of orthogonality in a modulation scheme and enabled technologies like 3G. It works by XORing many users' signals by fast-changing, orthogonal pseudo-noise (PN) sequences and combining them on a single carrier [4]. Because each PN coding sequence is orthogonal, a user can simply perform the same XOR operation with their unique PN code on the received signal to extract their data [4]. Also, incorporating fast-changing PN sequences spreads the frequency band occupied by the signal, making CDMA a spread spectrum technology [4]. Orthogonal frequency-division multiplexing is another technology that relies on orthogonality. It works by spacing subcarriers in frequency such that the nulls of each subcarrier align with the peaks of the other subcarriers. This compact arrangement of subcarriers allows for much greater spectrum efficiency. In fact, using OFDM over traditional FDM can save nearly half the bandwidth [39]. Modern OFDM implementations rely on an IFFT and an FFT operation, which are very computationally efficient [39]. OFDM is also inherently resilient to phenomena such as multipath fading and narrowband interference which plague other

multiplexing schemes [39]. OFDM has thus been instrumental in enabling technologies like *4G Long Term Evolution (LTE)* and *5G New Radio* (NR).

2.6.6 Out-of-Band Radiation

Out-of-band (OOB) *transmission* of radar systems can significantly impact other radio systems. To address this, regulatory entities set restrictions on the transmission frequency, transmission power, and the shape of the transmitted waveform in the frequency domain. One tool to help regulate these variables is the NTIA's *Radio Spectrum Engineering Criteria* (RSEC) emission mask. An emission mask defines the outline (in frequency) that a radar waveform should stay within to prevent undue interference with neighboring services. Some parameters controlled within this "mask" are -40 dB "chimney" bandwidth, OOB roll-off, and suppression levels of -X dB. The exact specifications of these parameters are given by a set of equations provided by the NTIA [40].

2.6.7 Figures of Merit

Determining the efficiency of a particular service in terms of occupied spectrum is another important aspect of spectrum management [41]. This allows radio engineers to decide which technologies are worth occupying parts of the spectrum. However, this can be difficult to do for two reasons. First, different types of radio systems, even similar ones, can differ enough that their spectrum efficiency calculations are incompatible [42]. Therefore, it is only appropriate to compare calculations of identical services; otherwise, the varying nuances of each service can obscure the result [42]. According to [41], no objective measure of spectrum efficiency currently exists that encompasses all services. Second, some services, like radar and unlicensed systems, can be diffi-

cult to gauge due to inconsistent and varying operation. “Spectral efficiency” is a type of spectrum efficiency metric that specifically refers to communication systems and is expressed in terms of bits per second per Hertz (bps/Hz). However, depending on the purpose, this metric may not convey enough information. Analogs of this calculation factor in things like coverage area, supported users, and financial burden.

2.6.8 Software-Defined Radio

Software-defined radio (SDR) has been instrumental in the progression of modern radio systems. Prior to SDR, radio systems were generally single-purpose. For example, a traditional radar could not easily become an FM receiver without extensive modification, even if most of its components could support this shift in functionality. If the same radar were implemented in software, however, a dramatic shift in functionality could be as simple as running a different file on one’s computer. As such, SDRs have opened the door to promising new technologies such as cognitive radio and radar [43, 44]. They also bridge the gap between conception and implementation, significantly reducing production time. In some ways, SDRs in the field of radio systems are analogous to 3D printing in the field of prototyping and manufacturing. Cheap SDRs like the RTL-SDR can be purchased for around $30 and grant the user basic control over frequencies ranging from 24 MHz to 1.766 GHz (RTL-SDR). More expensive systems like the Ettus X series offer more control but can cost the operator upwards of $24k [45]. The *GNU Radio project*, regardless of the hardware, attracts many SDR enthusiasts and practitioners regardless of their hardware. It is an open-source, easy-to-use assembly of advanced digital signal processing (DSP) tools that have become a staple in the RF community [46].

2.7 Current and Emerging Spectrum Sharing Characteristics in Radiocommunications

The Internet of Things is widely accepted as the future of radiocommunications among industry leaders in wireless technology. Manufacturers such as Samsung, Intel, and Qualcomm are devoting significant resources to making faster, cheaper, more efficient, and lower latency devices to support this progression [47]. These innovations, however, come at the price of increased bandwidth [47]. Failure to allocate the required bandwidth could have significant implications for a nation's economy [48]. 5G NR is the most promising technology to support these advancements, but existing spectrum allocations are insufficient [47]. Employing dynamic spectrum utilization techniques in preexisting *industrial, scientific, and medical* (ISM) bands, CBRS bands, 4G LTE bands, U-NII bands, and other spectrally inefficient bands can help remedy spectrum scarcity issues surrounding 5G. Furthermore, working closely with the DoD can help prevent instances of 5G interference with radio activities pertaining to national security and military operations [49].

2.7.1 The Department of Defense

The Department of Defense currently holds the largest amount of Federal spectrum, making it a frequent target of opportunity for the spectrum-hungry telecommunications industry [49]. While expanding 5G allocations threatens the reliability of existing DoD services, the Department understands the economic benefits of a strong 5G network. In fact, the DoD stands to benefit themselves from 5G deployment. Having a faster, more reliable, and more dynamic radio access network (RAN) could drive further innovation in previously unfeasible domains. For instance, the Army is experimenting with using

5G to enable enhanced augmented/virtual reality tactical training [49]). The Navy and the Air Force are working on using 5G to remotely access airplane diagnostics [49]. The DoD also stands to benefit from the development of highly agile radio capabilities that are robust in complex, "near-peer" environments — an interest that aligns with the development of 5G [50]. These mutual interests promote greater cooperation between both entities.

2.7.2 Interference Challenges with Radar Systems

One of the main systems that is vulnerable to 5G interference is high-powered radar. According to several wireless communications researchers, "the standard evolution from GSM (Global System for Mobile Communications) to the fifth generation (5G) has produced a progressive invasion of frequency bands traditionally used by radar systems" [51, p. 19]. The S and C bands (2-8 GHz) are heavily occupied by federal radar but are also essential for the ubiquitous operation of 5G networks [49]. 3GPP Release 17 (March 2022) cites plans to extend 5G coverage up to 71 GHz, which is likely targeting the 60 GHz ISM band [5]. The ISM bands are allocated for the use of devices that perform work, such as microwave ovens and industrial welding equipment [52]. These applications of RF usage are not generally affected by interference, so operating radiocommunication devices within these bands does not harm legacy allocations [52]. Thus, in 1985, the FCC began allowing spread-spectrum transmitters to operate without license in certain ISM bands [52]. The ISM bands are also wide in bandwidth. The 2.4 GHz ISM band is 83.5 MHz wide and supports many technologies, such as Wi-Fi, Bluetooth, and Home RF, as well as traditional ISM devices, like home microwaves [52]. The 60 GHz ISM band is no exception to these conditions. While suffering from severe atmospheric attenuation (about 21.6 dB of loss for the same transmission dis-

tance compared to 5 GHz), this band can still be useful for in-room communications [53]. Moreover, the bandwidth available at this frequency (500 MHz) can support data rates comparable to present wired communications standards [53]. Unfortunately, federal airborne radar systems also occupy this prospective band, so interference is likely unless collaborative measures are taken to avoid it [40]. Power allocation algorithms and joint co-design of systems have been shown to alleviate interference in this band, but more research is required in this area [51]. Similar circumstances are echoed in the K band (20-36 GHz), specifically in the 24 GHz range [51]. This is not just a problem in the United States, either. In China, studies have shown that 5G allocation in the n285 band (24.25-27.5 GHz) has caused interference with narrowband millimeter-wave radar at 24-24.25 GHz [54].

2.7.3 Citizens Broadband Radio Service

In October 2010, the NTIA began looking at certain bands of frequency in the UHF and SHF bands to allocate towards wireless broadband, hoping that it would spur "innovative new businesses" and a more efficient economy [55, p. iv]. One of the considered bands was the 3550-3700 MHz band, later called the "Citizens Broadband Radio Service" by the FCC in 2012 [56]. This band was primarily used for DoD radar systems, but the NTIA determined that it was also capable of supporting modern wireless broadband schemes without significantly affecting legacy systems [55]. In 2015, the FCC established a three-tiered organizational structure for this band: (1) *Incumbent Access*; (2) *Priority Access*; and (3) *General Authorized Access* [57]. Each tier communicates with a cloud-based *spectrum access system* (SAS) that coordinates which users may transmit at certain frequencies in specific geographical regions [57].

Incumbent users have the highest preference and represent legacy federal users,

Fixed Satellite Service (FSS), and, temporarily, (grandfathered) terrestrial wireless service [57]. Priority Access users are those with "critical quality-of-service needs," such as "hospitals" and "public safety entities" [57, p. 9]. They operate on a secondary basis to the incumbent users. Finally, General Authorized Access represents the "widest possible group of potential users," according to the FCC [58]. They must yield entirely to the previous tiers [57]. In 2020, the FCC authorized "full commercial deployment" of this band, paving the way for 5G deployment in CBRS [59]. The use of this band will allow carriers to deploy small cells where additional coverage is necessary, making 5G faster and more robust [57].

It is possible that other countries will adopt a similar approach as CBRS if they identify frequency bands with services that could accommodate additional devices. Many developed countries have the demand for such a solution, but its feasibility depends on the availability of suitable frequency bands. Although CBRS is specific to the United States, coordinated efforts at the international level, such as through the ITU-R, could help address transborder interference scenarios and promote global synchronization of frequency bands. The desire for such a system will likely increase as globalization continues to accelerate.

2.7.4 Wi-Fi 6

Wi-Fi 6 (802.11ax) is the next continuation of the IEEE 802.11 standard of WLAN. Deployed in 2020, it provides data rates that are over 2.5 times faster than previous generations [60]. It currently operates in the 2.4 GHz and 5 GHz bands. However, in April 2020, the FCC announced that unlicensed operations would be expanded into 1200 MHz of spectrum (5.925-7.125 GHz), "ushering in Wi-Fi 6 ... and boosting the growth of the Internet of Things" [60]. This allocation is a monumental step forward for

Wi-Fi because it more than quadruples the previous bandwidth allocated to it [61]. The incumbent services of this band include mobile, fixed, fixed satellite, and radioastronomy services that must remain in operation [62]. Like the other previously discussed bands, a series of rules must be made to prevent interference with these services [62]. The commission determined that an *Automatic Frequency Control* (AFC) system utilizing a centralized database of frequency ranges and maximum permissible powers for a location would best prevent interference [62]. This model of spectrum management has already been proven effective due to its similarities with the successful CBRS spectrum access system [62].

2.8 Fundamental Challenges with Spectrum Management

Spectrum allocation has historically been done by stacking new frequency allocations above existing ones on a chronological basis [4]. This is because time allows for technologies that utilize higher frequencies to become more established [4]. Unsurprisingly, though, this rather instinctive system for organizing spectrum acts as a metaphorical sedimentary rock, permanently casting obsolete technologies in the layers of spectrum allocation. Spectrum refarming delineates the process of reorganizing these legacy allocations to make room for services deemed more spectrally efficient [4]. MmWave 5G NR, for instance, does not have enough propagative penetration to reasonably provide consistent service to all users [63]. It is, therefore, imperative that low-band and mid-band frequencies be used in combination with mmWave [63, 64]. Existing allocations, though, completely occupy desired bands, so refarming preexisting 4G LTE bands for 5G NR is a likely step in modernizing wireless communication infrastructure [63]. This same process is an inevitable progression for every generation of broadband cellular network technology. On October 28, 2021, the FCC issued a PSA

alerting consumers to the planned retirement of most 3G networks in the U.S. by the end of 2022 “to make room for more advanced network services” [65]. The FCC warns that older devices that do not support 4G LTE or 5G NR will lose connectivity, including the ability to contact emergency services [65]. In fact, fixed hardware is a probable culprit for why 3G — an obsolete technology — is only recently being phased out.

2.8.1 Legacy Equipment

Legacy equipment is a central reason for the slow adaptation of spectrally efficient technology. The economic loss suffered during the shifting of technology can sometimes haze the perceived benefits of greater spectral efficiency. For this reason, the reallocation of presently inefficient bands can be a lengthy, bureaucratic process that almost always results in the monetary loss of at least one party [4]. To make the 3G retirement plan more palatable, many network carriers are offering free device upgrades to their affected users [65]. Network carriers will likely extend similar support for subsequent phase-outs, such as 4G and eventually 5G, to alleviate the financial burden associated those retirements. In other instances, however, legacy equipment operators are not as fortunate. Upgrading or replacing legacy equipment can impose a significant financial burden on industries, so proactive change can take years depending on how many users are negatively affected [4]. It is important for policymakers to consider the motivation for the proposed reallocation. Parties that emphasize the inefficiency of legacy users, rather than the improved efficiency of their own proposed technology, are likely operating with selfish intent and will only worsen the related spectrum scarcity issue [4].

2.9 Conclusion

In conclusion, radio frequency use is an ever-expanding frontier, on one hand, and a finite, competitive resource, on the other. It is highly valuable to both government and private industry, creating a fertile area for government regulation of private use. The major industrial benefit of RF use is that it allows systems to share data wirelessly. The related lure of vast financial reward brings industry innovators to the arena. Meanwhile, governmental use of RF drives the use of weather, national defense, aviation, and maritime services that are essential and therefore in the public good. Interference of those essential government operations must be prevented but in a manner that allows private industry to also make productive use of the spectrum. Spectrum management is the recognized key to the multi-use of radio frequency bands.

Chapter 3

The Fundamentals of OFDM in Communication Systems

3.1 Introduction

OFDM, as previously described, is a modulation technique that utilizes multiple narrowband subcarriers to transmit data. It has very efficient bandwidth utilization and is robust against narrowband interference and multipath fading. Each subcarrier is spaced orthogonally in frequency, meaning the peak of one subcarrier aligns with the zero crossings of the others. This allows OFDM to be almost twice as spectrally efficient compared to traditional frequency division multiplexing techniques. Also, since it modulates data on many different subcarriers, the loss of a few subcarriers due to narrowband interference can be easily corrected by using error correction techniques. Techniques like encoding, interleaving, and puncturing can be used to minimize errors and maximize throughput. Moreover, equalization is greatly simplified with OFDM. OFDM, however, is sensitive to frequency offset, has a high peak-to-average power ratio (PAPR), and requires precise timing and frequency synchronization [39].

3.2 Background

OFDM was introduced in 1966 by Robert W. Chang at Bell Labs. Chang's groundbreaking paper, titled, "Synthesis of band-limited orthogonal signals for multichannel data transmission," proposed to transmit data on multiple parallel narrowband orthogonal sub-channels. The proposed technique utilized analog modulation using the Fourier Transform and a bank of oscillators at the subcarrier frequencies. In 1971, Weinstein and Ebert eliminated the need for many oscillators by digitally implementing OFDM with the discrete Fourier Transform (DFT), greatly reducing implementation complexity. This made OFDM feasible for widespread implementation. Modern advances in digital FFT (a computationally efficient DFT) chips further improve the implementation complexity of OFDM and allow for techniques like Orthogonal Frequency Division Multiple Access (OFDMA) [66].

3.3 Transmitter and Receiver Design Structure

The basic OFDM transmitter design structure leverages an N-length *inverse discrete Fourier Transform* (IDFT) where N is the number of subcarriers, to produce IQ data from constellation mapping of bits to discrete time domain data. The real components of the time-domain data are passed through a *digital-to-analog converter* (DAC) and mixed with a carrier frequency generated by a *local oscillator* (LO). The imaginary components of the TD data are passed through an *analog-to-digital converter* (ADC) and mixed with the same local oscillator but phase-shifted by 90 degrees to produce orthogonal basis functions sine and cosine. Both resultant waveforms are added together and then transmitted as a single waveform.

The OFDM receiver design structure is tasked with undoing the various steps the

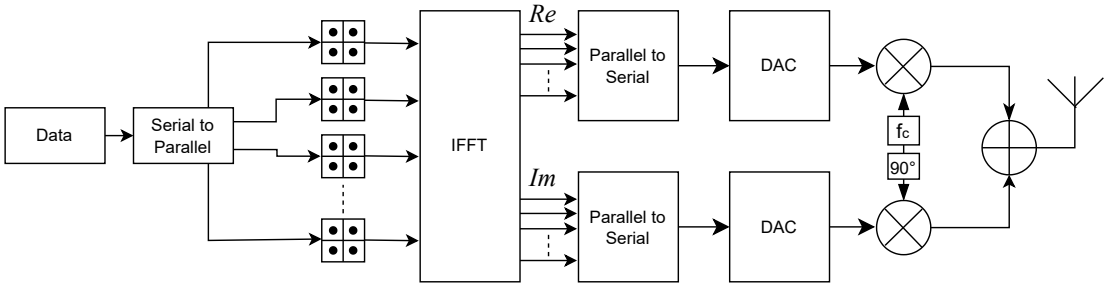

Figure 3.1: Simplified OFDM Transmitter Block Diagram

transmitter took to effectively transmit the data. This involves quadrature mixing the received signal with the same carrier frequency and low-pass filtering off reflected higher frequency components of each signal at $2f_c$. Both resultant *continuous time* (CT) signals are then passed through an ADC and taken as the real and imaginary values of an N_{carriers}-length DFT. This yields a parallel array of complex values that correspond to the same constellation points that were mapped at the transmitter. Due to the noise and channel effects found in real-world systems, the received constellation points will be different than the original ones. If all constellation points are equiprobable, as is often assumed, the receiver will map each received constellation point to the closest point on the expected constellation. If there is no significant interference and distortion, then these values will match the ones mapped at the transmitter and the data will be recovered. It is important to note that these diagrams are simplified arrangements and real-world systems have many additional components, like equalizers, cyclic prefix insertion, and encoders/decoders, to account for things like multipath delay spread and noise.

3.4 The Cyclic Prefix

A *cyclic prefix* (CP) is used in OFDM to combat inter-symbol interference (ISI) caused by multipath fading. The cyclic prefix is a copy of the last N_{CPE} samples of a

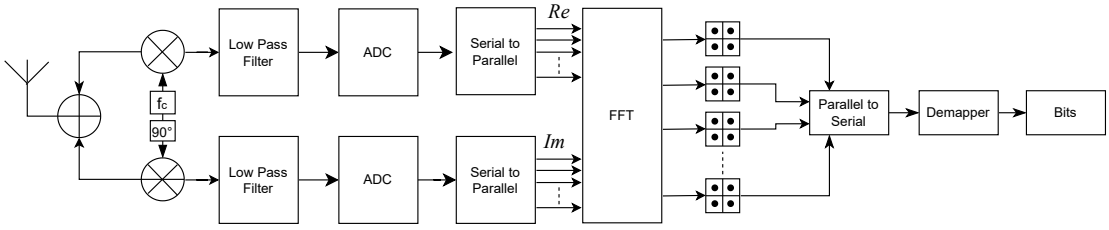

Figure 3.2: Simplified OFDM Receiver Block Diagram

symbol prepended to the front of the symbol in the guard interval. This preserves the orthogonality of subcarriers by including a full symbol of the delayed multipath reflection in the sampling interval. Increasing the cyclic prefix duration helps mitigate ISI caused by longer delay spreads, but it also increases the length of the OFDM symbol, which reduces throughput. This creates a tradeoff [39].

The cyclic prefix can also be used for timing and frequency synchronization by mixing the OFDM symbol with a time-delayed and conjugated version of itself then integrating across the guard time, T_G. This process, known as *autocorrelation*, allows timing estimation by observing the peak correlation value and frequency offset estimation by determining the phase of the maximum correlation [39].

Systems with large relative multipath delay spread use longer cyclic prefixes than systems with shorter delay spread. For example, LTE uses an extended CP duration of 16.7 µs [67], while Wi-Fi 6's longest configurable CP is 3.2 µs. This is because LTE signals have to propagate long distances in outdoor environments, which leads to longer delay spreads than indoor Wi-Fi applications. Delay spread is generally controlled by several system factors, like the carrier frequency, transmit power, and implementation of technologies like multi-user MIMO (MU-MIMO) which service more users by using multiple antenna elements to direct radiation in the direction of specific users. Different configurations of these variables factor into the required delay spread tolerance of a system.

3.5 Wireless Standards

In an OFDM communication system, there are a variety of design specifications that an engineer can tailor to the physical limitations of the channel and the desired application. These design specifications include things like subcarrier spacing, FFT size, cyclic prefix length, and constellation type/modulation order, as well as the OFDM frame structure discussed in the following section. Different standards have different formal descriptions for these parameters. For example, 802.11.ax, or Wi-Fi 6, uses a variety of FFT sizes depending on the available bandwidth of the channel, signal-to-noise ratio (SNR), and desired data rate. For instance, a 20 MHz Wi-Fi 6 channel contains 256 subcarriers and uses *quadrature amplitude modulation* (QAM) with a modulation order of up to 1024. Wi-Fi 6 also specifies frameworks for 40 MHz, 80 MHz, and even 160 MHz channels [68].

3.6 OFDM Frame Structure

The OFDM frame structure is organized into three constituent elements: the *preamble*, the *header*, and the *payload*. The preamble is used for synchronization, channel estimation, and frequency offset estimation. The header contains information about the characteristics of the data symbols, like the modulation order, packet length, and payload size so that the receiver is able to properly demodulate the data. Finally, the payload contains the actual data being transmitted. This frame structure is generally consistent through many major wireless standards like LTE and Wi-Fi with slight variations depending on their application [1, 69].

In the 802.11a standard frame structure, for instance, the preamble is 12 OFDM symbols comprised of short training symbols, used for timing acquisition and coarse

frequency acquisition, and long training symbols, used for channel estimation and fine frequency acquisition, as shown in Figure 3.3. The preamble is able to accomplish these goals by using favorable signal characteristics and a priori knowledge of the signal structures by the receiver [1].

In 802.11a, the header contains information about the data symbols, such as the data rate, which specifies the modulation type and coding rate. It also contains information about the number of bytes transmitted in the frame, which, along with the modulation order, coding rate, and data subcarriers per symbol (48), can be used to calculate the number of OFDM symbols transmitted in a frame as shown in the following equation,

$$N_{\text{OFDM}} = (R_{\text{code}}) \log_2(M)(N_{\text{carriers}} - N_{\text{null}}), \tag{3.1}$$

where N_{OFDM} is the number of OFDM symbols in one frame, M is the modulation order, N_{carriers} is the total number of subcarriers (i.e., the FFT size), N_{null} is the number of nulled (unused) subcarriers, and R_{code} is the coding rate [1].

Finally, the payload in the 802.11a standard contains the data. It is adaptable in size, containing anywhere from 1 to 4095 bits. It modulates bits as specified by the data rate parameter from the header in several constellation types: BPSK, QPSK, 16-QAM, and 64-QAM [1].

3.7 Error Correction Techniques

Encoding and *interleaving* are *error correction techniques* that are often used in OFDM systems to optimize throughput while minimizing errors. Encoding is the process of introducing redundancy into the data so that when an error occurs the receiver can still retrieve the original bitstream. This, of course, reduces the throughput of the

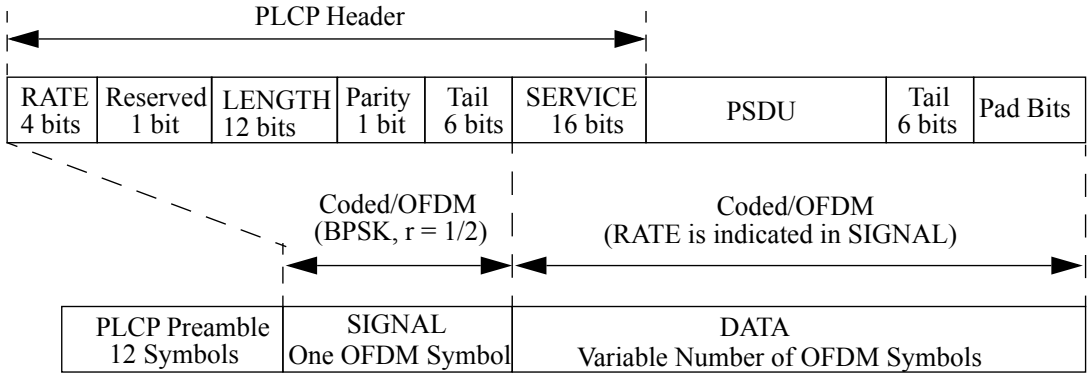

Figure 3.3: 802.11a OFDM frame structure [1]

system. Since groupings of bit errors from subcarriers lost to deep fades or narrowband interference reduces the error correction capabilities of the encoding/decoding process, an interleaver is used to "blend" the bits up and evenly distribute the errors, as illustrated in Figure 3.4. At the receiver, the bits are decoded and "unblended" in reverse order, yielding the original bitstream. *Puncturing* can be used to achieve higher data rates when the coding rate is too conservative for the current SNR. It works by removing certain bits of data from the input bitstream, transmitting, then inserting dummy bits in place of the removed bits before decoding the data [1].

3.8 Carrier Frequency Offset

OFDM systems are especially vulnerable to *carrier frequency offset* (CFO) caused by mismatched transmitter and receiver oscillators and Doppler shift. Small errors in frequency can result in significant *inter-carrier interference* (ICI) because any deviation from the subcarrier peaks causes neighboring subcarriers to not be completely nulled out, which damages orthogonality. It can also result in a loss in received power from the target subcarrier. An illustration of these factors can be observed in Figure 3.5. A system's oscillator tolerance before experiencing significant distortion is usually given

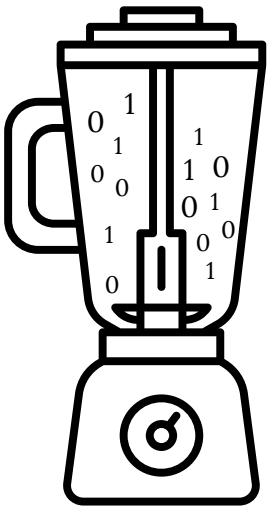

Figure 3.4: Error correction interleaver depicted as a physical blender mixing up bits

in parts per million (ppm). For instance, if an OFDM system at a carrier frequency of 5 GHz has a subcarrier spacing of 300 kHz, then its oscillator accuracy might need to be within a range of 3 kHz or have an accuracy better than 0.6 ppm. Generally, a carrier frequency offset of less than 1% is required to limit degradation to 0.1 dB. CFO correction, however, can greatly improve the tolerance for frequency errors. Moreover, pulse-shaping filters can be used to shape the subcarriers in such a way that when frequency offset does occur, there is not as much ICI [39].

In Paul Moose's 1994 paper, "A Technique for Orthogonal Frequency Division Multiplexing Frequency Offset Correction," he outlines a method for CFO correction using duplicate data symbols. Since the phase of the modulated subcarriers does not change between symbols, any observed change is due to CFO. The frequency offset is then estimated using a derived Maximum Likelihood Estimate (MLE) algorithm. A receiver can then shift the incoming signal in time by $e^{-2\pi \cdot \Delta f_{\text{est}} \cdot n/fs}$ to correct for the distortion. The performance of the algorithm is a function of the SNR of each subcarrier and the frequency offset. The estimated ratio of the carrier offset to the carrier spacing, $\hat{\epsilon}$, is

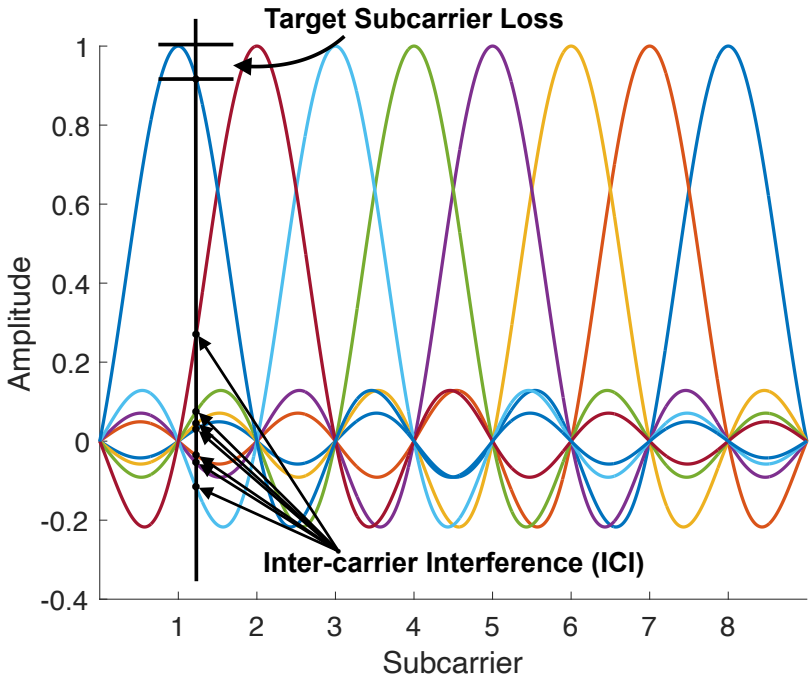

Figure 3.5: ICI and target subcarrier loss as a result of carrier frequency offset (CFO)

shown in Equation 3.2 [70],

$$\hat{\epsilon} = \frac{1}{2\pi} \tan^{-1} \left\{ \frac{\sum_{k=-K}^{K} (\mathrm{Im}[Y_{2k} Y_{1k}^*])}{\sum_{k=-K}^{K} (\mathrm{Re}[Y_{2k} Y_{1k}^*])} \right\}, \tag{3.2}$$

where Y_{1k} and Y_{2k} are two received symbols in the frequency domain (after channel effects and noise) corresponding to the same sequence, x_n, transmitted twice. These repeated, consecutive symbols are known in the OFDM frame structure as *training symbols*, as their sole purpose is to "train" the receiver to more accurately retrieve the transmitted data.

3.9 Pulse Shaping

Pulse-shaping can be applied to the individual subcarriers in the frequency domain so that their spectrum rolls off more rapidly. This reduces ICI by lowering the amplitude of the neighboring subcarriers when the OFDM system has an uncorrected frequency offset, as shown in Figure 3.6. Pulse shaping can also be used to limit out-of-band radiation. OOB radiation can decrease slowly when subcarriers are sinc pulses, as seen with the standard rectangular pulse-shaping window. A raised cosine window (eq. 3.3) with a rolloff factor of just 0.05 can significantly reduce OOB radiation, as shown in Figure 3.7. The roll-off factor, α, controls how fast the amplitude drops off in the frequency domain and how much the symbol duration increases in the time domain. The extensions between adjacent symbols in the time domain can be overlapped, though, so the symbol duration is only increased by a factor of 1/2 of α. Tradeoffs exist between limiting the reduction in throughput, decreasing ICI, and increasing out-of-band radiation. Other pulse-shaping windows, like the better than raised cosine pulse (BTRC) and the improved sinc power pulse (ISP), have been used to achieve desired performance of the system. It is important for an engineer to consider the uses of the system, the desired spectral mask, and desired throughput to determine the correct pulse-shaping window [71].

$$w(t) = \begin{cases} 0.5 + 0.5\cos\left(\pi + \frac{t\pi}{\alpha T_s}\right) & 0 \leq t \leq \alpha T_s \\ 1.0 & \alpha T_s \leq t \leq T_s \\ 0.5 + 0.5\cos\left(\frac{(t-T_s)\pi}{\alpha T_s}\right) & T_s \leq t \leq (1+\alpha)T_s \end{cases} \tag{3.3}$$

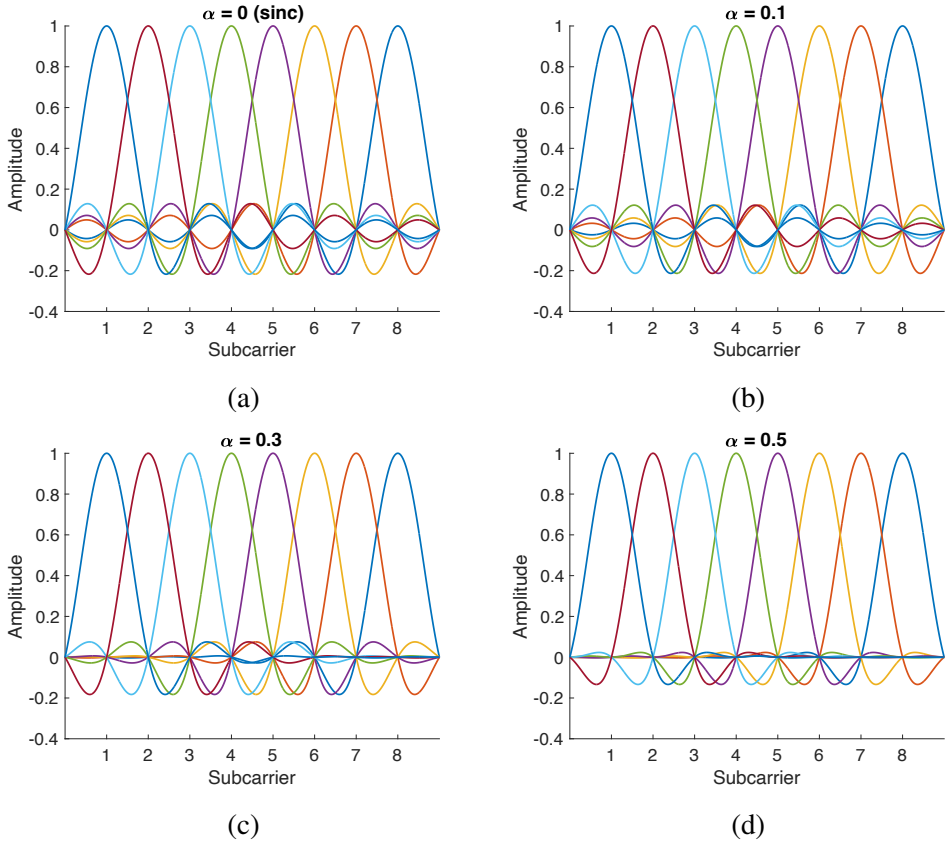

Figure 3.6: Orthogonally spaced raised cosine-shaped subcarriers with various rolloff factors: (a) $\alpha = 0$, which is a sinc pulse, (b) $\alpha = 0.1$, (c) $\alpha = 0.3$, (d) $\alpha = 0.5$

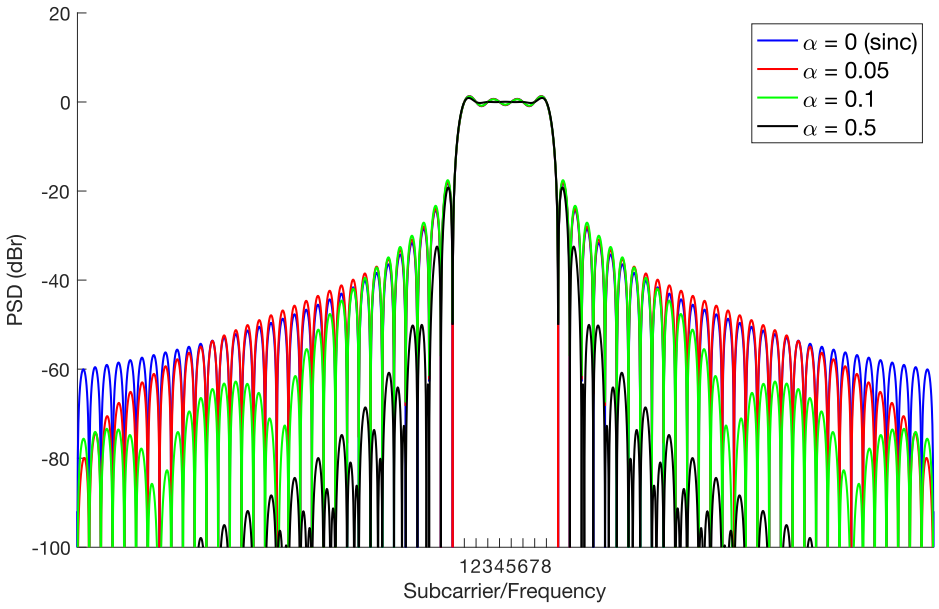

Figure 3.7: Depiction of OOB radiation of OFDM systems with 8 subcarriers orthogonally spaced in frequency with various rolloff factors: $\alpha = 0$, which is a sinc pulse, $\alpha = 0.05$, $\alpha = 0.1$, $\alpha = 0.5$

3.10 The Peak-to-Average Power Ratio Problem

OFDM systems often suffer from a high *peak-to-average power ratio* (PAPR) because each subcarrier is independently modulated, so when they add up it can result in a large-peaked time domain signal. This is a problem because analog-to-digital converters want to contain the full amplitude range of the received signal through the use of *automatic gain control* (AGC). When quantization occurs with a signal with high PAPR, then the resolution of the lower amplitude variations of the signal is limited to fewer quantization steps, and they can be lost as a result. Figure 3.8a shows the 3-bit (8 steps) ADC quantization for a signal with a low PAPR of 3 dB, and Figure 3.8b shows the 3-bit quantization steps for a signal with a high PAPR of 13 dB. The sampling rate for the quantization steps of both figures is twice the highest frequency, as per the

Nyquist sampling theorem. One can observe that the quantization steps of the signal with low PAPR much better encapsulate the behavior of the signal compared to the quantization steps of the signal with high PAPR. The simplest solution to high PAPR is to clip the high-amplitude portions of an OFDM symbol, but this destroys the orthogonality of the subcarriers and causes in-band and out-of-band interference. The OOB interference can be filtered off, though, which allows this method to be implemented in the real world [72].

There are many other techniques that can be used to reduce the average PAPR in an OFDM symbol. One such technique, called the *SeLected Mapping* (SLM) technique, is to generate a large number of OFDM sequences representing the same data and choose the one with the lowest PAPR. This is accomplished by multiplying the input data symbol by U phase sequences, each of length N. This chosen phase sequence is traditionally transmitted on a side of the OFDM transmission and the receiver uses this information to deconstruct the original data. Another approach is to intentionally transmit data symbols off from their constellation points in such a way that the subcarriers do not add up to tall peaks in the time domain [73].

3.11 Multipath Fading Channels

Transmitted OFDM symbols experience distortion known as *multipath fading*, which is caused by delayed reflections of the transmitted signal being picked up at the receiver. These delayed reflections are a result of the signal bouncing off various physical objects, like buildings, walls, or mountains, before arriving at the receiver. They are represented as an impulse response known as the *discrete-time* (DT) *channel response*, where each "tap," or delayed reflection, appears as a single weighted discrete time value as illustrated in Figure 3.9. By taking an N_{carriers}-point FFT of the discrete TD chan-

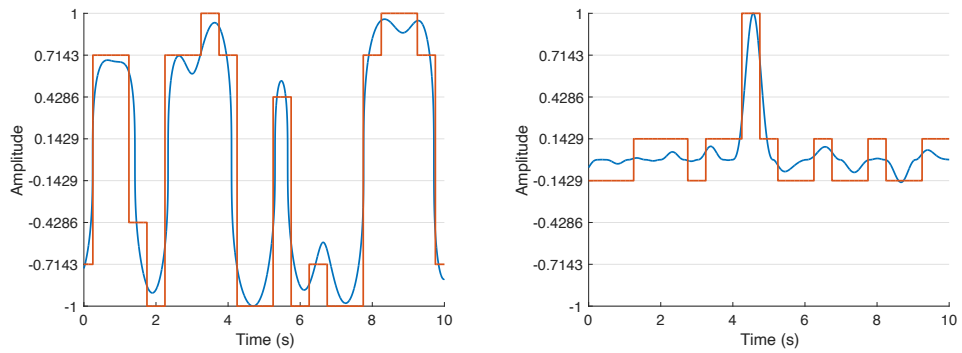

(a) (b)

Figure 3.8: 3-bit quantization of signal with a low PAPR of 3 dB (a) and a high PAPR of 13 dB (b)

nel response, one can obtain the frequency response of the fading channel, which shows the distortion experienced by each subcarrier. Equalization in OFDM serves to estimate this channel frequency response and correct for its distortions. A MATLAB simulation was made to analyze the effect that various multipath fading channels have on each subcarrier.

Consider an OFDM system with 64 subcarriers, a 20-dB SNR, and a four-tap channel impulse response of $g = [e^{-0} \quad e^{-1} \quad e^{-2} \quad e^{-3}]/\text{norm}(g)$ (or $g = [0.9300 \quad 0.3421 \quad 0.1259 \quad 0.0463]$), as shown in Figure 3.10. This channel impulse response is comprised of a dominant direct path (the e^{-0} term) and several decaying terms representing delayed reflections of the signal. The *magnitude* and *phase response* of the channel are shown in Figures 3.10a and 3.10b, with each subcarrier overlaid on their respective locations to map their individual distortions. The constellation diagrams of nine individual subcarriers (1, 8, 16, 24, 32, 40, 48, 56, and 64) are also shown in Figures 3.10c to 3.10k. One can then track the magnitude and phase distortions of each subcarrier from the frequency response plots to the constellation diagrams and observe how the multipath channel affects each subcarrier. For instance, subcarrier 8

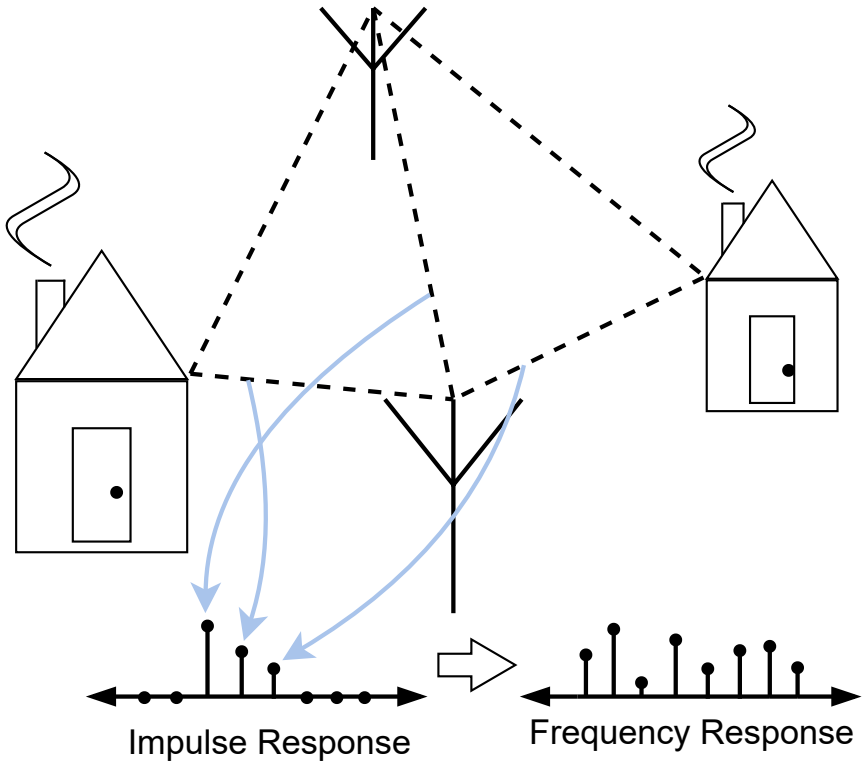

Figure 3.9: Illustration of the impact of a 3-tap multipath fading channel, including direct line-of-sight and time-delayed signal reflections, on an 8-subcarrier OFDM system

shows a magnitude scaling of approximately 2 dB and a phase rotation of approximately 0.31 radians, or roughly $-18°$. By observing the constellation for subcarrier 8 in Figure 3.10d, one can see that the received constellation points are slightly more spread out and rotated counterclockwise compared to the original QAM constellation [74].

Now consider the same 64 subcarrier OFDM system, except with a 12-tap normalized channel impulse response of $g = [0.0141 \quad -0.0493 \quad 0.0563 \quad 0.2252 \quad -0.3870 \quad 0.7036 \quad 0.4926 \quad 0.2111 \quad 0.0070 \quad -0.1055 \quad 0.0141 \quad 0.0070]$. Notice that this channel now has leading and trailing echoes and a longer delay spread. Since delay spread is inversely proportional to coherence bandwidth, or the bandwidth over

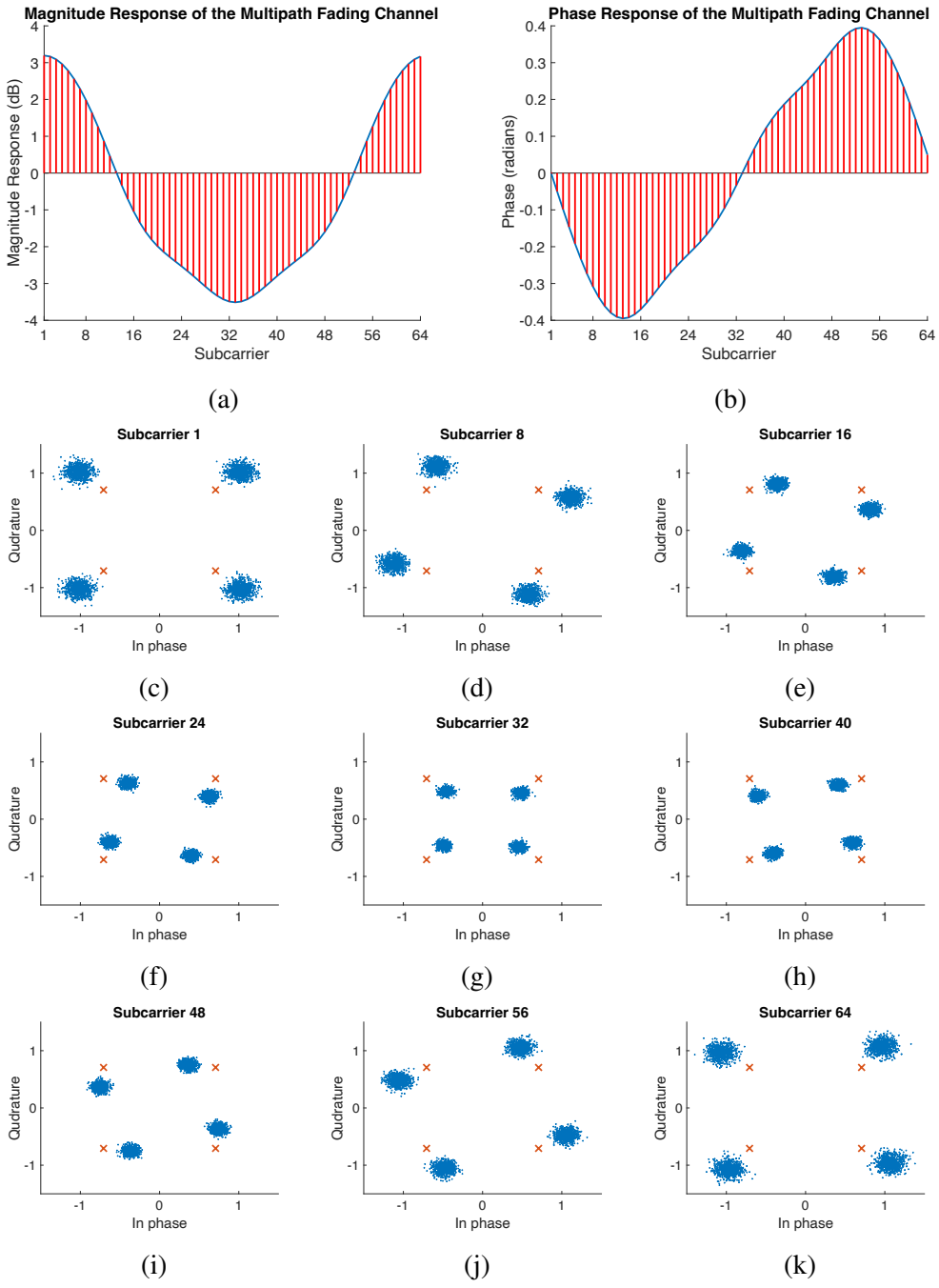

Figure 3.10: Magnitude (a) and phase (b) response of four-tapped multipath channel impulse response, normalized to unit energy, represented by $g = [e^{-0} \quad e^{-1} \quad e^{-2} \quad e^{-3}]$. Constellation plots for subcarriers 1 (c), 8 (d), 16 (e), 24 (f), 32 (g), 40 (h), 48 (i), 54 (j), and 60 (k) are provided.

which the channel can be seen as flat fading, the magnitude and phase responses appear more jagged, as seen in Figure 3.11.

3.12 Equalization

Equalization reduces the effect that multipath delay spread has on the frequency response of the channel by estimating and compensating for the distortions. In OFDM, equalization is traditionally easier than in traditional single-carrier systems due to the subcarriers being narrower than the coherence bandwidth of the channel. This is because the frequency response of the channel affects each subcarrier independently as if it were flat fading, so the equalization of each subcarrier is represented as a single complex multiplication operation at the receiver. This greatly simplifies the equalization process and improves robustness against fading and other channel effects like interference and noise.

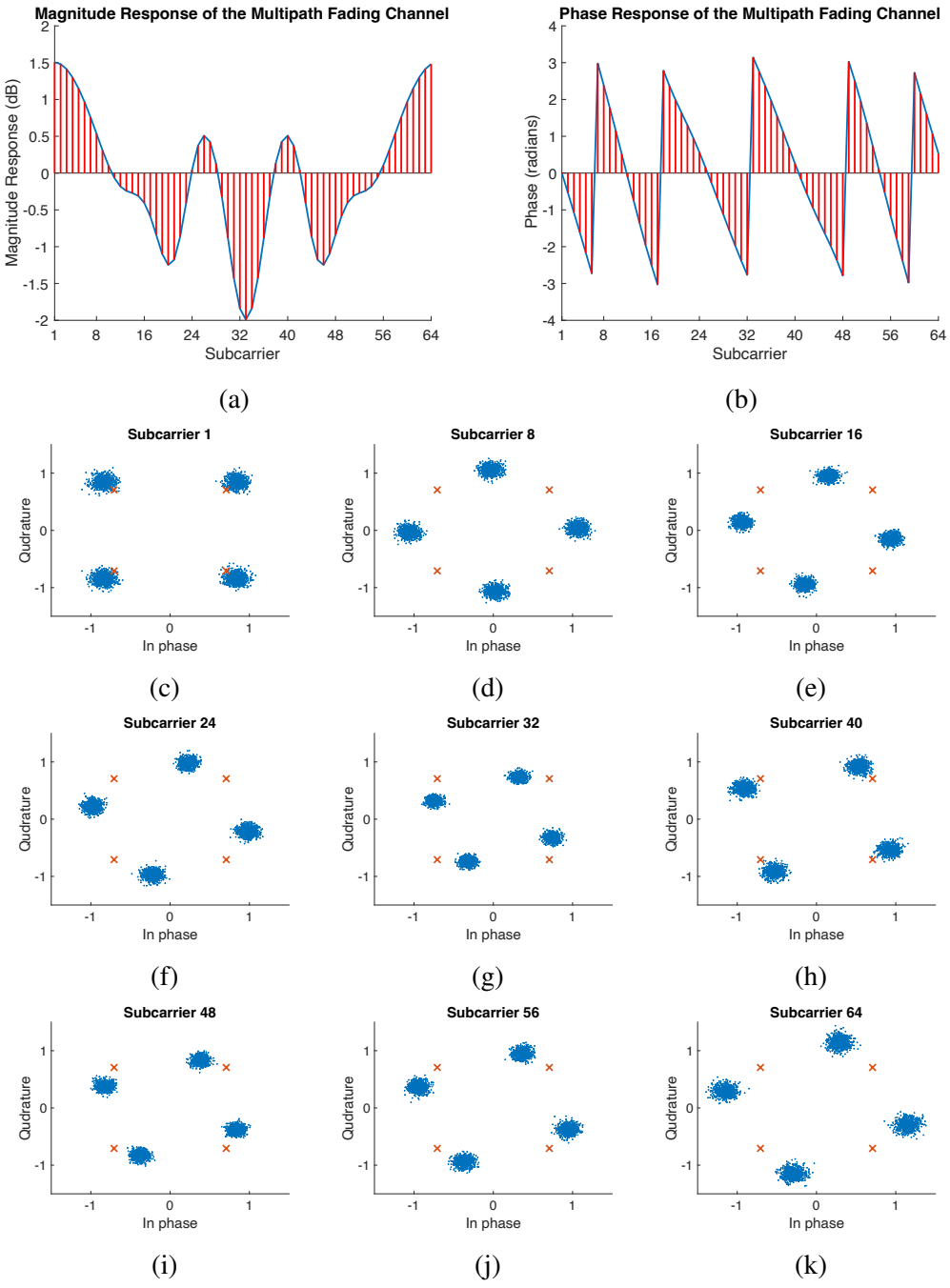

Figure 3.11: Magnitude (a) and phase (b) response of normalized four-tapped multipath channel impulse response represented by $g = [0.0141 \quad -0.0493 \quad 0.0563 \quad 0.2252 \quad -0.3870 \quad 0.7036 \quad 0.4926 \quad 0.2111 \quad 0.0070 \quad -0.1055 \quad 0.0141 \quad 0.0070]$. Constellation plots for subcarriers 1 (c), 8 (d), 16 (e), 24 (f), 32 (g), 40 (h), 48 (i), 54 (j), and 60 (k) are provided.

Chapter 4

The Fundamentals of Pulse-Doppler Radar

4.1 Introduction

A *pulse-Doppler radar* is a type of radiolocation system that transmits pulsed waveforms and receives reflections from nearby targets. By analyzing these reflections, a pulse-Doppler radar system can provide information about the distance and velocity of the target relative to the radar. It uses pulse-timing techniques to determine range information and Doppler processing to determine velocity information. There are many applications for pulse-Doppler radar, such as defense surveillance, air traffic control, and weather monitoring which solidify its importance in society.

4.1.1 Types of Radar Systems

4.1.1.1 Continuous Wave Radar vs. Pulsed Radar

There are two basic forms of radar: *continuous wave* (CW) radar and *pulsed radar*. A CW radar is a radar that operates with simultaneous transmit and receive, while pulsed radar transmits bursts of signals, monitoring the spectrum for return echoes between each successive transmission. CW radar is more suitable for low-power, short-range applications like police radars and automotive cruise control and does not suffer

from blind spots in range and velocity like pulsed-radar systems do. As alluded to in the introduction, a pulsed-radar system will be assumed for all of the demonstrations and calculations.

4.1.1.2 Monostatic Vs. Bistatic Radar Systems

Monostatic and *bistatic* are two different configurations for radar systems that differ in the location of the transmitter and the receiver. In a monostatic radar system, the transmitter and the receiver are colocated, which typically means they share an antenna. A shared antenna requires a *duplexer* to facilitate the rapid bidirectional switching between the transmit and receive chains. In a bistatic system, the transmitter and receiver are physically separated by a significant distance, offering benefits such as potentially better reflection characteristics from a target and more. These two radar systems are shown in Figure 4.1. Since the majority of radar systems employ a monostatic configuration, however, this chapter will assume a monostatic system for all analyses.

4.2 Basic Principles of a Pulsed Radar

A pulsed radar works by transmitting hundreds to thousands of electromagnetic pulses a second. After transmitting each pulse, the radar then observes the spectrum for echoes of the transmitted pulse reflecting back to the radar from objects in the envi-

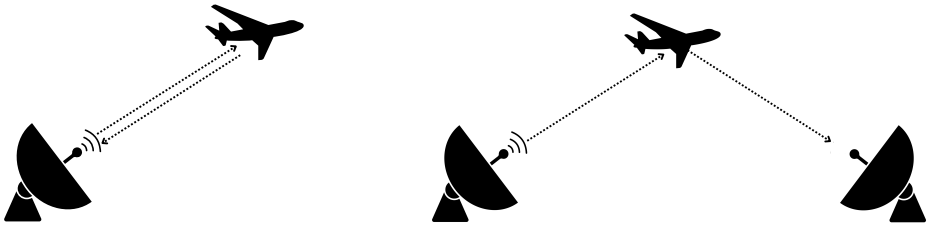

Figure 4.1: Depiction of two radar configurations: (a) monostatic, (b) bistatic

ronment, called *scatterers*, as shown in Figure 5.4c. Using *pulse timing techniques*, the radar is able to estimate the relative range of a scatterer of electromagnetic waves with respect to radar. The *pulse repetition frequency* (PRF) is the rate at which pulses are transmitted from the radar, and the *pulse repetition interval* (PRI) is the time duration between the start of one pulse and the start of the next, which is the reciprocal of the PRF. The *duty cycle* of a pulsed radar represents the amount of time spent transmitting divided by the PRI. Traditionally, the duty cycle of a pulsed radar is kept low (less than 1%) to ensure that the average power does not get too high [2].

4.2.1 Pulse Timing Techniques

Pulse timing techniques, as mentioned in the previous section, are used by a pulsed radar to estimate the relative range between the radar and a scatterer. The *maximum unambiguous range*, or the range at which a pulse can travel and return back to the radar before the next pulse is transmitted, is calculated as follows:

$$R_{ua} = \frac{c \cdot T_{PRI}}{2} \tag{4.1}$$

Here, T_{PRI} is the pulse repetition interval. and c is the speed of light, which is how fast an electromagnetic pulse travels. Logically, one may understand this equation as the distance traveled by the pulse (range $\cdot$ velocity) divided by two, since the pulse must return back to the radar. When a scatterer is further away than R_{ua}, the returned echoes will overlap into the next pulse's observation period, resulting in *range aliasing*. For instance, if $R_{ua} = 100$ meters and a *target*, or an object of interest, at 150 meters is in the path of the radar, then the radar will perceive this object at $150 - 100 = 50$ meters away, assuming the target's radar cross-section (RCS) is high enough to return enough power to the radar for detection [2].

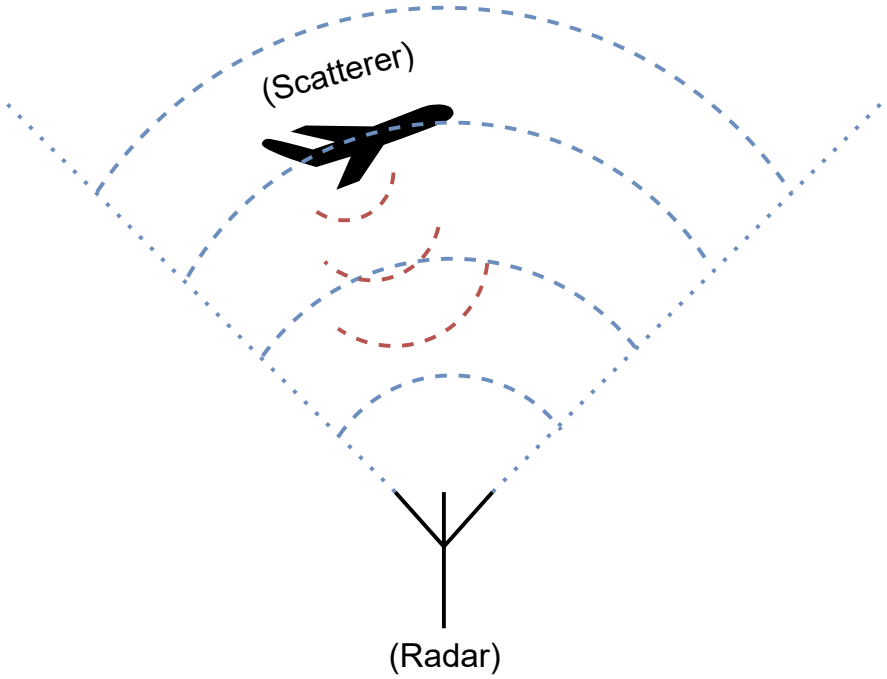

Figure 4.2: Simple pulsed radar system transmitting and receiving signal reflections from an airplane

4.2.2 Radar Cross Section

Radar cross-section is a fundamental property of an object that refers to its detectability in the eyes of the radar. An object's RCS is calculated from the following equation,

$$\sigma = 4\pi R^2 \left(\frac{Q_b}{Q_t} \right), \tag{4.2}$$

where R is the radar range, Q_t is the incident radiation power density at the target, and Q_b is the backscattered radiation power density at the radar. RCS is a hypothetical quantity that represents the area that would be required for the intercepted transmitted power density at the target to create the backscattered power density that was observed at the radar, resulting in the $\left(\frac{Q_b}{Q_t} \right)$ term. The $4\pi R^2$ term comes from the surface area of a sphere with radius R since the backscattered radiation is modeled as radiating

isotropically (though it never really is)[2].

4.2.3 Clutter, Noise, Interference, and Jamming

The performance of a pulsed radar system can be severely impacted by *clutter*, *noise*, *interference*, and *jamming*. In general, clutter refers to surface or volume scattering resulting from the ground or sea, or meteorological patterns like rain, hail, or clouds. Since clutter is subject to complex scattering behavior, it is modeled stochastically as a random process. Moreover, the unique statistical properties of clutter – like its probability distribution and its spatial correlation characteristics – allow it to be distinguished from targets. In contrast to noise, clutter is multiplicative, non-white in nature, and affected by the positioning of the radar relative to the sources of clutter [2].

Noise is a major source of performance degradation in radar. Noise typically comes in two forms: *internal noise* and *external noise*. Internal noise is produced by the radar, while external noise is received through the radar's antenna from outside sources. *Thermal noise* is a type of internal noise that arises when electrical conductors are at a non-zero temperature in Kelvin. Another type of internal noise is *shot noise*, which is caused by the discrete, quantum behavior of electric current. *Atmospheric noise* and *cosmic noise* are types of external noise that come from things like lightning storms and extraterrestrial background radiation, respectively [2].

Radar interference occurs when another electromagnetic signal is being transmitted in the same space, time, and frequency as the radar. It is most commonly addressed by rules and regulations seeking to organize the spectrum to prevent such occurrences. Still, bad actors and improperly configured devices regularly transmit out of line. One familiar example of this is the interference caused by U-NII devices on the FAA's Terminal Doppler Weather Radar, as previously discussed in Section 2.6. Norman,

Oklahoma, home of the University of Oklahoma's *Advanced Radar Research Center* (ARRC), has two FCC-reported instances of U-NII devices causing interference requiring FCC agents from Dallas, Texas to use direction-finding techniques to track down the offenders. Another instance in Edmond, Oklahoma involves a wireless provider setting a U-NII device's operating country as Nicaragua and disabling the DFS setting to circumvent laws and restrictions. This resulted in a nearby news network's TDWR experiencing harmful interference [75]. In this thesis, a novel radar interference mitigation technique for OFDM waveforms will be discussed in Chapters 5 and 6.

Jamming occurs when a malicious emitter deliberately interferes with the operations of a radar. While radar signal processing seeks to improve the *signal-to-interference ratio* (SIR), jamming attempts to worsen it. *Noise jamming* is the technique that transmits an amplified noise signal in an effort to increase the perceived noise at the radar receiver. Other more advanced techniques try to mimic target echoes so that the radar hallucinates false targets [2].

4.2.4 Coordinate Systems

Radar systems are typically represented using spherical coordinates because they detect things radially from their perspective. The spherical coordinate system is defined in terms of *range* (R), *azimuth* (θ), and *elevation* (ϕ). Range is the distance from the radar to the target, azimuth is the horizontal angle shift with respect to the boresight direction (the direction that the antenna is pointing) and elevation is the vertical angle shift with respect to the boresight direction. Since targets move in the Cartesian coordinate system (x, y, z), radar signal processing often requires transforming between coordinate systems, which can be challenging [2].

4.2.5 Figures of Merit

Figures of merit seek to quantify the performance of a radar, with the key figures of merit for radar detection being the *probability of detection* (P_D) and the *probability of false alarm* (P_{FA}). P_D refers to a radar's ability to detect a target within one coherent processing interval, as discussed in Section 4.3. On the other hand, P_{FA} is the probability that a radar mistakenly detects a target when there is none. It is, therefore, desirable to maximize P_D and minimize P_{FA}. However, achieving this can be challenging because the mechanisms that increase P_D also increase P_{FA}. Generally, the only way to increase the spread between both probabilities is to maximize the SIR through various radar signal processing techniques [2].

For tracking, the figures of merit are the accuracy of range, angle, and velocity estimations, with velocity estimation discussed in Section 4.3. These estimations are dependent on the resolutions for each merit and the SIR. The objective of radar signal processing, again, is to enhance these performance measures so that the radar is more accurate and predictable [2].

4.2.6 Radar Resolutions: Range, Angular, and Cross-Range

Resolution is a fundamental parameter of a radar system that determines its ability to distinguish between two equal-strength scatterers that are closely spaced in range, angle, cross-range, or Doppler shift (velocity) [2]. A target can be resolved in one dimension, such as range, and be unresolved in another dimension, such as angle. In this section, the *range*, *angular*, and *cross-range resolution* of a radar system will be discussed, while Section 4.3 addresses *Doppler resolution*.

The range resolution in an unmodulated, constant-frequency pulse is determined by

the following equation:

$$\Delta R = \frac{cT_p}{2}, \tag{4.3}$$

where T_p is the pulse duration. In simple terms, Equation 4.3 states that for objects spaced less than $\frac{cT_p}{2}$ apart, the trailing edge of the first scatterer is not recorded at the receiver before the leading edge of the second scatterer, as can be intuitively understood from Figure 4.3. This results in the radar's inability to differentiate between both objects [2].

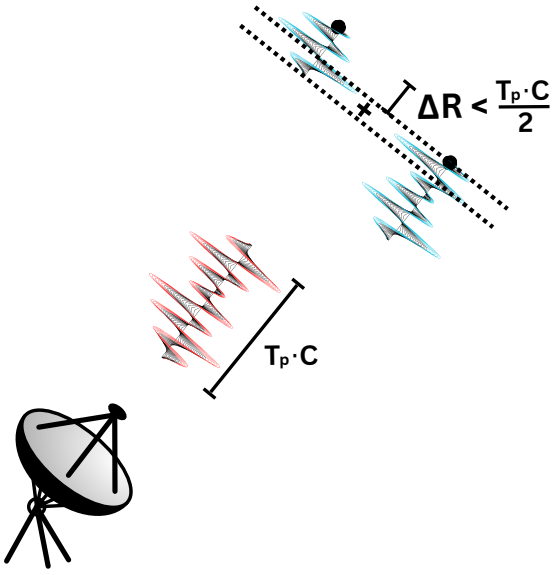

Figure 4.3: Illustration of two unresolved targets that do not fulfill the requirements of the range resolution equation (Equation 4.3)

The result from Equation 4.3 for simple waveforms is derived from a generalized ΔR equation that is true for all waveforms, including *pulse compression waveforms*, as discussed in Section 4.2.11. The generalized equation is derived from the following relationship for simple pulses:

$$T_p = 1/\beta, \tag{4.4}$$

where β is the bandwidth. Thus, ΔR can be written in the following form [2]:

$$\Delta R = \frac{c}{2\beta}. \tag{4.5}$$

Equation 4.3 shows that decreasing T_p allows for finer range resolution. This, however, issues complications as a lower pulse duration results in less transmitted energy (for the same transmitted power level), and less energy means worse detection and estimation performance. Pulse compression waveforms can overcome this apparent trade-off by decoupling β from T_p, and increasing the time-bandwidth product to a value greater than one [2].

Angular resolution is determined by the directivity (discussed in Section 4.2.7.1) of the transmitting antenna and applies to both the azimuth and elevation dimensions. Often, the *3-dB beamwidth*, θ_3, which is a measure of the angular spread of the antenna marking an approximately 50% drop-off of the maximum power density, is used to approximate the angular resolution by capturing the shape of the main lobe. For an ideal antenna aperture,

$$\theta_3 = 2 \arcsin\left(\frac{1.4\lambda}{\pi D_y}\right), \tag{4.6}$$

where D_y is the aperture size in the Y direction. Utilizing higher transmission frequencies typically means narrower antenna beamwidths, thus better angular resolution. Also, increasing the physical size of the antenna allows for more narrow beamwidths, thus better angular resolution [2].

The cross-range (CR) resolution, ΔCR, measures the resolution in the directions perpendicular to the range and is rigidly defined by the following equation:

$$\Delta CR = 2R \sin\left(\frac{\theta_3}{2}\right). \tag{4.7}$$

However, ΔCR can be approximated by the equation:

$$\Delta CR \approx R\theta_3, \tag{4.8}$$

since $\sin(x) = x$ for small x due to the small-angle approximation. Notice from this equation that ΔCR degrades as R increases, while range resolution has no dependency on range [2].

A radar takes measurements in three dimensions: range, azimuth, and elevation. From these, one can form two and three-dimensional *resolution cells* that illustrate the resolution capabilities of the radar. A three-dimensional cell is shown in Figure 4.4. The volume of this resolution cell is defined by the following equation:

$$\Delta V = \frac{\pi}{4} R^2 \theta_3 \phi_3 \Delta R, \tag{4.9}$$

where θ_3 is the 3-dB azimuth beamwidth and ϕ_3 is the 3-dB elevation beamwidth. Notice that the volume exponentially increases with R [2].

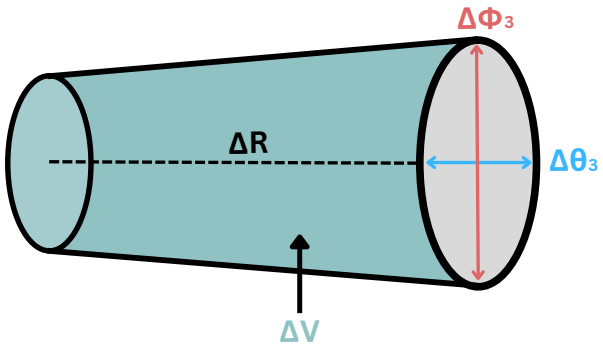

Figure 4.4: 3-dimensional resolution cell formed from the range resolution ΔR, the azimuth angle resolution $\Delta\theta_3$, and the elevation angle resolution $\Delta\phi_3$

4.2.7 Antennas

As discussed in Chapter 2, there are many types of antennas, each with their own qualities and characteristics. A deeper dive into the metrics of these antennas can help illuminate the various factors that determine a radar's performance capabilities.

4.2.7.1 Directivity

Directivity is a measure of how effectively an antenna can focus its radiation in a specific direction. High directivity means that the antenna has a more concentrated radiation pattern, while low directivity means that the radiation pattern is more diffuse. The hypothetical *isotropic antenna*, which radiates equally in all directions, has the lowest possible directivity of 1. If fact, directivity is often expressed in relation to the isotropic antenna and is quantified in units of dB(isotropic), or "dBi," which enables the comparison of an antenna's radiation pattern to that of an isotropic antenna.

4.2.7.2 Radiation Pattern and Sidelobe Control

An antenna's *radiation pattern* consists of *main lobes* and *sidelobes*. The main lobe is the primary lobe, where maximum radiated power occurs. The sidelobes are lower in power and typically unwanted byproducts of generating the main lobe. An illustration of an antenna radiation pattern is shown in Figure 4.5. Sidelobe suppression is important because unwanted scatterers in the direction of the sidelobes can reflect the transmitted waveform back to the radar, which increases radar interference.

4.2.7.3 Antenna Power Gain Equation and Effective Aperture

The *antenna power gain* (G) is the ratio of the peak radiation intensity of an antenna to the radiation intensity of an isotropic antenna that has equal input power. Typically,

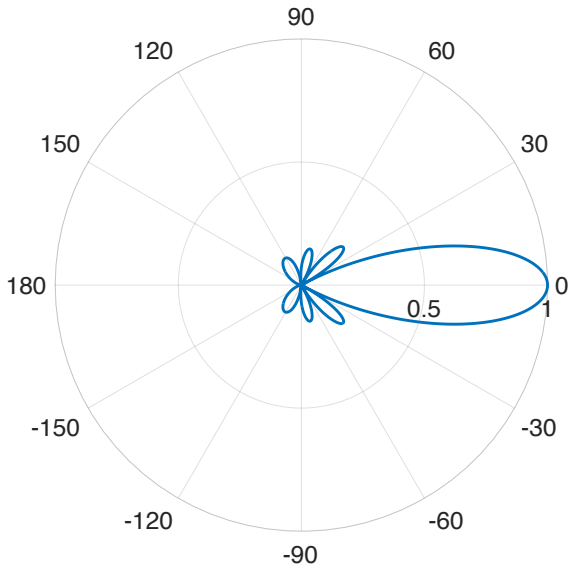

Figure 4.5: Antenna radiation pattern plotted on a polar coordinate system. There is one prominent main lobe located at 0° and several sidelobes at various other angles.

G can be loosely approximated using the following equation:

$$G \approx \frac{26,000}{\theta_3 \phi_3} \text{ [}\theta_3\text{, }\phi_3 \text{ degrees]} = \frac{7.92}{\theta_3 \phi_3} \text{ [}\theta_3\text{, }\phi_3 \text{ radians]}. \tag{4.10}$$

A typical antenna power gain value ranges from 10 dB (broad fan-beam) to 40 dB (narrow pencil beam) [2].

The *effective aperture* (Ae) of an antenna is a fictional area that is required to receive an incident wave's power density, resulting in the same power actually captured by the receive antenna. As such, it can be represented as follows:

$$Ae = \frac{P}{W} \text{ [m}^2\text{]}, \tag{4.11}$$

where P is the power received and W is the power density [2].

The effective aperture is related to the power gain through the following equation:

$$G = \frac{4\pi}{\lambda^2} \cdot Ae, \tag{4.12}$$

where λ is the wavelength [2].

4.2.8 The Radar Range Equation

The *radar range equation* provides the expected received return echo power based on information about the radar system and the target. The equation for instantaneous received power is presented below:

$$P_r = \frac{P_t G_t G_r \lambda^2 \sigma}{(4\pi)^3 R^4 L_s L_a} \text{ [W]}, \tag{4.13}$$

where P_t is the instantaneous transmit power, G_t is the transmit gain, G_r is the receive gain, σ is the RCS, L_s is system losses, and L_a is atmospheric losses. Notice how P_r is directly proportional to P_t, indicating improved target detection with increased transmit power.

4.2.9 The Transmitted and Received Signals

A transmitted pulsed signal can be represented in the following form,

$$x(t) = \sqrt{2}\, a(t) \cos[2\pi F_0 t + \theta(t)], \tag{4.14}$$

where $a(t)$ is the pulse envelope, F_0 is the carrier frequency, and $\theta(t)$ is the phase modulation term. The envelope, $a(t)$, is typically constant modulus (on-off pulsing) to maximize energy, such that $a(t) = A \ \forall \ t \in [0 \quad T_p]$. The average power of the

transmitted signal is shown in the following derivation [2]:

$$P_{\text{av}} = \lim_{T\to\infty} \frac{1}{T} \int_{-T/2}^{T/2} |x(t)|^2 \, dt, \tag{4.15}$$

$$P_{\text{av}} = \lim_{T\to\infty} \frac{1}{T} \int_{-T/2}^{T/2} 2a^2(t) \cos^2[2\pi F_0 t + \theta(t)] dt. \tag{4.16}$$

The identity $\cos^2(\alpha) = \frac{1+\cos(2\alpha)}{2}$ is used to replace $\cos^2[2\pi F_0 t + \theta(t)]$ in the previous equation (4.16).

$$P_{\text{av}} = \lim_{T\to\infty} \frac{1}{T} \int_{-T/2}^{T/2} 2 \left(\frac{a^2(t)}{2} + \frac{a^2(t)}{2} \cos[4\pi F_0 t + 2\theta(t)] \right) dt \tag{4.17}$$

$$P_{\text{av}} = \lim_{T\to\infty} \frac{1}{T} \int_{-T/2}^{T/2} a^2(t) dt + \lim_{T\to\infty} \frac{1}{T} \int_{-T/2}^{T/2} a^2(t) \cos[4\pi F_0 t + 2\theta(t)] dt \tag{4.18}$$

Since $a(t)$ is typically constant amplitude A, Eq. 4.18 becomes,

$$P_{\text{av}} = \lim_{T\to\infty} \frac{1}{T} \int_{-T/2}^{T/2} A^2 dt + \lim_{T\to\infty} \frac{1}{T} \int_{-T/2}^{T/2} A^2 \cos[4\pi F_0 t + 2\theta(t)] dt. \tag{4.19}$$

The term $\lim_{T\to\infty} \frac{1}{T} \int_{-T/2}^{T/2} A^2 dt$ becomes A^2 and the term $\lim_{T\to\infty} \frac{1}{T} \int_{-T/2}^{T/2} A^2$ $\cos[4\pi F_0 t + 2\theta(t)] dt$ goes to zero since the cosine function is even and the integral is across one period. Thus,

$$P_{\text{av}} = A^2. \tag{4.20}$$

The received radar return signal from a scatterer located at a range of $\frac{ct_0}{2}$ is given by the equation,

$$y(t) = \sqrt{2}\, \hat{a}(t - t_0) e^{j[(2\pi F_0 (t-t_0) + \theta(t-t_0) + \phi(t)]} + n(t). \tag{4.21}$$

The $\hat{a}$ term represents the scaled amplitude of returned pulses after propagation attenu-

ation, the t_0 time delay comes from the two-way travel of the radar pulse, $\phi(t)$ denotes the phase modulation from the target interaction, like Doppler shift, for example, and $n(t)$ is the noise term [2].

4.2.10 Complex Representations of the Transmitted and Received Waveforms

A signal can be viewed from two perspectives: *passband* and *complex baseband* (or *complex envelope*). The passband representation of a signal is real-valued and modulated on a carrier frequency, suitable for transmission over a physical medium such as air. The passband representation of the transmitted and received radar waveforms is shown in Equations 4.14 and 4.21, respectively. However, the *complex baseband* representation removes the carrier frequency from the waveform with a coherent receiver, leaving only the essential information. It is useful for mathematical analysis and signal processing purposes, such as filtering and equalization. Since they are complex-valued and centered around zero frequency, they cannot be transmitted over the air.

The complex baseband representation of a transmitted radar waveform $\tilde{x}(t)$ shown in Equation 4.14 is illustrated in the following form:

$$\tilde{x}(t) = a(t)e^{j\theta(t)}. \tag{4.22}$$

The transmitted waveform $x(t)$ can be written in terms of this complex envelope as follows:

$$x(t) = \sqrt{2}\,\Re\big\{x_c(t)e^{j2\pi F_0 t}\big\}, \tag{4.23}$$

where $\Re\{\bullet\}$ denotes the real part of the complex expression.

Similarly, the complex baseband representation of the received radar waveform $\tilde{y}(t)$

shown in Equation 4.21 can be seen in the following form:

$$\tilde{y}(t) = \hat{a}(t - t_0)e^{j[\theta(t-t_0)+\phi(t)]}, \tag{4.24}$$

The received waveform $y(t)$ can now be represented in terms of this complex envelope as follows:

$$y(t) = \sqrt{2}\,\Re\{y_c(t)e^{j2\pi F_0 t}\} + n(t). \tag{4.25}$$

Note that the factor of $\sqrt{2}$ found in the passband equations (Eq. 4.14 and Eq. 4.21) is used to ensure that the power is consistent between the passband and complex baseband representations.

4.2.11 Pulse Compression Waveforms

By manipulating the phase or frequency of the waveform against time using the $\phi(t)$ term in the complex baseband waveform equation (Eq. 4.22), one can decouple range resolution from bandwidth in Equation 4.5. This alters Equation 4.5 to the following form:

$$T_p > \frac{1}{\beta}, \tag{4.26}$$

making the time-bandwidth product, or the *pulse compression gain*, $T_p\beta$, greater than unity. This manipulation can occur within the scope of an individual pulse, called *intra-pulse modulation*, or across multiple pulses, called *interpulse modulation*. The result of this technique is the creation of a *pulse compression waveform*, which is a widely employed technique used in radar signal processing that resolves the range resolution energy tradeoff that was discussed in Section 4.2.6. One of the most prevalent forms of pulse compression waveform is the *linear frequency modulation* (LFM) or "chirp" waveform [2].

LFM works by linearly sweeping the instantaneous frequency of a waveform across a range of frequencies $[\frac{-\beta}{2}, \ \frac{\beta}{2}]$ throughout the pulse duration T_p, as shown in Figure 4.6. This means that the LFM frequency function can be represented in the following form:

$$f_{LFM} = \pm \left(\frac{\beta}{T_p} t - \frac{\beta}{2} \right) \tag{4.27}$$

where the sign indicates whether the chirp is increasing in frequency or decreasing in frequency. The phase function, $\theta(t)$, in Equation 4.22 is determined by integrating the instantaneous frequency as shown in the following equation:

$$\phi(t) = 2\pi \int_0^t f(\zeta) d\zeta + \theta_0, \tag{4.28}$$

where θ_0 is the initial phase. Therefore,

$$\theta_{LFM}(t) = \pm 2\pi \int_0^t \left(\frac{\beta}{T_p} \zeta - \frac{\beta}{2} \right) d\zeta + \theta_0, \tag{4.29}$$

which results in the following LFM phase function expression $\theta_{LFM}(t)$:

$$\theta_{LFM}(t) = \pm \pi \left(\frac{\beta}{T_p} t^2 - \beta t \right) \tag{4.30}$$

Now, the complex baseband waveform equation (Eq. 4.22) can be updated to include the LFM phase function:

$$\tilde{x}_{LFM}(t) = a(t) e^{j\theta_{LFM}(t)}, \tag{4.31}$$

$$\tilde{x}_{LFM}(t) = a(t) e^{\pm j\pi \left(\frac{\beta}{T_p} t^2 - \beta t \right)}, \tag{4.32}$$

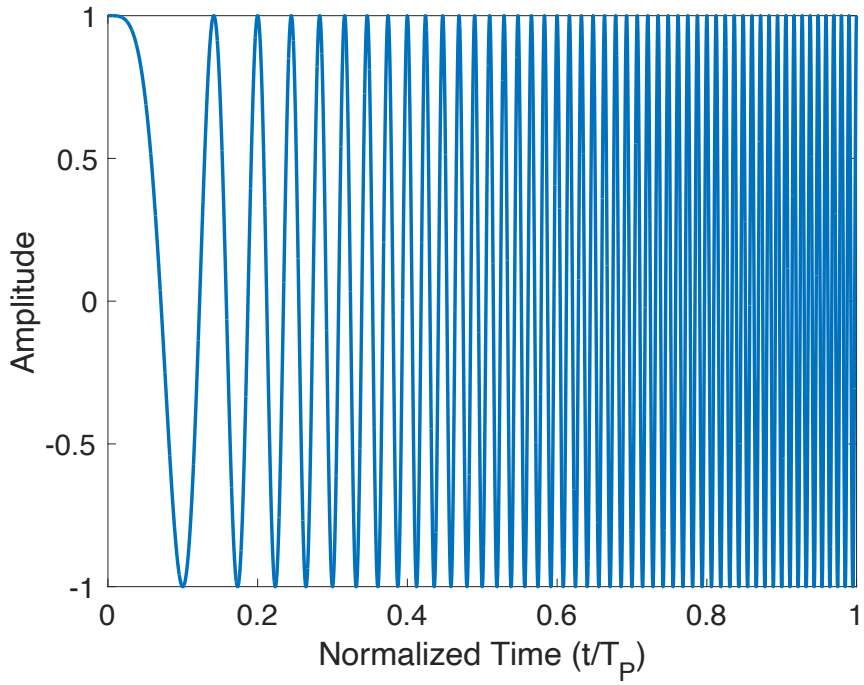

Figure 4.6: Real time-domain LFM waveform with time-bandwidth product of 100 [2]

4.2.12 Matched Filtering

Matched filtering is a powerful technique used in signal processing to maximize the SNR of the received waveform. It is called a matched filter because it "matches" the shape of the transmitted pulse. The technique optimizes the receiver frequency response by taking a cross-correlation of the received waveform with the known transmitted waveform, which maximizes the presence of the signal and minimizes the presence of noise. [2]

When the received waveform is convolved with a matched filter, the output is a waveform with peak locations corresponding to the time delay (or range) between the transmitter and the target. The amplitude of the peak is proportional to the RCS of the target and transmitted power. Different waveforms have different matched filter

characteristics, as will be discussed in Section 4.2.14. The matched filter response is the time-reversed conjugate of the transmitted waveform, so the length of the matched filter is the same length as the transmitted waveform, which is T_P. This implies that the output of the matched filter, resulting from the convolution of two continuous-time signals of length T_P, is $2 \cdot T_P$. Additionally, for pulse-compression waveforms, T_M must be greater than or equal to T_P to satisfy causality [2].

To derive the matched filter result discussed in the previous paragraph, consider the received waveform $y(t)$ expressed in the following form:

$$y(t) = (x(t) + n(t)) * h(t), \tag{4.33}$$

$$y(t) = x(t) * h(t) + n(t) * h(t), \tag{4.34}$$

where $x(t)$ is the radar waveform, $n(t)$ is the corrupting noise signal, and $h(t)$ is the receiver filter response. This can be rewritten as,

$$y(t) = y_s(t) + n_0(t), \tag{4.35}$$

where $y_s(t)$ is the filtered signal response and $n_0(t)$ is the filtered noise response. Thus,

$$Y(f) = \mathfrak{F}\{y(t)\} = Y_s(f) + N_0(f), \tag{4.36}$$

$$Y(f) = X(f)H(f) + N(f)H(f). \tag{4.37}$$

Matched filtering is used to maximize the SNR at time T_M. The power of the signal at time T_M is given by the following equation:

$$|y_s(T_M)|^2 = \left| \frac{1}{2\pi} \int_{-\infty}^{\infty} X(f)H(f)e^{j2\pi f T_M} df \right|^2, \tag{4.38}$$

and the noise power for white noise with power spectral density (PSD) σ_w^2 W/Hz is given by the equation:

$$n_p = \frac{\sigma_w^2}{2\pi} \int_{-\infty}^{\infty} |H(f)|^2 \, df. \tag{4.39}$$

The SNR is therefore given by:

$$\text{SNR} = \frac{|y_s(T_M)|^2}{n_p}, \tag{4.40}$$

$$\text{SNR} = \frac{\left| \int_{-\infty}^{\infty} X(f) H(f) e^{j2\pi f T_M} df \right|^2}{\sigma_w^2 \int_{-\infty}^{\infty} |H(f)|^2 \, df}, \tag{4.41}$$

The Cauchy-Schwarz inequality states that:

$$\left| \int_a^b f(x) g(x) dx \right|^2 \leq \left(\int_a^b |f(x)|^2 \, dx \right) \left(\int_a^b |g(x)|^2 \, dx \right), \tag{4.42}$$

with equality when $g(x) = \alpha f^*(x)$. Thus,

$$\left| \int_{-\infty}^{\infty} X(f) H(f) e^{j2\pi F T_M} df \right|^2 \leq \left(\int_{-\infty}^{\infty} \left| X(f) e^{j2\pi f T_M} \right|^2 df \right) \left(\int_{-\infty}^{\infty} |H(f)|^2 \, df \right), \tag{4.43}$$

$$\text{SNR} \leq \frac{\left(\int_{-\infty}^{\infty} \left| X(f) e^{j2\pi f T_M} \right|^2 df \right) \left(\int_{-\infty}^{\infty} |H(f)|^2 \, df \right)}{\sigma_w^2 \int_{-\infty}^{\infty} |H(f)|^2 \, df}. \tag{4.44}$$

The upper bound is satisfied when,

$$H(f) = \alpha X^*(f) e^{-j2\pi f T_M}. \tag{4.45}$$

Therefore, the impulse response of the matched filter is given by,

$$h(t) = \mathfrak{F}^{-1}\{H(f)\} = \alpha x^*(T_M - t). \tag{4.46}$$

Evaluating Equation 4.41 with 4.45,

$$\text{SNR}_{\text{MF}} = \frac{\left| \int_{-\infty}^{\infty} X(f)\alpha X^*(f) e^{-j2\pi f T_M} e^{2\pi j f T_M} df \right|^2}{\sigma_w^2 \int_{-\infty}^{\infty} \left| \alpha X^*(f) e^{-j2\pi f T_M} \right|^2 df} \tag{4.47}$$

$$\text{SNR}_{\text{MF}} = \frac{\left| \alpha \int_{-\infty}^{\infty} |X(F)|^2 df \right|^2}{\sigma_w^2 \int_{-\infty}^{\infty} |\alpha|^2 \left| X^*(f) e^{-j2\pi f T_M} \right|^2 df} \tag{4.48}$$

$$\text{SNR}_{\text{MF}} = \frac{\left| \int_{-\infty}^{\infty} |X(f)|^2 df \right|^2}{\sigma_w^2 \int_{-\infty}^{\infty} |X^(f)|^2 df} \tag{4.49}$$

$$\text{SNR}_{\text{MF}} = \frac{\int_{-\infty}^{\infty} |X(F)|^2 df}{\sigma_w^2} \tag{4.50}$$

$\int_{-\infty}^{\infty} |X(f)|^2 df$ is the energy of $x(t)$, E, thus,

$$\text{SNR}_{\text{MF}} = \frac{E}{\sigma_w^2}. \tag{4.51}$$

Equation 4.51 shows the maximum attainable SNR. Any additional filtering or processing will reduce the SNR. An important thing to notice is how it only depends on the energy of the transmitted signal, not the modulation type used or other factors [2].

4.2.13 Doppler Mismatch in Matched Filtering

The preceding matched filter derivation assumes that the target is not moving so there is no Doppler shift, as described in Section 4.3.1. If the target velocity is known, the matched filter can be adjusted to account for the Doppler shift, as shown in the following equation:

$$h(t) = \alpha x'^*(-t) = \alpha x^*(-t) e^{+j2\pi F_D t}, \tag{4.52}$$

where $x'(t)$ is the received waveform with Doppler shift F_D, and $T_M = 0$ seconds. Thus, the frequency response is simply:

$$H(f) = \alpha X^*(f - F_D). \tag{4.53}$$

As one can observe from these equations, the matched filter for $x'(t)$ can be acquired by simply shifting the $x(t)$ matched filter in frequency to account for the Doppler shift [2].

If the matched filter is not tuned to the Doppler shift of the target, there will be Doppler mismatch, which can affect the receiver's detection ability. It is useful to define a variable that represents the Doppler mismatch: $F_{\text{diff}} \equiv F_D - F_i$, where F_i is the Doppler shift that the filter is matched to. Generally, small Doppler mismatches of $F_{\text{diff}} \ll \frac{1}{T_p}$ do not have any significant impact on matched filter performance. Large mismatches, on the other hand, can greatly reduce the peak output amplitude [2].

The peak matched filter output $y(0)$, where $T_M = 0$ (for simplicity), is shown in the following equation:

$$|y(0)| = \left| \frac{2\alpha \sin\left(\frac{2\pi F_{\text{diff}} T_p}{2}\right)}{2\pi F_{\text{diff}}} \right|. \tag{4.54}$$

Plotting $|y(0)|$ against F_{diff} yields the graph shown in Figure 4.7. One can clearly observe from Figure 4.7 that the Doppler mismatch curve has a Rayleigh resolution of $\frac{1}{\tau}$.

It is important to note that Doppler mismatch is not always undesirable since it can be advantageous to filter for targets moving at certain velocities.

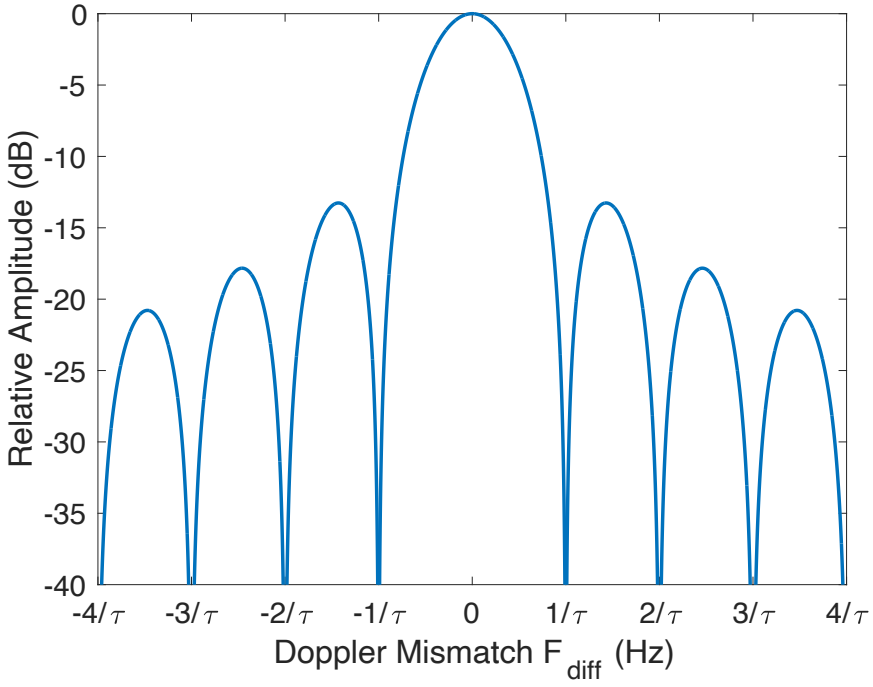

Figure 4.7: Relative peak matched filter output amplitude $|y(0)|$ (dB) vs. Doppler mismatch F_{diff} (Hz) [2]

4.2.14 The Ambiguity Function

The *ambiguity function* is a valuable tool that is used to characterize the performance of a waveform paired with its matched filter. It is a two-dimensional function that provides radar signal processing engineers with valuable insights into a waveform's performance under various Doppler conditions. The *complex ambiguity function* is defined as,

$$\hat{A}(t; F_D) = y(t; F_D) = \int_{-\infty}^{\infty} x(s) e^{j2\pi F_D s} x^*(s-t) ds. \tag{4.55}$$

The $e^{j2\pi F_D s}$ term comes from the Doppler shift of $x(t)$ when reflecting off a moving target, $\alpha = 1$ for unit gain, and T_M is assumed to be zero. The ambiguity function,

$A(y; F_D)$, is thus defined as the magnitude of the complex ambiguity function:

$$A(y; F_D) = |\hat{A}(y; F_D)|. \tag{4.56}$$

The ambiguity function provides key insights when examining a waveform's sidelobe behavior, range and Doppler resolutions, and range and Doppler ambiguities. A *Doppler cut* of an ambiguity function is the matched filter output with a constant frequency displacement from the matched filter and the received waveform caused by a target's Doppler shift. The *zero Doppler cut* is a special case of the ambiguity function that is equal to the autocorrelation of the waveform in question. For instance, two depictions of the ambiguity function of LFM are shown in Figure 4.8. The three-dimensional depiction of the LFM ambiguity function is shown in Figure 4.8a, while two Doppler slices of the ambiguity function are shown in Figure 4.8b. In the case of Figure 4.8b, one can observe a displacement in the range of the peak for the Doppler-shifted return signal, which will cause the receiver to mistake the target as closer than it really is [2].

There are many factors to consider when choosing a waveform. An engineer must consider the application of the radar system to determine the most suitable waveform for the task at hand.

To determine a waveform's range and Doppler resolutions, one can examine its ambiguity function. The range resolution, ΔR, is equivalent to half the width of the main lobe in the range dimension. Similarly, the Doppler resolution, ΔF_D, corresponds to half the width of the main lobe in the Doppler dimension. Recall from Eq. 4.5 that $\Delta R = \frac{c}{2\beta}$, meaning that the main lobe width in the range dimension is $\frac{c}{\beta}$ when there is perfect Doppler match. As Doppler mismatch increases, the main lobe's width can increase significantly, leading to a reduction in the range resolution.

The sidelobes present when analyzing a Doppler cut of a waveform's ambiguity

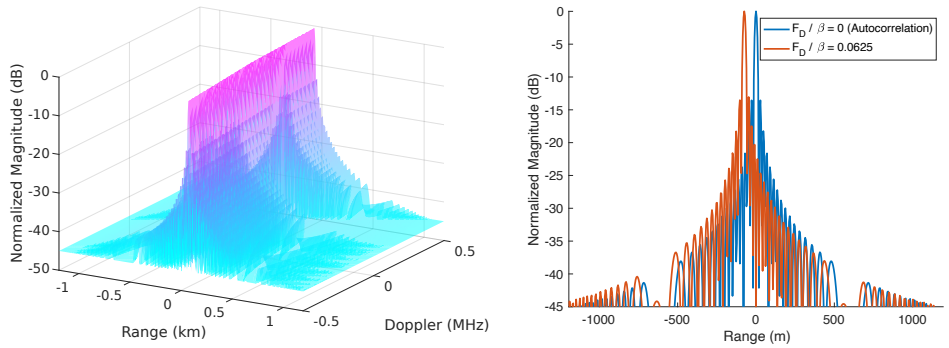

(a) (b)

Figure 4.8: Two depictions of an 8 MHz bandwidth LFM waveform ambiguity function are shown: (a) Three-dimensional ambiguity function, (b) Two Doppler cuts from the ambiguity function: one at zero Doppler (the autocorrelation function) and one at $\frac{F_D}{\beta} = 0.0625$

function can determine a waveform's tendency to mask weaker target reflections with the sidelobes of a stronger target. The peak sidelobe level is a common metric that is used to determine the quality of a waveform. Generally, the lower the sidelobes, the better the waveform. This is an important design consideration, especially for radar systems operating in environments with multiple targets of various RCSs.

Range ambiguities generally show up as multiple peaks in a Doppler cut of an ambiguity function. Some waveforms, such as Frank and Barker 13, which are phase-coded waveforms, generate multiple peaks when confronted with Doppler shifts, while other waveforms, such as LFM, P3, and P4 codes, demonstrate greater resilience against range ambiguities. Thus, if the radar application anticipates target returns from targets moving at non-trivial velocities, the latter waveforms may be more suitable for implementation.

4.2.14.1 Properties of the Ambiguity Function

The ambiguity function possesses three important properties that will be discussed in this section.

1. **Energy Bound Property:** The ambiguity function is bounded by the energy of the transmitted waveform, E, which occurs at location $A(0,0)$. This can be expressed as,

$$|A(t, F_D)| \leq |A(0,0)| = E. \tag{4.57}$$

2. **Conservation of Energy Property:** The total area under the surface of the ambiguity function is equal to the squared energy of the transmitted waveform. This means that when energy is removed from one area of a waveform's ambiguity surface, it must be added to another area of the surface. This can be expressed by the following property:

$$\int_{-\infty}^{\infty}\int_{-\infty}^{\infty} |A(t, F_D)|^2 dt dF_D = E^2. \tag{4.58}$$

3. **Symmetry Property:** The ambiguity function is symmetric across the range-Doppler diagonal according to the following expression:

$$A(t, F_D) = A(-t, -F_D). \tag{4.59}$$

4.3 Pulse-Doppler Processing

Doppler processing techniques play a critical role in many modern target-tracking radar systems. A pulse-Doppler radar utilizes Doppler processing to determine vital velocity information about its target. This is not only useful for target classification

and trajectory tracking but also helps distinguish targets from ground clutter. This section will discuss various aspects of Doppler processing, such as the Doppler effect and range-Doppler maps.

Pulse-Doppler processing populates a matrix of fast-time and slow-time radar data within a *coherent processing interval* (CPI). One CPI contains data from many pulses, allowing the radar to gather Doppler information that would be otherwise imperceptible with modern instrumentation.

4.3.1 The Doppler Effect

As previously introduced in Chapter 2, the Doppler effect is a fundamental phenomenon that allows radars to determine velocity information of moving targets. This enables technologies such as police radar guns, weather radar, and military radar systems. The Doppler effect occurs when the frequency of an RF emission appears shifted due to a relative motion between the signal source and an observer. Generally, radar systems consider a positive relative velocity $(v_r > 0)$ as a target moving away from the radar, and a negative relative velocity $(v_r < 0)$ as a target approaching the radar. The relative velocity can be defined as,

$$v_r = v\cos(\phi), \tag{4.60}$$

where ϕ is the angle between the target's velocity vector and the vector pointing from the target to the radar. It is important to emphasize that a change in range between the radar and the target must occur for the Doppler effect to take place. Consequently, a target moving perpendicularly to an observer will not emit a Doppler-shifted signal, as illustrated in Figure 4.9 [2].

The Doppler frequency shift, F_D, can be calculated by the following formula:

$$F_D = \frac{2v_r}{c - v_r} F_0, \tag{4.61}$$

where F_0 is the center frequency of the transmitted signal.

4.3.2 The Range-Doppler Map

Range-Doppler maps are excellent visualization tools for viewing multiple targets at different ranges and velocities. To create a range-Doppler map, the radar populates a matrix of IQ data from a coherent radar receiver. One axis (typically the vertical axis) corresponds to *fast-time* data, and the other corresponds to *slow-time* data [2].

The fast-time dimension contains individual samples gathered during the radar's observation period for an individual pulse return. A discrete matched filter is performed in this dimension using the known transmitted waveform and peaks appear at the locations of the range bins with targets present. Samples in the fast-time dimension are separated by the sampling time, T_s, which is represented by the following expression as,

$$T_s = \frac{1}{\beta}. \tag{4.62}$$

Samples in fast-time are often referred to as *range bins*, where each range bin corresponds to:

$$\Delta R = \frac{c}{2\beta}, \tag{4.63}$$

which is equivalent to the range resolution defined in Eq. 4.5 [2].

The slow-time dimension, on the other hand, represents samples across consecutive pulses. An FFT across this dimension can obtain the Doppler frequency shift caused by moving targets. This approach allows for more cycles to emerge due to the presence of

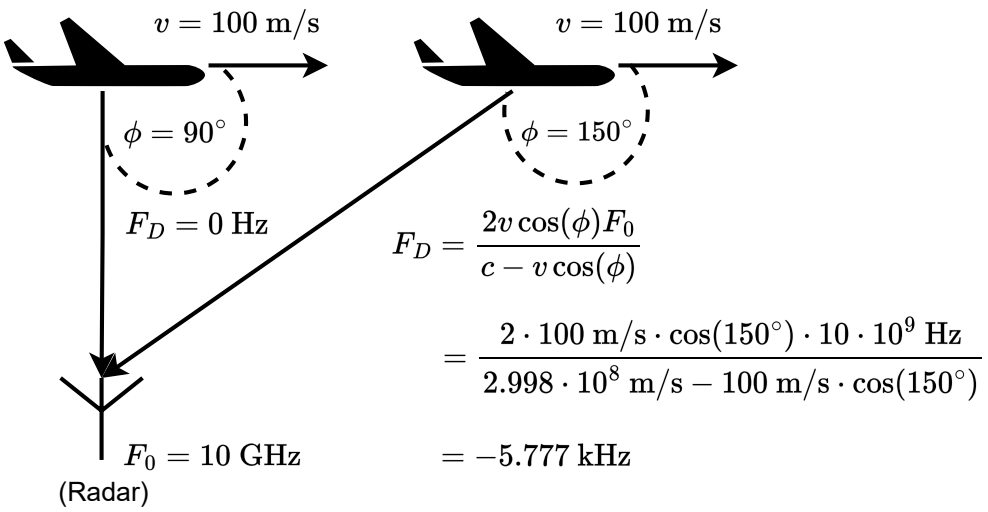

Figure 4.9: Illustration of the Doppler effect showcasing two distinct scenarios: one features a stationary target (relative to the radar) resulting in no Doppler shift, and another features a relative motion between the radar and the target that produces a Doppler shift in the returned signal frequency. Both targets are traveling at the same velocity and can be seen as the same target simply progressing in time.

Doppler frequencies than would be possible in the fast-time dimension, enhancing the accuracy of Doppler frequency shift detection. Alternatively, one could extend a single pulse to the length of an entire CPI, but the range resolution of such pulse would be much higher [2].

As the individual samples in slow time are separated by the PRI, the Doppler axis is limited by $[-\frac{\text{PRF}}{2}\ \frac{\text{PRF}}{2}]$ (Hz). Any frequencies occurring outside of this bound will be aliased, appearing as incorrect Doppler frequency locations.

The formulation of an IQ matrix from radar data is shown in Figure 4.10. After matched-filtering in fast-time and an FFT in slow-time, a range-Doppler map is formed, as shown in Figure 4.11. The *clear region* in slow-time distinguishes the area between the zero-Doppler clutter (for a stationary radar) and the Doppler bounds $[-\frac{\text{PRF}}{2}\ \frac{\text{PRF}}{2}]$ (Hz) which is appropriate for detecting targets [2].

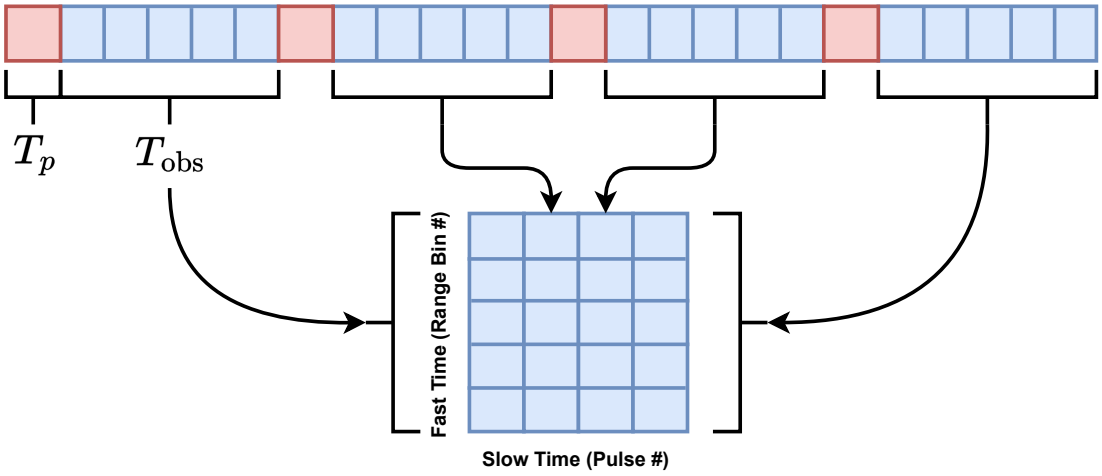

Figure 4.10: Formulation of an IQ matrix of radar data making up one coherent processing interval

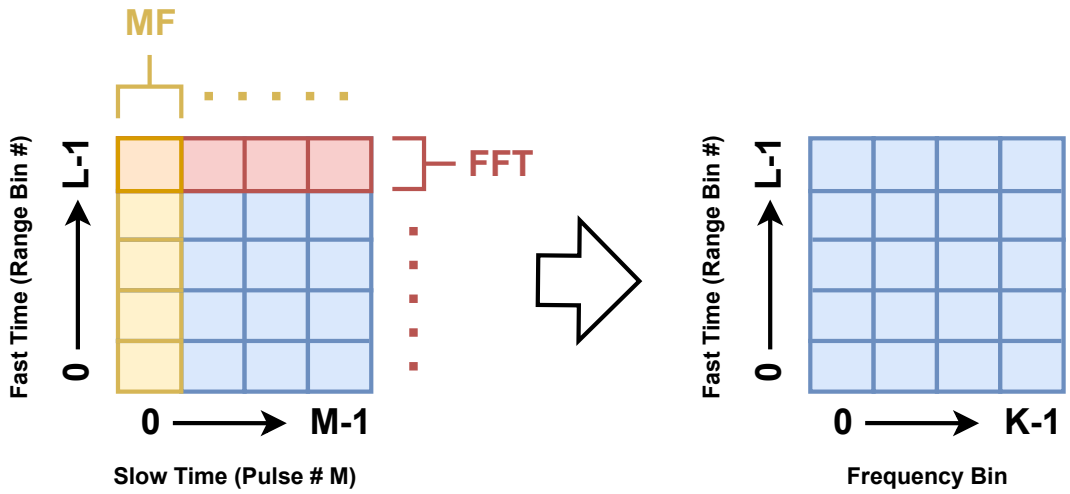

Figure 4.11: Range-Doppler matrix formed from radar IQ data. Note that the number of slow-time samples, M, does not always equal the number of frequency samples, K (often $K > M$). This illustration is a continuation of the IQ matrix shown in Figure 4.10.

Chapter 5

Framing the Problem: Radar Interference of OFDM Waveforms

5.1 Introduction

Modern *internet service providers* (ISPs) and wireless device manufacturers cater to millions of customers, often in densely populated urban areas, with an increasing demand for higher throughput and support for more devices. These companies, as discussed in Chapter 2, lobby for and acquire more and more spectrum resulting in congestion in many bands, like the S-band and the C-band, where signal characteristics are favorable for both radar and communications applications [3, 76]. The CBRS band from 3550 MHz to 3700 MHz and the 5 GHz bands used for Wi-Fi 6 and U-NII devices, as discussed previously, are a few such examples. Legacy users of these bands are naval radar systems and Terminal Doppler Weather Radar (TDWR), respectively, posing complications for radar interference of communication waveforms, like the seemingly ubiquitous OFDM. According to [3], however, "the intermittent nature and wide bandwidth make interfering OFDM waveforms difficult to eliminate at the radar receiver."

The current approaches to this problem look at filtering off as much interfering radiation as possible [3], or dynamically changing operating frequencies to a channel that is not being interfered with. However, a novel *Reconstruction and Elimination of Co-*

channel OFDM Interference Leakage (RECOIL) algorithm can be used to reconstruct the interfering waveform from the demodulated bits and subtract it from the radar receiver after reapplying the multipath channel and scaling the power appropriately. The RECOIL technique leverages the idea that OFDM waveforms contain data that can be retrieved to a certain degree of noise and channel distortion. This simulation results of this technique can inform new regulatory transmission guidelines, enabling more RF usage in the same fixed band of frequencies.

5.2 How the RECOIL Algorithm Works

Communications interference at a radar receiver can be represented as,

$$y(t) = a \cdot r(t) + n_r(t) + b \cdot c(t) + n_c(t), \tag{5.1}$$

where $r(t)$ is the received radar waveform, $n_r(t)$ is the noise experienced by the received radar waveform, $c(t)$ is the received communications waveform, $n_c(t)$ is the noise experienced by the received communication waveform, and a and b are the scaling factors of the radar and communications waveforms. The RECOIL algorithm serves to remove the $b \cdot c(t)$ term from the radar receiver, $y(t)$.

The RECOIL algorithm works by first demodulating the OFDM symbol using the same OFDM system parameters that the interfering waveform was created with. These system parameters are the number of subcarriers, the subcarrier spacing, the cyclic prefix length, the constellation type, the modulation order, and the center frequency. Timing synchronization and multipath channel estimation are also critical for the performance of OFDM demodulation. These parameters could be difficult to obtain since the nature of stray interfering OFDM symbols could imply a lack of coordination be-

tween the two systems.

After demodulation, the interfering OFDM waveform is remodulated using the same parameters that it was demodulated with. This sequential demodulation then remodulation process is known as *demod-remod*. This effectively yields the $c(t)$ term by itself, assuming there are no bit errors. In practice, bit error rates in excess of 20% can still greatly reduce interference power using the RECOIL algorithm. The scaling term, b, must then be estimated to yield the final $b \cdot c(t)$ term. Estimating b to infinite precision is impractical, however, so a scaling mismatch term is included in the MATLAB simulations, which leaves residual interference depending on its value. The final estimated term is represented as $\hat{b} \cdot \hat{c}(t)$, where $\hat{b}$ is the estimated scaling term and $\hat{c}(t)$ is the estimated interfering OFDM waveform.

Finally, the reconstructed OFDM interference term, $\hat{b} \cdot \hat{c}(t)$, is subtracted from the radar receiver at the same time instance that it occurred. Assuming that $\hat{c}(t) = c(t)$, this yields:

$$y(t) = a \cdot r(t) + n_r(t) + [b - \hat{b}] \cdot c(t) + n_c(t). \tag{5.2}$$

As the $\hat{b}$ term approaches b, the overall $[b - \hat{b}] \cdot c(t)$ term approaches zero, thereby eliminating the OFDM interference term and leaving,

$$y(t) = a \cdot r(t) + n_r(t) + n_c(t). \tag{5.3}$$

5.3 Contributing Factors

When attempting the real-world application of this technique, it is important to consider the context in which it will be deployed. Many application-specific simplifications and other complexities arise from the nature of the problem and should be considered before attempting any real-world application of this interference mitigation technique.

Many of these impeding factors stem from the assumed lack of coordination between the in-band radar and the rogue OFDM interferer. Other simplifications can be made because the radar does not actually need the demodulated bits other than use them to reconstruct the interfering waveform.

5.3.1 Problem-Driven Simplifications

Since the radar does not rely on the transmitted data, error correction techniques (such as decoding and interleaving) can be ignored. While knowledge of error correction techniques can improve performance, they are not necessary for the operation of this algorithm. Additionally, newer wireless standards, such as Wi-Fi 6, LTE, and 5G NR, use OFDMA to allocate different subcarriers of an OFDM symbol to different users. Since OFDMA involves subcarrier allocation, it can be treated like OFDM for the purpose of removing radar interference.

An important aspect of this technique is that it remains effective even when the received OFDM waveforms experience significant noise, interference, and channel distortion. In a traditional communications system, these corruptions of the transmitted waveform can significantly impact a system's usefulness depending on its throughput requirements. A communication system's channel capacity is given by the equation,

$$C = \beta \log_2 \left(1 + 10^{\frac{\mathrm{SNR_{dB}}}{10}}\right) \tag{5.4}$$

where C is the channel capacity in bits per second (bps), and β is the bandwidth in Hertz. By plotting the channel capacity against the SNR, one can observe significant throughput degradation from a high to low SNR, as shown in Figure 5.1. For instance, there is a 2.88x reduction in channel capacity from 30 dB to 10 dB, which, for the purposes of wireless communications, could mean the difference between high-speed

video streaming and barely being able to send an email. With the RECOIL algorithm, a 10 dB SNR can completely remove interference in some cases (depending on system factors). Therefore, the radar receiver does not have to receive OFDM symbols in the same way that communications receivers do. Generally, as long as the cumulative Euclidean distance of each constellation point is improved with respect to its true value, the performance of this interference mitigation algorithm will show improvement.

5.3.2 Complications

5.3.2.1 The Impact of Lost Samples

The first complication with this technique is that the radar receiver is turned off while the radar is transmitting. Depending on the pulse duration of the radar waveform and the timing of the transmission, significant portions of the communications signal can be lost.

To analyze the impact of lost samples on received constellations, an OFDM communication system simulation was created. The simulation assumed a radar pulse duration of 1 µs and an OFDM symbol duration of 12.8 µs (or 14.4 µs with a cyclic prefix) in accordance with IEEE 802.11ax specifications [68]. This means that $\frac{1}{14.4} \approx 6.94\%$ of the samples were lost (the duty cycle of the pulsed radar), or 80 consecutive samples for an FFT size of 1024 plus a CP size of 128. By zeroing out a specific number of received samples, the simulation varied the start position of the length of lost bits to determine the impact on the system's bit error rate (BER).

The BER results, illustrated in Figure 5.2, show that there is little difference in performance regardless of where the lost samples occur, as long as they occur after the cyclic prefix. Additionally, simulations with an FFT size of 256 produced a very similar BER but with higher variance, indicating that the FFT size does not greatly

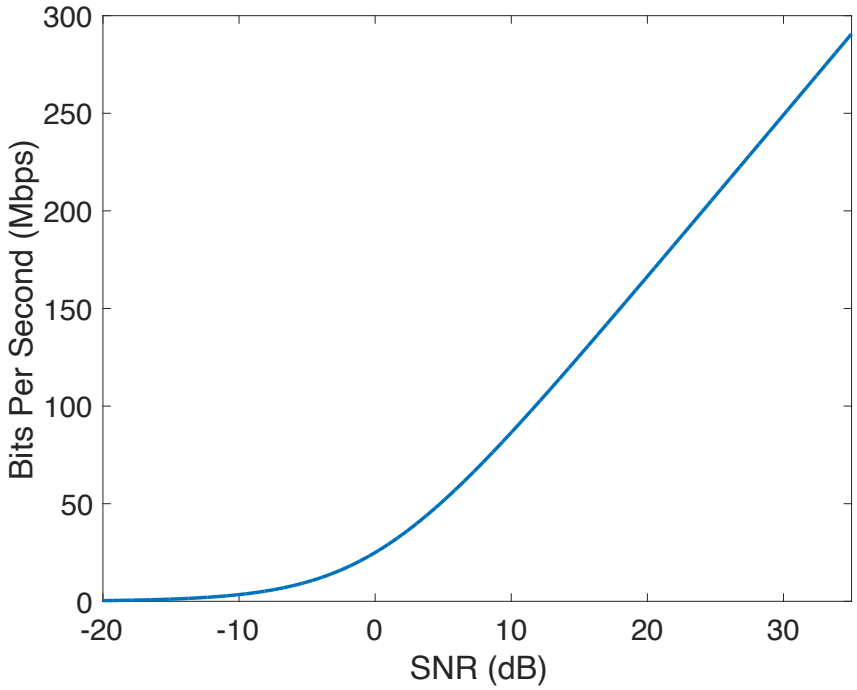

Figure 5.1: Channel capacity vs. SNR in dB plot for a 25 MHz channel

affect performance. The main contributing factor is the ratio of lost samples to FFT size (or the relative time duration of the radar pulse to the OFDM symbol). If multipath were taken into account, lost samples from the cyclic prefix would likely still have less impact on system performance due to the weakened nature of delayed reflections relative to the direct path. The constellation points depicted in Figure 5.3 are centered around their true values, similar to what might be expected in a channel with high additive white Gaussian noise (AWGN). The distribution of interference appears to be consistent across all subcarriers.

5.3.2.2 Unknown OFDM Parameters of the Interfering Waveform

Performing interference subtraction is complicated by not knowing the OFDM parameters of the interfering waveform, such as the number of subcarriers, cyclic prefix

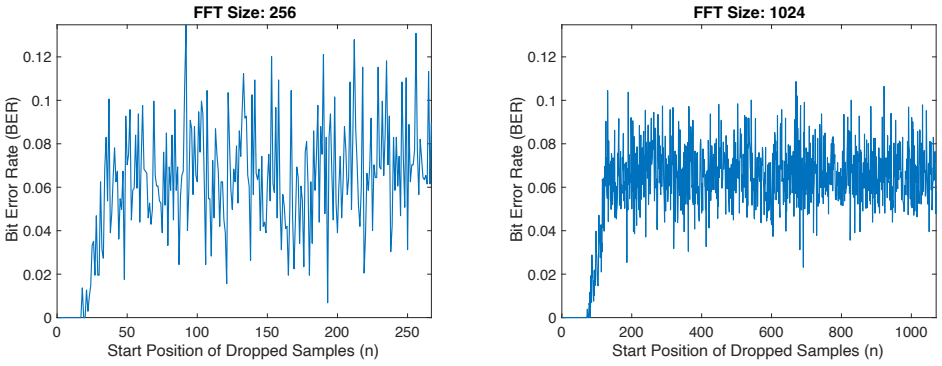

(a) (b)

Figure 5.2: Simulated BER of two OFDM systems plotted as a function of start position, n: (a) FFT size of 256 with CP length of 32 and 20 consecutive lost samples, and (b) FFT size of 1024 with CP length of 128 and 80 consecutive dropped samples

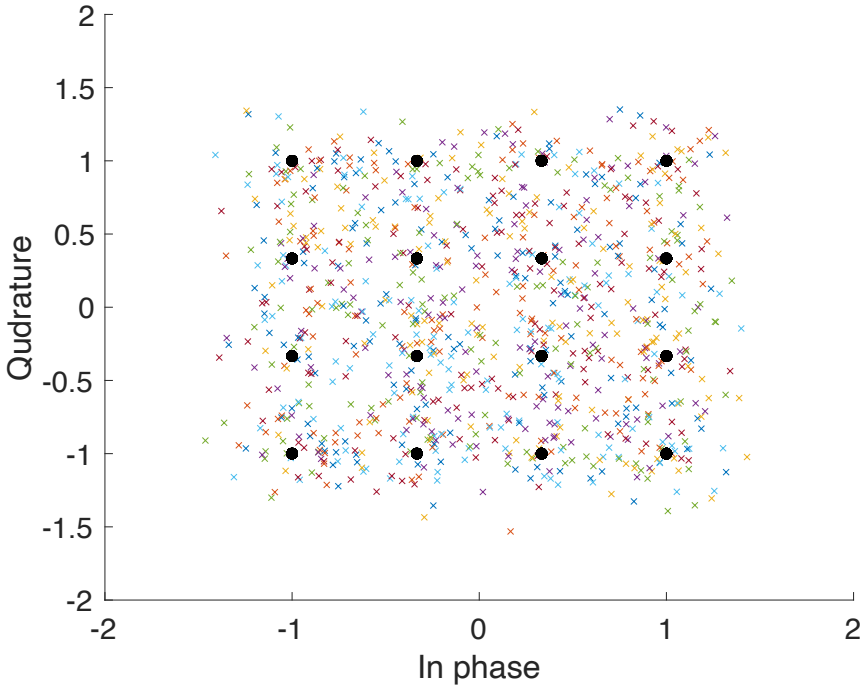

Figure 5.3: Received 16-QAM constellation of OFDM system with an FFT size of 1024, a CP length of 128, and 80 consecutive lost samples

length, subcarrier spacing, constellation type/modulation order, exact carrier frequency of the modulated waveform, and so on. Additionally, estimating the channel effects, signal power, and timing synchronization is crucial for the receiver to properly equalize and demodulate the waveform. These parameters and variables are likely unknown to the receiver when there is limited context of the interfering waveform. Furthermore, estimating these parameters by processing isolated OFDM signals requires sophisticated statistical methods and digital signal processing techniques that may introduce inaccuracy and error.

Take, for instance, the problem of blind constellation estimation. Traditionally, a communication system's transmitter and receiver agree on a signal constellation that maps complex baseband frequency domain IQ data to comprehensive sets of bits. These constellations come in many forms, but the most common ones are M-PSK (Phase Shift Keying) and M-QAM (Quadrature Amplitude Modulation) (Figure 5.4), where M is the modulation order, or the number of constellation symbols per constellation. Since there are two values for a bit (zero and one), a constellation's modulation order is $M = 2^b$, where b is the number of bits per constellation symbol. However, in the case of interfering OFDM symbols, the modulation order and the type of constellation could be unknown, creating a challenge in demodulating OFDM symbols.

One approach to this problem is to examine received constellation point groupings to reconstruct the constellation of the transmitted data. Unlike the K-means algorithm, which requires a priori knowledge of the number of groups present in the data points, the density-based spatial clustering of applications with noise (DBSCAN) algorithm can find groups without any such knowledge. This is important since the modulation order could be unknown to the receiver. By averaging each dimension of the returned group of points, one can form a symbol book estimate of the constellation of the transmitted signals. The receiver can then use this symbol book estimate in a traditional

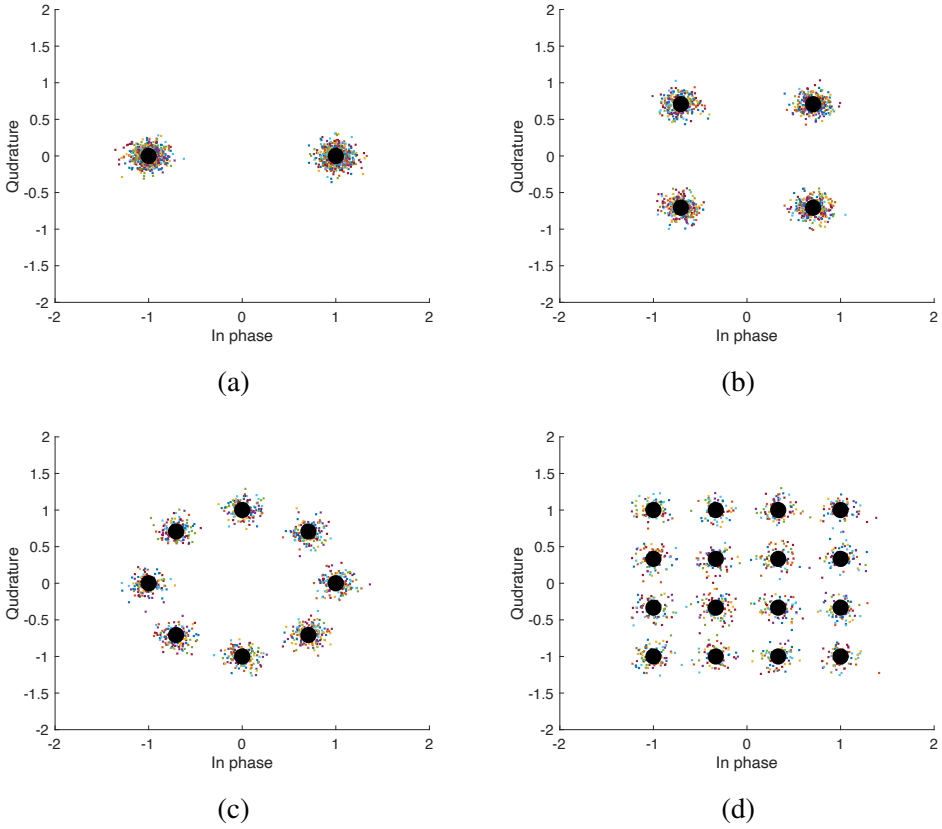

Figure 5.4: Various basic constellation types with noise: (a) BPSK, (b) QPSK, (c) 8-PSK, (d) 16-QAM

fashion to demod-remod the received interfering OFDM symbol for the RECOIL algorithm. One should note that the ordering of the symbol book estimate does not matter in the context of the RECOIL technique because all that demod-remod is doing is snapping the received constellation points to their nearest symbol book point. This process is what takes advantage of the known structure of OFDM to generate a higher resolution version of the received interfering OFDM symbol.

The $dbscan$ MATLAB function takes three inputs: the data points to be grouped, an $epsilon$ value that specifies the neighborhood search radius of each point, and a $minPts$ value that sets a threshold on the number of other data points that must be found within the data point in question in order for it to return a cluster. The algorithm iterates through all of the input data points to determine if they meet the requirements of a cluster. When a new data point is found to meet this criterion, all neighboring data points are grouped in the same cluster and tested for the same criteria. If the neighboring data points are contained within the same cluster as the initial "core point," then the points within the newly tested point's neighborhood that are not included in that core point's neighborhood are added to the cluster. This process repeats for all of the points in the cluster. Any initially tested point that does not meet the grouping criterion is deemed a "noise point" and is not grouped in a cluster. The algorithm is complete when all of the points in the data set are either sorted into clusters or labeled as a noise point. MATLAB sorts all of the tested data points into their respective clusters, which are then used for calculating a symbol book estimate [77].

A MATLAB simulation was built to analyze the performance of the DBSCAN algorithm for constellation reconstruction in various simulated environments. The first simulated transmission is a 64-subcarrier OFDM system with a 16-QAM modulation scheme. The number of transmitted OFDM symbols is 500 pulses with a 20 dB signal-to-noise ratio. The received constellation is shown in Figure 5.5a. One can quite clearly

see 16 distinct groupings of constellation symbols arranged in a 4x4 grid, indicating a 16-QAM constellation. The DBSCAN algorithm is performed with an $epsilon$ value of 0.2 and a $minPts$ value of $(N_{symb})(N_{\mathrm{FFT}})\left(\frac{1}{50}\right) = 640$ where N_{symb} is the number of transmitted symbols and N_{FFT} is the number of subcarriers. The DBSCAN algorithm indeed returns 16 clusters. The new symbol book obtained from averaging both dimensions in each cluster is shown in Table 5.1. The BER for both symbol books is 0 in both cases and the DBSCAN algorithm results and overlaid exact constellation symbol locations are shown in Figure 5.5b.

The second simulated transmission has a decreased SNR of 10 dB. As one can observe from Figure 5.6a, the constellation groupings are still visually present, but their presence is somewhat less distinct than in the 20 dB case. The $epsilon$ and $minPts$ values were kept the same at 0.2 and 640, respectively, and the DBSCAN algorithm again returned 16 distinct constellation points for the symbol book estimate. The symbol book and estimated symbol book values are shown in Table 5.2. The BER was about 5.64% with the real symbol book and about 5.70% with the estimated symbol book. This result indicates minimal RECOIL performance degradation for medium to high SNR environments with unknown constellations. The DBSCAN results and overlaid exact constellation symbols are shown in Figure 5.6b.

A third transmission at a 5 dB SNR suggests a steep performance drop-off in the DBSCAN algorithm in high-noise environments for constellation reconstruction. Visually, one can still make out a vague square outline in the received constellation, indicating an M-QAM constellation. However, the individual constellation point groupings are no longer distinctly present, as seen in Figure 5.7a. The $epsilon$ and $minPts$ values were kept the same at 0.2 and 640, respectively, but the DBSCAN algorithm only found one symbol grouping, which can not be used to form a symbol book estimate. The $epsilon$ and $minPts$ values were also experimentally varied, but no combination

Symbol Book	Symbol Book Estimate	Euclidean Error
-1-1i	-0.999-0.9982i	0.002
-1-0.3333i	-1-0.3332i	0.0001
-1+0.3333i	-0.9983+0.3296i	0.0041
-1+1i	-0.9998+0.9998i	0.0003
-0.3333-1i	-0.3328-1.0004i	0.0007
-0.3333-0.3333i	-0.3337-0.3329i	0.0006
-0.3333+0.3333i	-0.3341+0.3328i	0.0009
-0.3333+1i	-0.3343+0.9991i	0.0013
0.3333-1i	0.3338-1.0019i	0.002
0.3333-0.3333i	0.3336-0.3351i	0.0018
0.3333+0.3333i	0.3328+0.3311i	0.0023
0.3333+1i	0.3323+0.9998i	0.001
1-1i	0.9993-1.0012i	0.0014
1-0.3333i	1.0006-0.3328i	0.0008
1+0.3333i	1.0009+0.3332i	0.0009
1+1i	0.9991+1.0004i	0.001

Table 5.1: Tabulated symbol book and symbol book estimate constellation points for a 64 subcarrier OFDM system with 500 transmitted OFDM symbols on a 16-QAM constellation and an SNR of 20 dB, with error indicated by the euclidean distance between the points

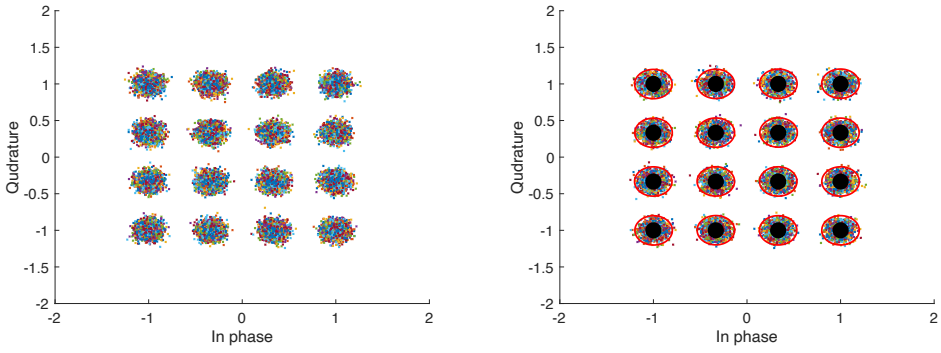

(a) (b)

Figure 5.5: Received constellation for 64 subcarrier system with 500 transmitted symbols on a 16-QAM constellation at a 20 dB SNR. The constellation is depicted in two figures: (a) an unprocessed constellation, (b) overlaid DBSCAN decisions shown as red circles, and exact constellation point locations shown as black dots.

Symbol Book	Symbol Book Estimate	Euclidean Error
-1-1i	-0.9968-1.0066i	0.0074
-1-0.3333i	-0.9985-0.3536i	0.0203
-1+0.3333i	-0.9706+0.3364i	0.0295
-1+1i	-1.0075+0.9955i	0.0088
-0.3333-1i	-0.3177-0.9475i	0.0548
-0.3333-0.3333i	-0.3373-0.2846i	0.0489
-0.3333+0.3333i	-0.3357+0.3384i	0.0056
-0.3333+1i	-0.3352+0.9772i	0.0229
0.3333-1i	0.3563-0.9938i	0.0238
0.3333-0.3333i	0.3256-0.3288i	0.009
0.3333+0.3333i	0.3174+0.3153i	0.0241
0.3333+1i	0.3523+0.9817i	0.0263
1-1i	0.9749-0.9967i	0.0253
1-0.3333i	0.9654-0.3334i	0.0346
1+0.3333i	0.9853+0.3341i	0.0147
1+1i	0.9711+0.9702i	0.0415

Table 5.2: Tabulated symbol book and symbol book estimate constellation points for a 64 subcarrier OFDM system with 500 transmitted OFDM symbols on a 16-QAM constellation and an SNR of 10 dB, with error indicated by the euclidean distance between the points

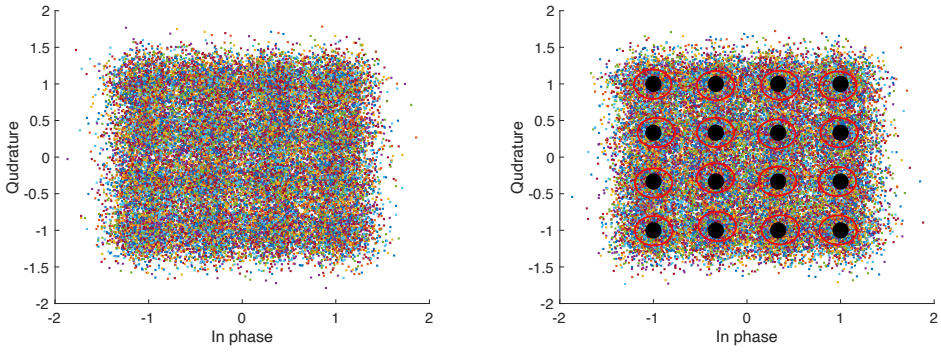

(a) (b)

Figure 5.6: Received constellation for a 64 subcarrier system with 500 transmitted symbols on a 16-QAM constellation at a 10 dB SNR. The constellation is depicted in two figures: (a) an unprocessed constellation, (b) overlaid DBSCAN decisions shown as red circles, and exact constellation point locations shown as black dots.

of values tested resulted in an increase in performance.

Further research in this area has the potential to improve performance. For example, one could potentially leverage the fact that modulation orders are typically represented as powers of 2, such as 2^1, 2^2, 2^3, and so on. Additionally, further research could address a potential limitation of this implementation of the DBSCAN algorithm, which is its failure to account for an adequate number of points, on average, to detect constellation points of constellations with higher modulation orders, such as 64QAM. The use of a $minPts$ threshold value of $(N_{symb})(N_{\mathrm{FFT}})\left(\frac{1}{50}\right) = 640$, where $N_{symb} = 500$ and $N_{\mathrm{FFT}} = 64$, would exceed the average number of points of 500 per 64QAM constellation symbol. In order to account for these modulation orders, the $minPts$ threshold value must be lowered, which could impact the performance of other constellation types. Also, $epsilon$ would need to account for the minimum distance between constellation points of the constellation with the highest supported modulation order.

Other researchers [78] have explored using an adaptive DBSCAN algorithm to optimize constellation reconstruction. It does this by defining a validity index, $S\_Dbw(c)$, which is the sum of two terms: inter-cluster density, $Dens\_bw(c)$, and intra-cluster variance, $Scat(c)$, of the clusters. The $epsilon$ value of the DBSCAN algorithm is iterated over to minimize the validity index. When the validity index reaches its minimum, the clusters are at their peak separation and compactness. The optimal modulation order is then taken as the input value, c. The algorithm was reportedly able to correctly identify QPSK at 0 dB SNR over 90% of the time.

5.3.2.3 The Radar/OFDM Relative Power Dilemma

Another important consideration is the relative OFDM to radar transmission power ratio. The interfering OFDM transmission is affected by the radar transmission in the same way that the radar is affected by the OFDM transmission. When the relative

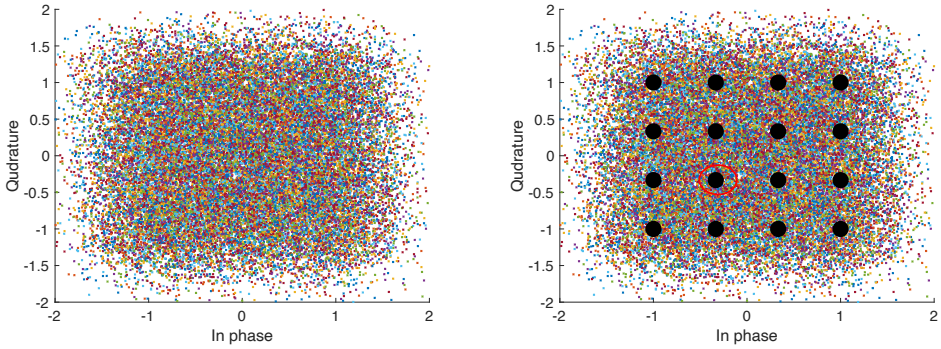

(a) (b)

Figure 5.7: Received constellation for 64 subcarrier system with 500 transmitted symbols on a 16-QAM constellation at a 5 dB SNR. The constellation is depicted in two figures: (a) an unprocessed constellation, (b) overlaid DBSCAN decisions shown as red circles, and exact constellation point locations shown as black dots.

radar transmission power is high compared to the OFDM transmission power, this can dramatically affect the accuracy of OFDM waveform demodulation. This results in a loss in performance of subtracting out interfering OFDM waveforms. To avoid this, radar return power must be limited so that it does not significantly corrupt the OFDM demod-remod process and subsequent subtraction. Interestingly, the radar benefits from receiving high relative OFDM interference because it helps overpower the received radar transmission and AWGN.

Chapter 6

A Breakdown of Key Factors and Performance: Informing New Regulations

6.1 Introduction

Various MATLAB simulations were created to investigate the effects of performing the RECOIL algorithm on IQ data from a monostatic pulse-Doppler radar system in various environments. These simulations work by injecting randomly-generated OFDM symbols into radar IQ data, with waveform spacing controlled by a density factor that regulates the level of OFDM interference present in the received IQ data before interference subtraction. These simulations account for lost samples during radar transmission and scaling mismatch issues arising from estimating the power of an unknown OFDM waveform. In addition, they can test the effects of various factors, such as additive white Gaussian noise (AWGN), FFT size, constellation type/modulation order, and relative OFDM to radar power, among others.

To facilitate analysis, these simulations assume a priori knowledge of the interfering OFDM symbols' constellation type, modulation order, FFT size/number of subcarriers, and subcarrier spacing. Moreover, it should be noted that these simulations do not account for multipath channel effects and assume perfect synchronization between the radar and the OFDM symbols.

6.2 Methodology

This section will explain the process of simulating OFDM interference to a pulse-Doppler radar system and removing the interference with the RECOIL algorithm. There are four distinct elements in the simulation that this section will describe: simulating OFDM interference, demodulating the OFDM waveforms, remodulating the OFDM waveforms, and subtracting the remodulated waveforms from the corrupted radar IQ data.

6.2.1 Simulating OFDM Interference

1. Create radar IQ data matrix using the specified radar configuration and target information described in Section 6.2.5. The dimensions of this matrix are $[\mathrm{N_{samps}}, \mathrm{N_{pulses}}]$, where $\mathrm{N_{samps}}$ is the number of samples per pulse and $\mathrm{N_{pulses}}$ is the number of pulses in the CPI.

2. Create an array of indices where the OFDM symbols start. Space them randomly and uniformly, ensuring they do not intersect. A symbol density factor is used to determine how many interfering OFDM symbols are contained with the CPI. The maximum index value is less than the total number of samples in the CPI, calculated as follows:

$$\mathrm{tot_{samps}} = (\mathrm{N_{lost}} + \mathrm{N_{samps}}) * \mathrm{N_{pulses}} \tag{6.1}$$

where,

$$\mathrm{N_{samps}} = \left\lfloor \frac{2 * \mathrm{r_{swath}}}{c} \cdot \frac{1}{\mathrm{F_s}} \right\rfloor, \tag{6.2}$$

$$\mathrm{r_{swath}} = \frac{c \cdot \mathrm{PRI} \cdot (1 - \mathrm{duty})}{2}, \tag{6.3}$$

and,

$$N_{lost} = \text{round}(1 - T_{obs}) \cdot N_{samps}. \tag{6.4}$$

3. Populate a column matrix of time-domain OFDM symbols by generating several symbols that equal the length of the array of indices, as specified in step 2. Each symbol should have a specified cyclic prefix length of N_{CPE} and a length of N_{FFT}, and should be created from a set of randomly generated bits to ensure ample variability.

4. Make an array of zeros with a length of tot_{samps}, then insert generate OFDM symbols starting at each index value from the array of indices in step 2.

5. Form a matrix of dimensions $[N_{samps} + N_{lost}, N_{pulses}]$ from the resulting array from step 4. Remove the last N_{lost} rows of the matrix corresponding to the lost samples from when the radar is transmitting. The resulting matrix's dimensionality matches the radar IQ data matrix.

6. Add AWGN corresponding to the specified OFDM SNR to the matrix.

7. Add the matrix of OFDM symbols to the radar IQ data. Scale the OFDM power appropriately based on the specified relative OFDM to radar power, adjusting for potential real-world discrepancies in estimated OFDM power using a specified scaling mismatch term. The final resulting matrix represents the received corrupted radar IQ data.

6.2.2 Demodulating the OFDM Waveforms

8. Add N_{lost} rows of zeros corresponding to the lost samples to the corrupted radar IQ data. Transform the matrix into an array.

9. Using the array of indices created in step 2 and a priori knowledge of the OFDM FFT size, extract the time-domain OFDM symbols from the matrix in step 8. Populate a column matrix of these extracted interfering OFDM symbols.

10. If any of the final N_{CPE} elements within the matrix columns of step 9 (considering each column as an OFDM symbol vector) are equal to zero, replace them with the corresponding row element from the same column at index of idx $-$ N_{FFT}. This modification prevents any unwanted protrusions in residual interference curves seen in Section 6.3.5 caused by setting the last N_{CPE} elements of the OFDM symbol to zero when a duplicate of that segment is readily available in the actual cyclic prefix.

11. Demodulate the OFDM symbols to extract the transmitted data bits, taking care to remove the rows of the matrix corresponding to the cyclic prefixes of the OFDM symbols.

6.2.3 Remodulating the OFDM Waveforms

12. Remodulate the OFDM symbols from the extracted data using the same OFDM system parameters as the interfering symbols. This sequential demod-remod process effectively "snaps" the received IQ points to their nearest legitimate constellation point from a symbol book, creating an informed estimate of the transmitted interfering OFDM waveforms.

13. Populate these symbols in the columns of a matrix and take an IFFT to get the complex time-domain interference data.

14. Generate a zero vector of length tot_{samps}, add the OFDM waveforms at the correct indices according to the array of indices from step 2, turn the vector into a matrix

of dimensions $[N_{samps} + N_{lost}, N_{pulses}]$, remove the last N_{lost} rows of the matrix corresponding to the lost samples during radar transmission, and scale the amplitudes to match the transmitted OFDM symbols. This process replicates steps 4, 5, and 7 in the previous section.

6.2.4 Interference Subtraction

15. Subtract the scaled matrix of OFDM symbols from step 14 from the received corrupted radar IQ data from step 7. The result is interference-free (under ideal conditions) radar IQ radar data making up one CPI. Pulse-Doppler processing can now be used for more accurate target detection and a clearer range-Doppler map. The results of the RECOIL algorithm vary depending on various factors of the system. An in-depth analysis of these factors will be performed in Section 6.3.

6.2.5 Radar System Configuration

The configuration of the radar system can influence the outcome of the RECOIL algorithm. Therefore, to ensure consistency, the radar configuration will be held constant throughout the duration of the results and analysis. While slight variations in performance may occur as parameters are adjusted, the analysis aims to provide a comprehensive indication of performance across a broad range of radar systems.

The radar system is modeled as a monostatic pulse-Doppler radar operating at a carrier frequency of 2.5 GHz and a bandwidth of 25 MHz. The waveform utilized is LFM, with a sampling frequency of 50 MHz (oversampling factor of 2). There are 1028 pulses in a CPI with a PRF of 20 kHz. The radar's duty cycle is 0.1. The number of received samples per pulse, calculated from Equations 6.2 and 6.3, equals 2250.

The radar's transmit power is 4 kW, with a noise figure of 8 dB. The antenna gain

is 24 dB, and the system losses are 3 dB. The load resistance is assumed to be 50 Ω.

6.2.6 Target Information

The simulation models three targets located at ranges of 3.6 km, 7 km, and 4 km, with range rates of -300 m/s, 450 m/s, and 200 m/s, respectively. All targets have an RCS of 50 m^2. These targets were selected to demonstrate the interference improvement across a comprehensive view of the range-Doppler map.

6.3 Results and Analysis

This section will focus on analyzing a few key factors and their influence on the performance of the RECOIL algorithm. Notably, these factors include: the OFDM signal-to-noise ratio, the constellation type/modulation order, the FFT size, the relative OFDM to radar power, and the observation period. The chosen performance metrics are interference improvement and normalized residual interference.

Sections 6.3.1, 6.3.2, and 6.3.3 are titled according to the variable that appears in the legends of their accompanying figures.

In this section, *interference improvement* is defined as the ratio of the OFDM interference power present before and after interference subtraction, expressed in dB by taking its 10log10. To obtain the residual interference matrix, the radar IQ data matrix is subtracted from the resulting IQ matrix after interference subtraction. The power of the residual interference matrix used in the interference improvement calculation is determined by averaging the absolute value squared of its elements. *Normalized residual interference* is defined as the residual interference power before and after interference subtraction divided by the max of the residual interference power before interference subtraction for all x-axis quantities. The curves are then expressed in dB by taking their

10log10.

6.3.1 OFDM SNR

The SNR of the interfering OFDM symbols plays a critical role in the performance of the RECOIL algorithm. This metric determines how well the received constellations can be demodulated, consequently impacting the effectiveness of interference subtraction. The SNR contributes to the dispersion observed around the received constellation points, with lower SNR increasing the bit error rate. As such, a decline in SNR can have a severe negative impact on interference subtraction.

The following table establishes three cases that will be analysed in this section:

Parameter	**Case 1**	**Case 2**	**Case 3**
Observation period	100%	99%	97.5%
Scaling mismatch	0%	1%	1%
N_{FFT}	256	256	256
N_{CPE}	32	32	32
Constellation	16QAM	16QAM	16QAM
Symbol Density	$\sim 75\%$	$\sim 75\%$	$\sim 75\%$
OFDM SNR (dB)	–	–	–
Relative OFDM Power (dB)	–	–	–

Table 6.1: Three RECOIL performance simulation cases used to analyze the impact of the SNR of the interfering OFDM symbols

6.3.1.1 Interference Improvement vs. Relative OFDM to Radar Power

Figure 6.1 illustrates the relationship between interference improvement and the relative OFDM to radar average power for Case 1, as specified in Table 6.1. The relative OFDM to radar power determines how much impact the radar signals have on the OFDM demodulation process. The legend of this figure distinguishes between various OFDM signal-to-noise ratios ranging from 0 dB to 25 dB. From this figure, one can

discern that a higher relative OFDM to radar average power results in superior interference improvement since the competing radar signals carry less weight. In instances where both SNR and relative OFDM power are increased, the enhancement in interference improvement can be significant and, in some cases, completely eliminated. This can be seen in the case where the SNR is 25 dB and the relative power exceeds about 20 dB.

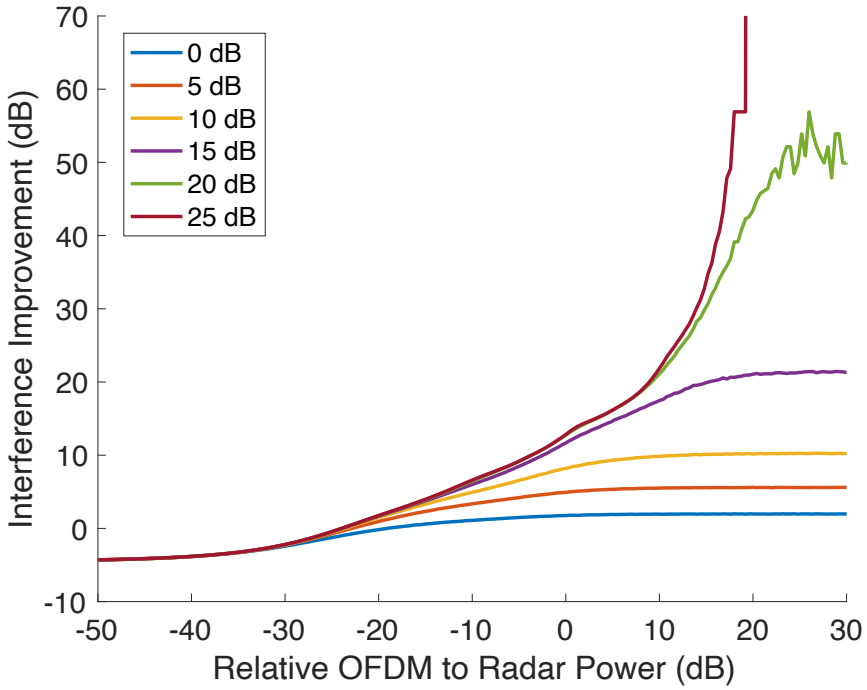

Figure 6.1: Interference Improvement vs. Relative OFDM to Radar Average Power plot for Case 1 in Table 6.1

Case 2, as described in Table 6.1, slightly modifies Case 1 by changing the observation period from 100% to 99% and the scaling mismatch from 0% to 1%. Case 1 does not account for lost samples from radar transmission and scaling mismatch from non-ideal received OFDM waveform scaling. In many ways, Case 1 can be seen as the "ideal case," while Case 2 is a more realistic case. The interference improvement vs.

relative OFDM to radar average power plot for Case 2 is shown in Figure 6.2.

Notice how Figure 6.2 lacks curves that indicate complete interference removal. The interference improvement is now constrained by the lost samples and scaling mismatch. All the curves in this plot plateau at some value of relative OFDM power, indicating little to no further improvement with increased relative OFDM power.

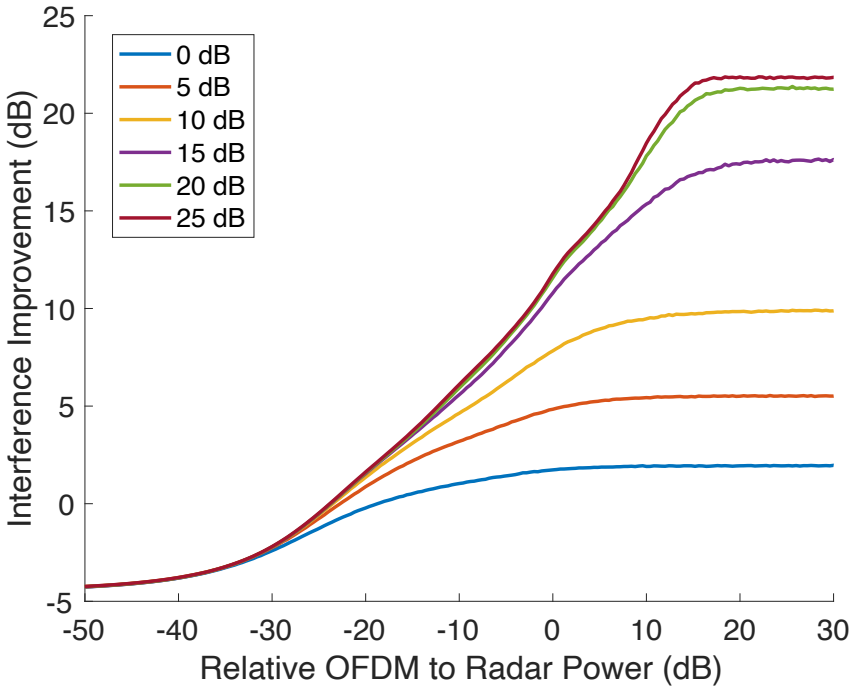

Figure 6.2: Interference Improvement vs. Relative OFDM to Radar Average Power plot for Case 2 in Table 6.1

Finally, consider Case 3, as described in Table 6.1. Case 3 is the same as Case 2 except the observation period is further decreased to 97.5%. Figure 6.3 illustrates the effect of more lost samples, with slightly lower interference improvement plateaus than those in Figure 6.2.

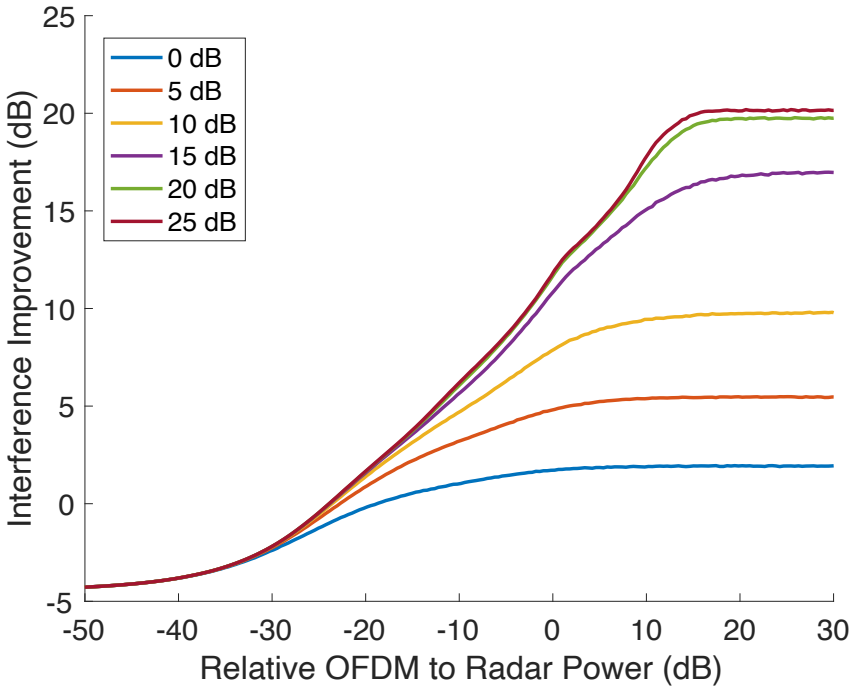

Figure 6.3: Interference Improvement vs. Relative OFDM to Radar Average Power plot for Case 3 in Table 6.1

6.3.1.2 Normalized Residual Interference vs. Relative OFDM to Radar Power

Consider again Case 2 in Table 6.1. Figure 6.4 presents the normalized residual interference after interference subtraction in relation to the relative OFDM to radar power. It is evident in this case that the residual interference increases for all curves, with lower residual interference corresponding to a higher SNR.

Interestingly, there is a relatively flat range of relative OFDM powers between approximately -25 dB and 15 dB (varying based on the SNR) where the residual interference does not increase proportionally to the relative OFDM to radar power. This effect is more noticeable in higher SNR curves and can be attributed to the algorithm's interference improvement counteracting the increased interference from the growing power of the interfering OFDM symbols. In fact, this power range aligns with the upper and

lower plateaus of the interference improvement plot seen in Figure 6.2. When the interference improvements plateau, the residual interference curves become linear. For constellations with lower modulation orders, such as BPSK, the interference improvement can actually overpower a corresponding increase in interfering OFDM power, as seen in Figure 6.8.

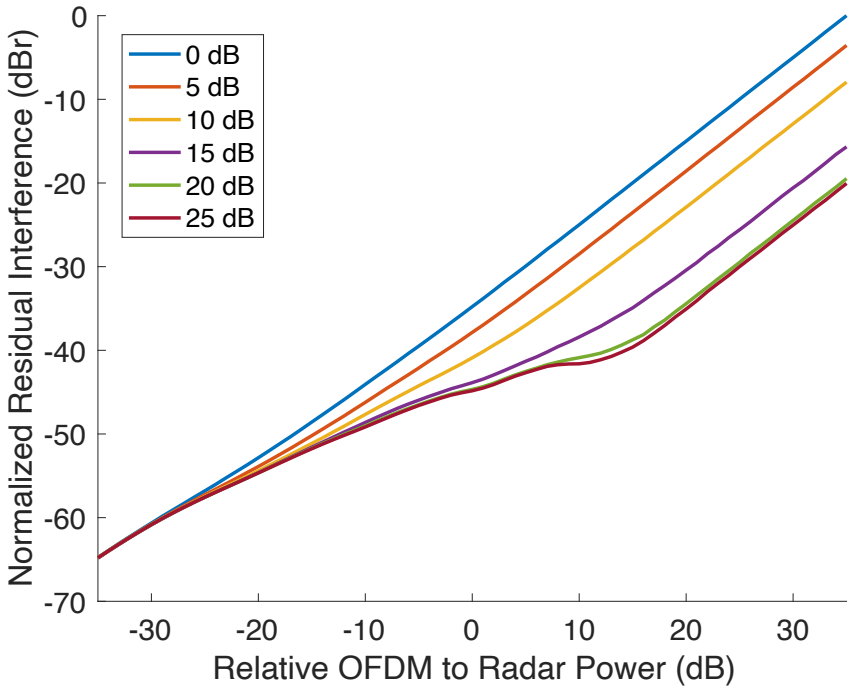

Figure 6.4: Normalized Residual Interference vs. Relative OFDM to Radar Average Power plot for Case 2 in Table 6.1

6.3.2 Constellation Type/Modulation Order

The constellation type and modulation order of interfering OFDM symbols play a crucial role in determining system performance. As the OFDM SNR and the number of lost samples rise, constellations featuring closely-packed symbols exhibit more rapid degradation compared to those with greater spacing between symbols. This oc-

curs because both factors contribute to increased dispersion around each constellation point, as was illustrated in Figures 5.4 and 5.2. This section will analyze five common constellations used in communications systems: BPSK, QPSK, 8PSK, 16QAM, and 64QAM.

The following table establishes three cases that will be referenced in this section:

Parameter	**Case 4**	**Case 5**	**Case 6**	**Case 7**
Observation period	99%	97.5%	95%	–
Scaling mismatch	1%	1%	1%	1%
N_{FFT}	256	256	256	256
N_{CPE}	32	32	32	32
Constellation	–	–	–	16QAM
Symbol Density	$\sim 75\%$	$\sim 75\%$	$\sim 75\%$	$\sim 75\%$
OFDM SNR (dB)	25	25	25	25
Relative OFDM Power (dB)	–	–	–	25

Table 6.2: Three RECOIL performance simulation cases used to analyze the impact of the SNR of the interfering OFDM symbol's constellation type and modulation order

6.3.2.1 Interference Improvement vs. Relative OFDM to Radar Power

Figure 6.5 illustrates the interference improvement in relation to the relative OFDM to radar average power for Case 4 of Table 6.2. Lower modulation order constellations, such as BPSK and QPSK, show significant improvement as OFDM power increases. However, 8PSK, 16QAM, and 64QAM all peak lower in interference improvement due to the combined effects of the 1% scaling mismatch and lost samples from the 99% observation period causing dispersion around each received constellation point. BPSK and QPSK, being more spread out, are less affected by this issue and exhibit more robustness. As scaling mismatch and lost samples increase further, QPSK will begin to deteriorate, followed by BPSK, as will be seen in Figures 6.6 and 6.7 corresponding to Cases 5 and 6.

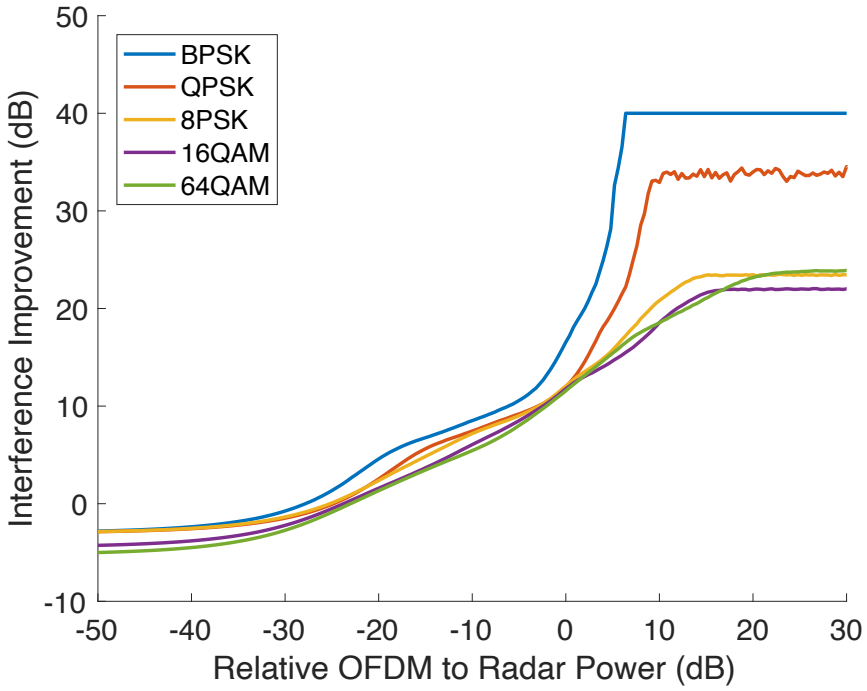

Figure 6.5: Interference Improvement vs. Relative OFDM to Radar Average Power plot for Case 4 in Table 6.2

In Case 5, the observation period is reduced to 97.5% from 99% in Case 4, resulting in an increased number of lost samples per radar pulse. Figure 6.6 shows the interference improvement vs. relative OFDM to radar average power for this scenario. Notice that the QPSK curve now levels off much lower than the BPSK curve, making it akin to the 8PSK, 16QAM, and 64QAM plateaus. This can be attributed to QPSK's denser constellation symbol configuration, which causes more rapid deterioration in the presence of increasing lost samples.

In Case 6, the observation period is reduced from 97.5% to 95%, leading to an even greater increase in the number of lost samples per pulse. Notice that all of the plateaus of the curves shown in Figure 6.7 are now comparable. This is because the dispersion around the constellation symbols caused by the lost samples has intensified to a degree

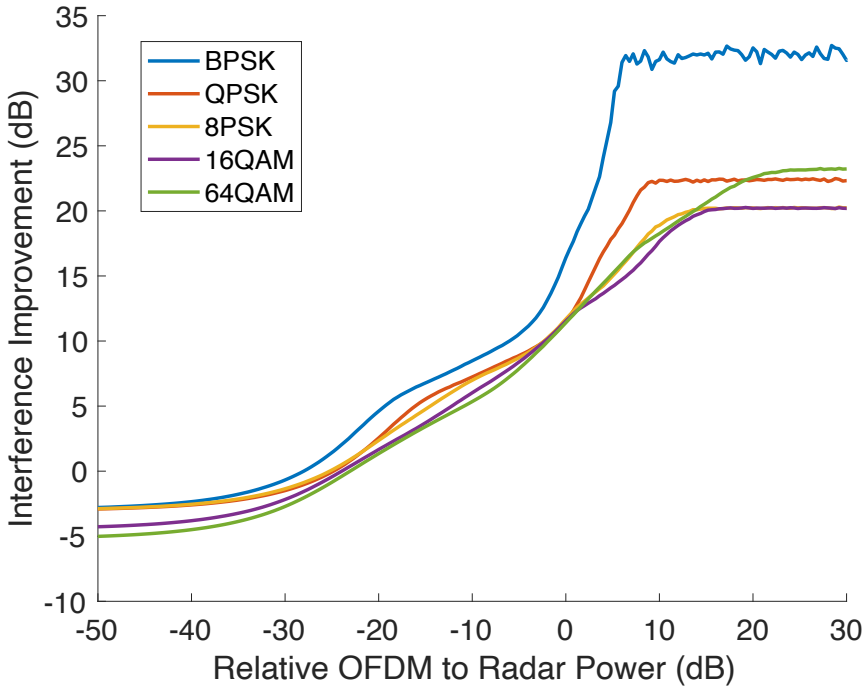

Figure 6.6: Interference Improvement vs. Relative OFDM to Radar Average Power plot for Case 5 in Table 6.2

where all the constellations are now considerably impacted.

6.3.2.2 Normalized Residual Interference vs. Relative OFDM to Radar Power

Consider again Case 4 in Table 6.2. Figure 6.8 shows the normalized residual interference against the relative OFDM to radar power plot for this case. Constellations with lower modulation orders exhibit a pronounced dip in the range of 5 dB to 20 dB of relative OFDM power. This suggests that, in some cases, the residual interference can decrease with an increase in the relative power of the interfering OFDM waveforms, as was hinted in Section 6.3.1.2. This occurs because higher relative OFDM to radar power results in less radar interference to the OFDM waveforms, which improves demodulation accuracy. For BPSK, QPSK, and 8PSK, the rate of interference

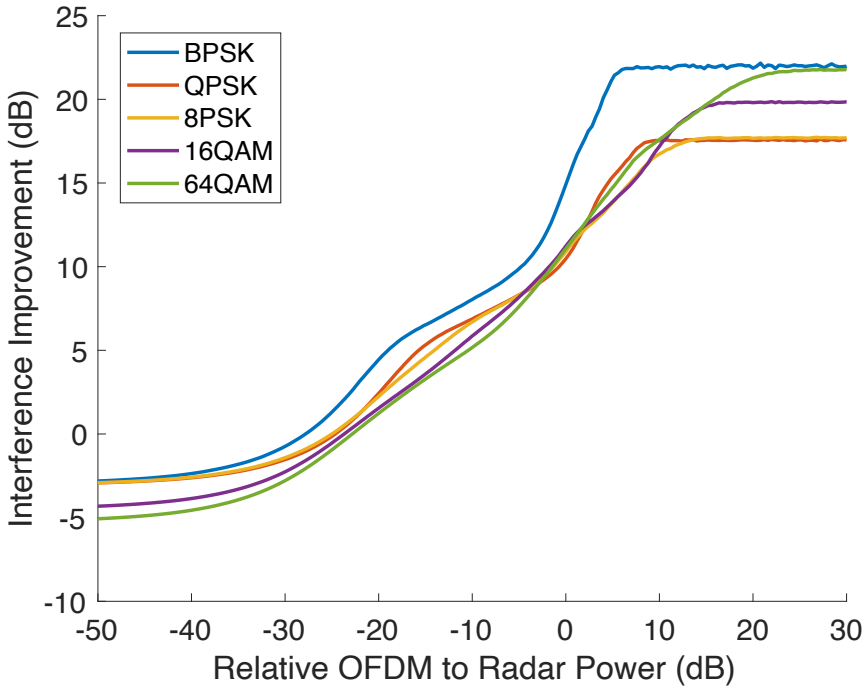

Figure 6.7: Interference Improvement vs. Relative OFDM to Radar Average Power plot for Case 6 in Table 6.2

improvement surpasses the rate of interference increase for the mentioned range of OFDM power levels, leading to a dip in the curves.

6.3.2.3 Interference Improvement vs. Observation Period

Figure 6.9 shows how the interference improvement changes with the observation period for Case 7 in Table 6.2. The curves for each constellation remain relatively flat until the observation period reaches 0.9, after which they start to increase. At around 0.99, four of the five curves begin to plateau at 40 dB, with BPSK plateauing first, followed by QPSK, 8PSK, and 16QAM. 64QAM peaks the latest, at approximately 37 dB. The plateaus being at 40 dB and not infinity is because of the scaling mismatch term affecting the OFDM symbol amplitude. The constellations begin to sort themselves by

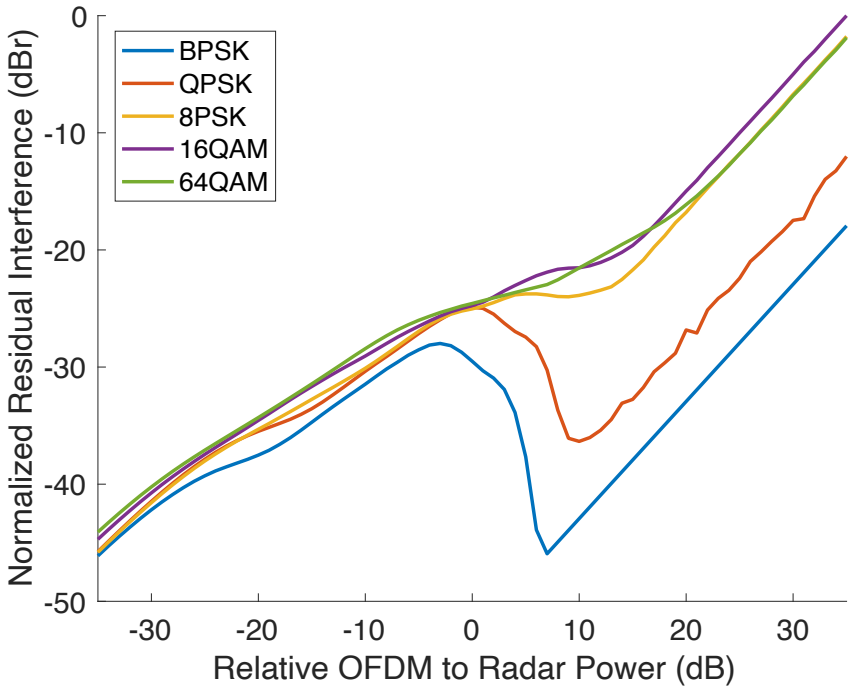

Figure 6.8: Normalized Residual Interference vs. Relative OFDM to Radar Average Power plot for Case 4 in Table 6.2

modulation order as the observation period increases, with QPSK surpassing 64QAM at around 0.975 and 8PSK surpassing 16QAM at 0.975. Typically, pulsed radars have higher observation periods, often greater than 99% [2], so, in general, the lower the modulation order, the better the performance of the RECOIL algorithm.

BPSK is the most robust to lost sample, for every observation period.

6.3.3 FFT Size

The FFT size is important because it determines the length of the time domain OFDM waveform, thus the impact that the lost samples have on OFDM demodulation. As the FFT size decreases, the negative impact of a constant amount of lost samples increases, as previously discussed in Section 5.3.2.1. However, because OFDM symbols

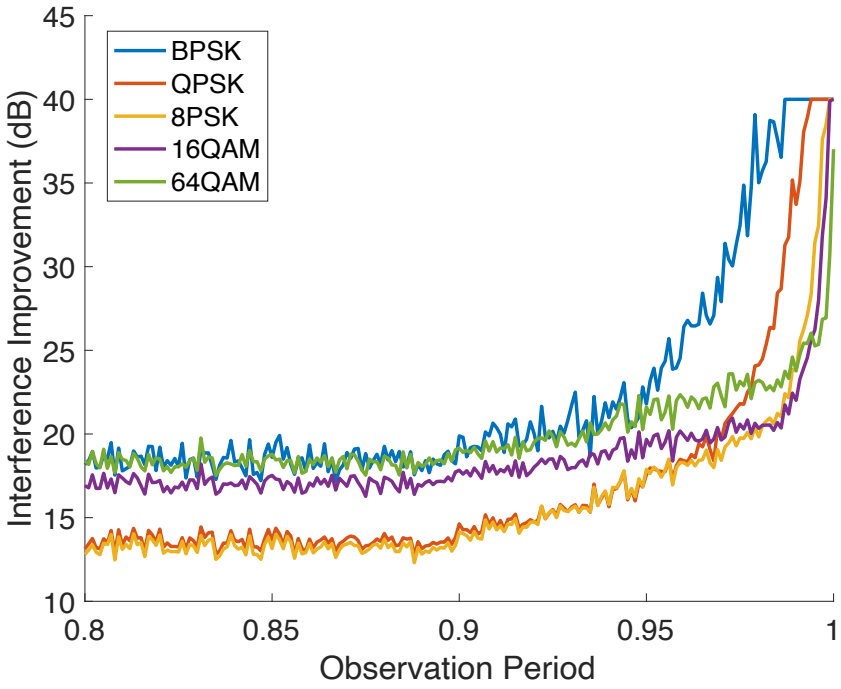

Figure 6.9: Interference Improvement vs. Observation Period plot for Case 7 in Table 6.2

with larger FFT sizes contain more samples and are spaced randomly and uniformly throughout the CPI, more received OFDM waveforms are corrupted by the lost samples for higher FFT sizes. As a result, smaller FFT sizes are more favorable in many cases.

This section will analyze RECOIL algorithm performance for five common OFDM communication system FFT sizes: 64, 126, 256, 512, and 1024.

The following table establishes two cases that will be referenced in this section:

6.3.3.1 Interference Improvement vs. Relative OFDM to Radar Power

Figure 6.10 shows how the interference improvement changes with the relative OFDM to radar power for Case 8 in Table 6.3. As one can observe, up until the curves

Parameter	Case 8	Case 9
Observation period	99%	99%
Scaling mismatch	1%	1%
N_{FFT}	–	–
N_{CPE}	$N_{FFT}/8$	$N_{FFT}/8$
Constellation	16QAM	16QAM
Symbol Density	$\sim 75\%$	$\sim 75\%$
OFDM SNR (dB)	25	–
Relative OFDM Power (dB)	–	25

Table 6.3: Two RECOIL performance simulation cases used to analyze the impact of the SNR of the interfering OFDM symbol's FFT size

start to plateau at a relative OFDM power of about 10 dB, the lower the FFT size, the better the overall performance. However, once the curves peak, they arrange themselves in an interesting order: the best interference improvement occurs with an FFT size of 64, followed by similar interference improvement between the 128 and 512 curves, then 1024, and finally 256. This suggests that the RECOIL algorithm's performance based on FFT size, while somewhat predictable for lower relative OFDM powers, can be difficult to define in saturation.

The behavior of these curves can be understood by recognizing the two contributing factors: the ratio of lost samples to FFT size (or the percentage of samples lost per OFDM symbol) and the percentage of received OFDM symbols affected. While smaller FFT sizes result in a higher ratio of lost samples to FFT size for a constant number of samples lost, there are fewer overall symbols affected since the likelihood of a symbol intersecting with the lost samples is lower (for a constant number of symbols per pulse, or "symbol density"). For larger FFT sizes, the residual interference is more spread out across the range bins, while smaller FFT sizes tend to have more concentrated residual interference near the range bin boundaries where the lost samples occur. This concept will be revisited in Section 6.3.5.

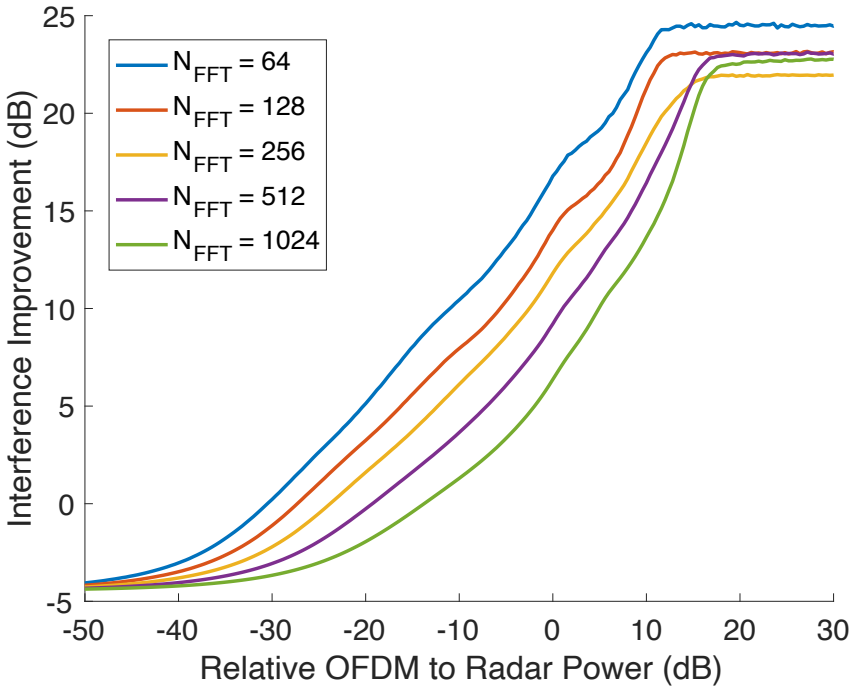

Figure 6.10: Interference Improvement vs. Relative OFDM to Radar Average Power plot for Case 8 in Table 6.3

6.3.3.2 Interference Improvement vs. OFDM SNR

Figure 6.11 shows the interference improvement relative to the OFDM SNR plot for Case 9, as listed in Table 6.3. It can be observed that up until an OFDM SNR of about 20 dB, all of the curves are ordered by FFT size. In this context, an FFT size of 64 demonstrates the best improvement, while a size of 1024 shows the worst improvement. As the curves saturate, FFT sizes of 512 and 1024 begin to overtake the smaller ones, suggesting that neither smaller nor larger FFT sizes inherently guarantee better interference improvement, as was also observed in the previous section (6.3.3.1).

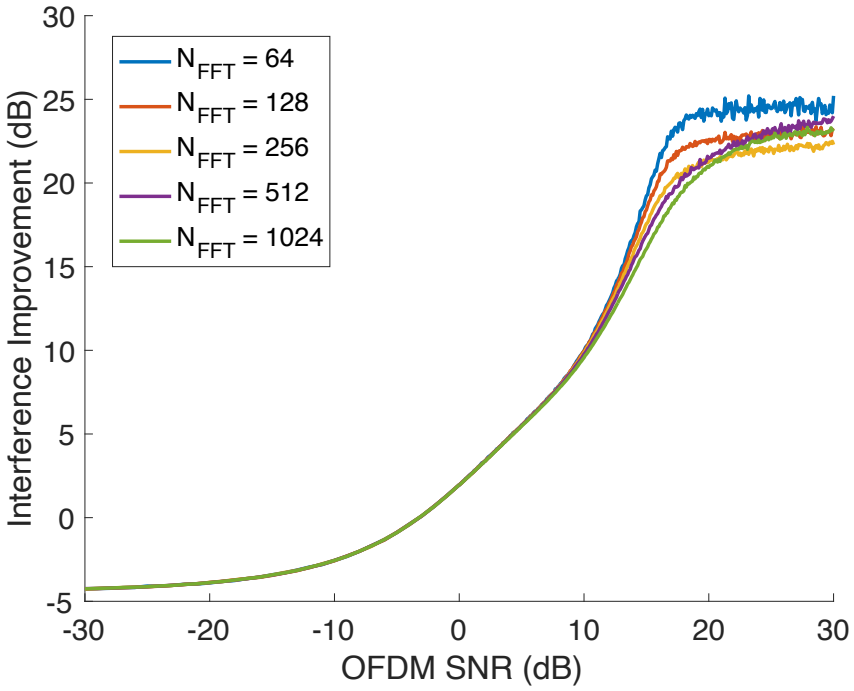

Figure 6.11: Interference Improvement vs. OFDM SNR plot for Case 9 in Table 6.3

6.3.4 The Received Constellation Plots

The constellation plots of the received OFDM waveforms show various factors that affect the algorithm's performance. Consider the following cases in the table below:

Parameter	**Case 10**	**Case 11**
Observation period	99%	97.5%
Scaling mismatch	1%	1 %
N_{FFT}	256	256
N_{CPE}	32	32
Constellation	–	–
Symbol Density	$\sim$ 75%	$\sim$ 75%
OFDM SNR (dB)	25	10
Relative OFDM Power (dB)	25	10

Table 6.4: Two RECOIL performance simulation cases used to analyze the impact of lost samples on the received OFDM waveform constellations

The received constellations for Case 10 for BPSK and 16QAM are shown in Figure 6.12. One can clearly observe that BPSK shown in Figure 6.13a is more robust to noise, lost samples, and interference than QPSK shown in Figure 6.13b. However, the dispersion around each constellation symbol in 16QAM is still relatively contained within each symbol's decision region, so the interference improvement of the RECOIL algorithm is still significant (23.51 dB vs 40.00 dB for BPSK).

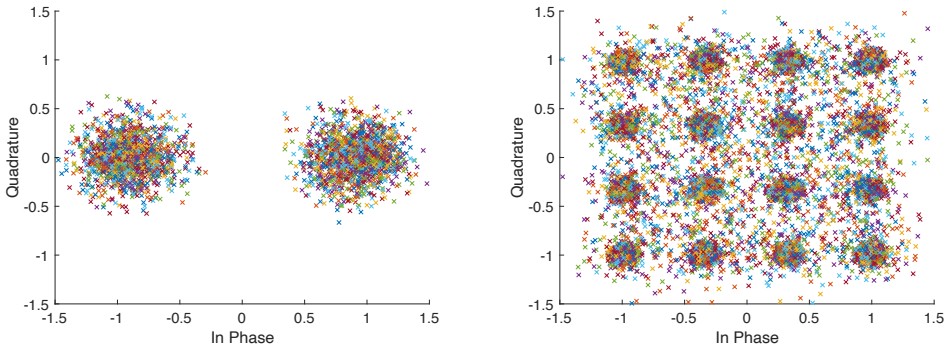

(a) (b)

Figure 6.12: Two received constellations for Case 10 from Table 6.4: (a) BPSK, (b) 16QAM

Figure 6.13 shows two received constellations for Case 11 from Table 6.4. It is evident that the dispersion around the constellation symbols is much higher compared to Figure 6.12. The BPSK constellation symbols are more spread out and, as a result, are less affected by corrupting factors than 16QAM. In this scenario, 16QAM can only achieve 9.62 dB in interference improvement, while BPSK attains 24.71 dB, surpassing 16QAM's performance in Case 10.

6.3.5 Average Residual Interference Plots

The average residual interference across the range bins is illustrated in this section. This section will illustrate how interference is distributed across the range bins depend-

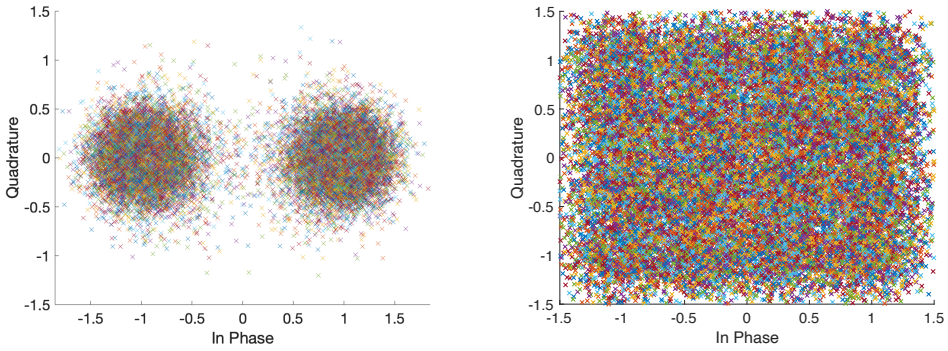

(a) (b)

Figure 6.13: Two received constellations for Case 11 from Table 6.4: (a) BPSK, (b) 16QAM

ing on various factors. The residual interference plots presented here are directly related to the range axis of the range-Doppler maps shown in the next section (6.3.6).

The following table establishes three cases that will be referenced in this section:

Parameter	**Case 12**	**Case 13**
Observation period	95%	97.5%
Scaling mismatch	1%	1%
N_{FFT}	256	512
N_{CPE}	32	64
Constellation	16QAM	QPSK
Symbol Density	$\sim 75\%$	$\sim 75\%$
OFDM SNR (dB)	20	10
Relative OFDM Power (dB)	20	10
Target Locations (km)	[3.6, 7.0, 4.0]	[2.5, 5, 5.5]
Target Velocities (m/s)	[-300, 450, 200]	[-100, -300, 500]

Table 6.5: Three RECOIL performance simulation cases used to analyze the average residual interference across the range bins

Consider the residual interference plot for Case 12 shown in Figure 6.14. The *with interference subtraction* curve shows the average residual interference following the application of the RECOIL algorithm. The first important observation is that the curve is much higher in amplitude toward the range bin boundaries. This is due to the lost

samples affecting the received OFDM symbol demodulation process. It tapers off because the FFT size is smaller than the number of samples per pulse, so only the received OFDM symbols near the boundaries lose samples. As the FFT size increases, the boundary slopes becomes more gradual. This is because a constant number of lost samples has a reduced impact on the received constellation for a larger FFT size (or symbol length), and more symbols are affected than before, as discussed in Section 6.3.3.

The middle residual interference protrusion shown in Figure 6.14 is caused by the presence of interfering received radar pulses at the corresponding range bins. As received radar power increases, the OFDM demodulation process becomes less effective, yielding higher residual interference. This, in turn, has the potential to obscure the radar pulse. This creates a catch-22 situation where the very presence of the radar pulse yields higher interference, making detection of the radar waveform more difficult. However, if the received waveform is powerful enough to cause worsened RECOIL performance, it is usually detectable through the decreased performance. Nevertheless, the potential of obscuring other targets at the same range is very real.

Figure 6.15 shows the average residual interference plot for Case 13 in Table 6.5.

Case 13 alters many parameters found in Case 12, such as the observation period, FFT size, CPE to FFT size ratio, constellation type/modulation order, relative OFDM power, OFDM SNR, and target ranges and velocities. These changes result in an altered residual interference plot, as shown in Figure 6.15, compared to the one in Figure 6.14. The overall residual interference appears much higher, and the slopes seem much more gradual due to the increased FFT size. Moreover, there are two distinct protrusions from the prominent returned pulses, in contrast to the one distinct peak shown in Figure 6.14.

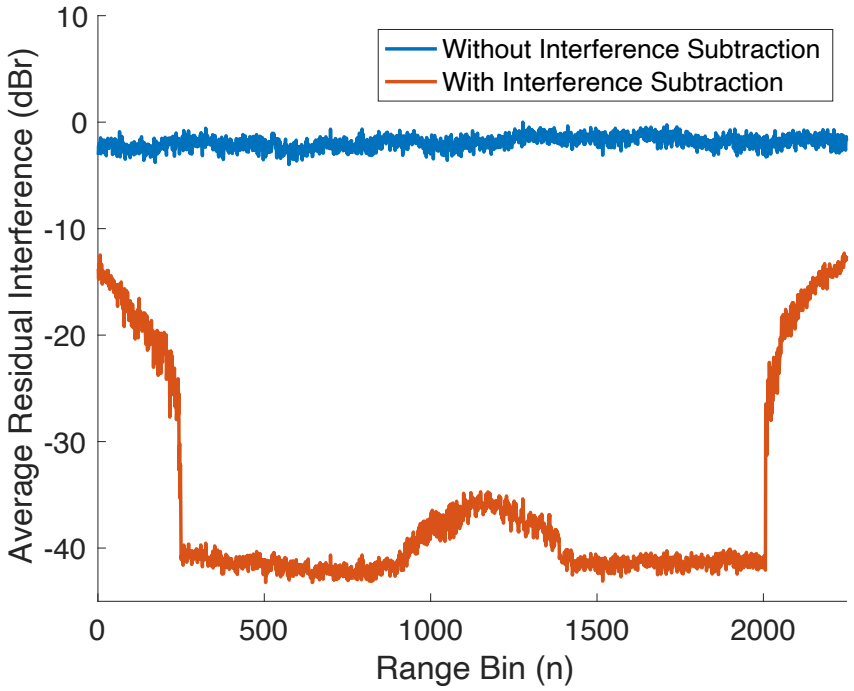

Figure 6.14: Average residual interference plot across received radar range bins for Case 12 in Table 6.5

6.3.6 Range-Doppler Maps

The range-Doppler map is a visualization tool to see received radar targets from a pulse-Doppler radar, as discussed in Section 6.3.6. The range-Doppler maps for both cases presented in Table 6.5 are shown in this section.

The range-Doppler maps without interference, with interference prior to subtraction, and after interference subtraction for Case 12 are presented in Figures 6.16, 6.17, and 6.18, respectively. Notably, the residual interference after subtraction (Figure 6.18) appears prominently at the boundaries of the range bins, and a string of interference is visible across the range bins with prominent targets. In this case, the targets are perceptible before and after interference subtraction, but they are much more defined in the post-subtraction map. However, the target with a velocity of 450 m/s at a range of 7 km

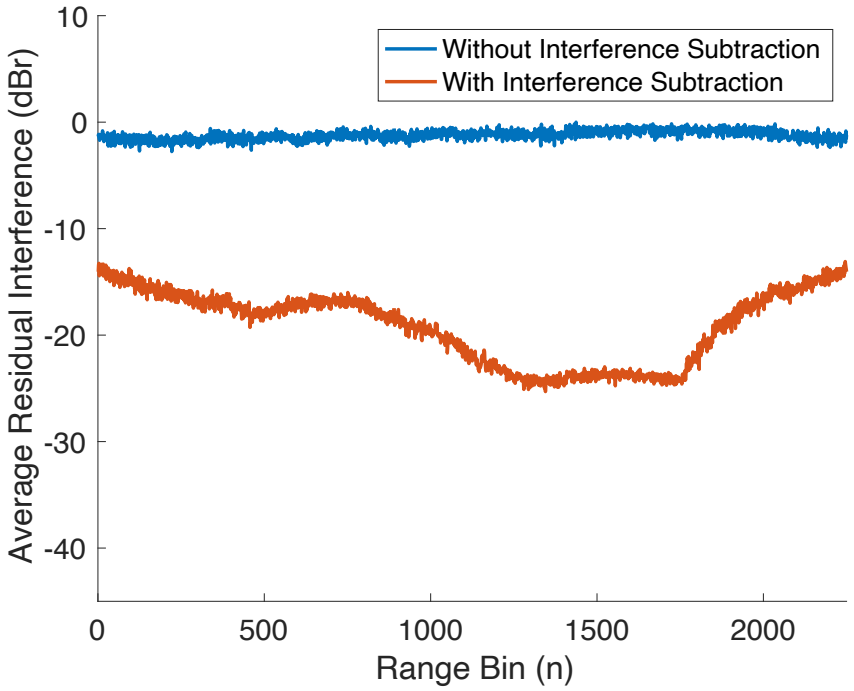

Figure 6.15: Average residual interference plot across received radar range bins for Case 13 in Table 6.5

is difficult to observe in both cases because it is buried in the residual interference near the range bins.

The range-Doppler maps for Case 13 are presented in Figures 6.19, 6.20, and 6.21. In this case, the residual interference is much more gradual and evenly distributed in Figure 6.21 than in Figure 6.18. The difference between before and after interference subtraction for Case 13 is clearly visible. Notably, in Figure 6.21 the target with a velocity of 500 m/s at a range of 5.5 km is almost completely concealed within the interference before subtraction, but visually apparent after interference subtraction.

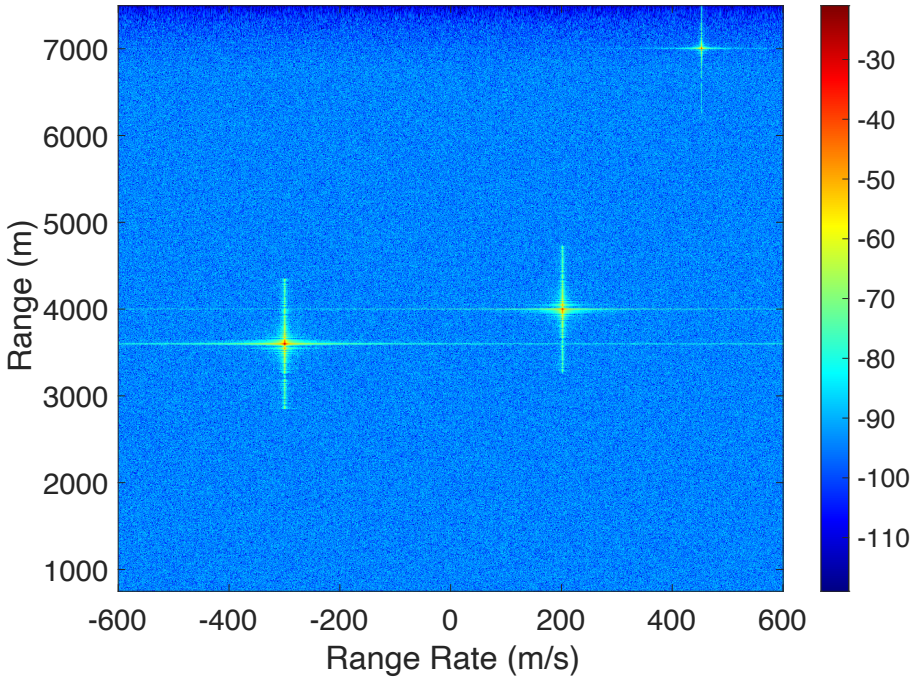

Figure 6.16: Range-Doppler map for Case 12 without interference

6.4 Informing New Regulations

The U-NII and CBRS frequency bands in the United States present promising applications for the RECOIL algorithm as they feature both radar and communication system usage. By enabling communication systems to transmit at higher power levels, more users could be served over longer distances and at faster data rates. Moreover, allowing these systems to operate freely in these bands instead of yielding to incumbent radar systems would guarantee uninterrupted service. However, radar systems are highly sensitive, and current regulations take great care to strictly limit harmful interference. Additionally, upgrading the hardware of many radar systems to support the algorithm would be a time-consuming and costly process.

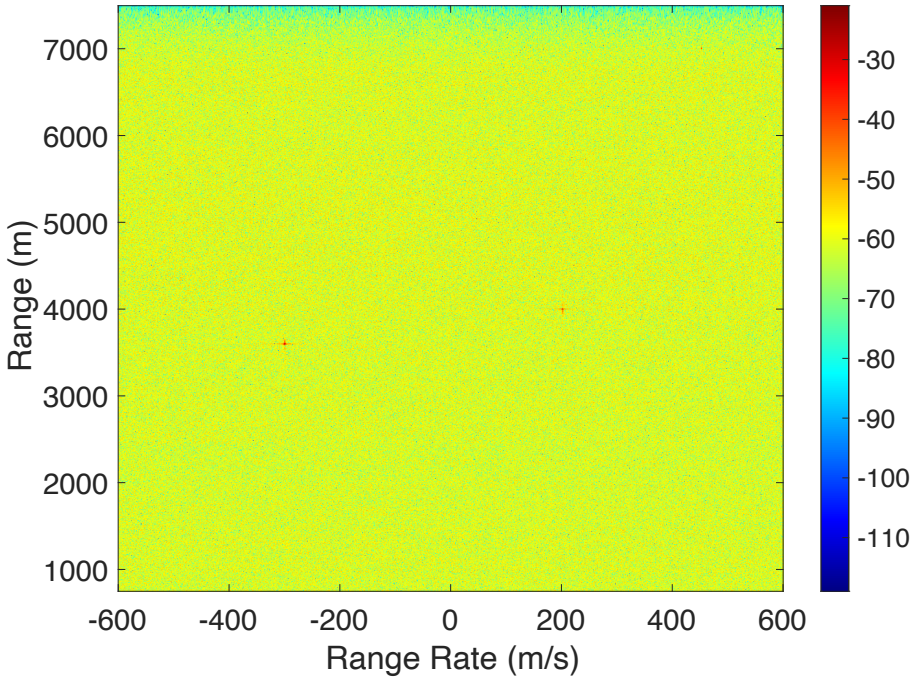

Figure 6.17: Range-Doppler map for Case 12 with interference

6.4.1 Redefining U-NII Regulations

Many U-NII devices operating in the 5 GHz band adhere to the principles of DFS, as previously discussed in Section 2.6. The technical rules that govern DFS assume that if a U-NII device receives a specific amount of radar power, then the radar will receive a proportional amount of interfering power from the U-NII device, assuming that signal propagation conditions are equal in both directions, which is often the case. This technique ensures that incumbent radar systems remain unaltered, as all of the coordination is done within the U-NII devices themselves [32].

A detection threshold is established at the U-NII device receiver, which, when crossed, indicates that the radar is likely receiving enough interference from the U-NII device to cause degradation in target detection performance. Therefore, the U-NII

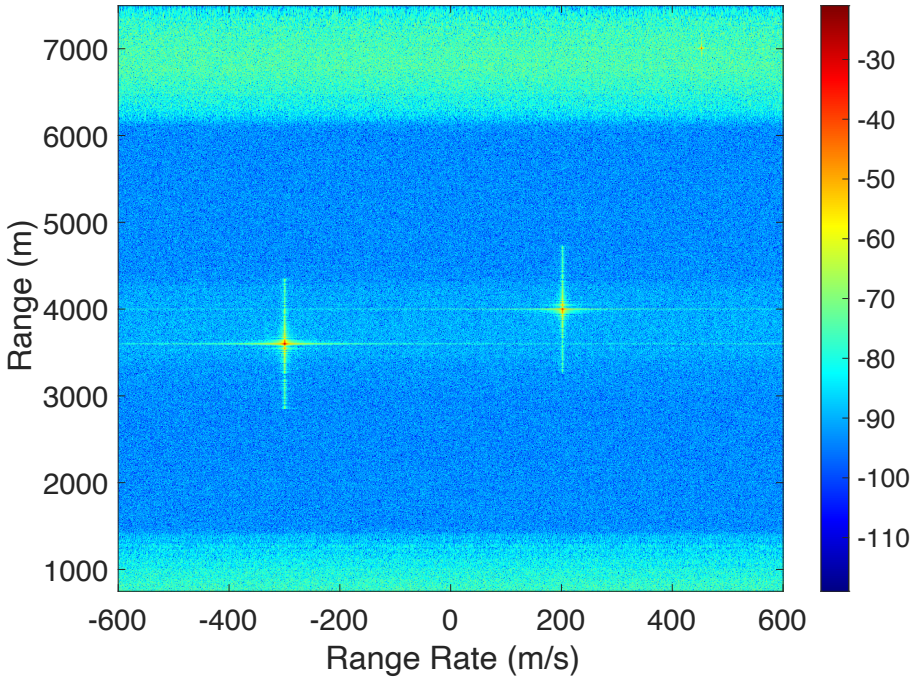

Figure 6.18: Range-Doppler map for Case 12 after interference subtraction with the RECOIL algorithm

device must cease transmission on that channel. In most radars, this threshold is about 6 dB lower than the radar's thermal noise. For a 5 GHz transmission frequency, a radar power detection threshold of -64 dBm at the U-NII device receiver is the determined optimal threshold [32].

Generally, the RECOIL algorithm can be an effective tool for radars that share frequency bands with communication devices without altering any existing regulations. In the case of a stray interferer, a radar may be able to significantly reduce interference, or, in some cases, completely remove interference, as seen in Figure 6.1. It is important to note that this scenario typically implies a lack of coordination between the U-NII device and the radar. In such cases, the radar would have to estimate many of the OFDM parameters, such as constellation type/modulation order, FFT size, cyclic prefix

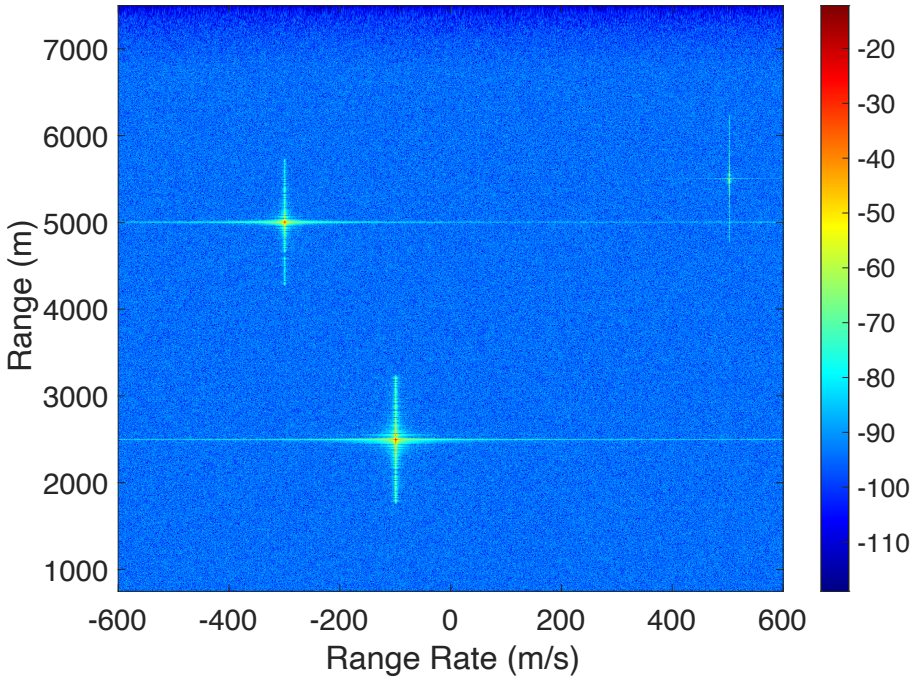

Figure 6.19: Range-Doppler map for Case 13 without interference

length, and so on. As a result, interference improvement could be significantly lower than the results shown in Section 6.3.

The current DFS framework operates under the assumption that higher interfering OFDM power adversely affects radar performance. However, the findings of this chapter reveal that this conviction is not always accurate. In fact, an increase in transmit power by an interfering OFDM transmitter using the RECOIL algorithm may actually benefit the radar. For example, consider the BPSK curve depicted in Figure 6.8. An increase in the relative OFDM to radar power from 0 to 10 dB decreases residual interference by over 10 dB. Thus, it may be possible to increase the preexisting DFS triggering threshold without compromising radar performance. Furthermore, implementing adaptive thresholds based on the OFDM system parameters of the U-NII device and the results of Section 6.3 could further optimize interference levels. A U-NII device could

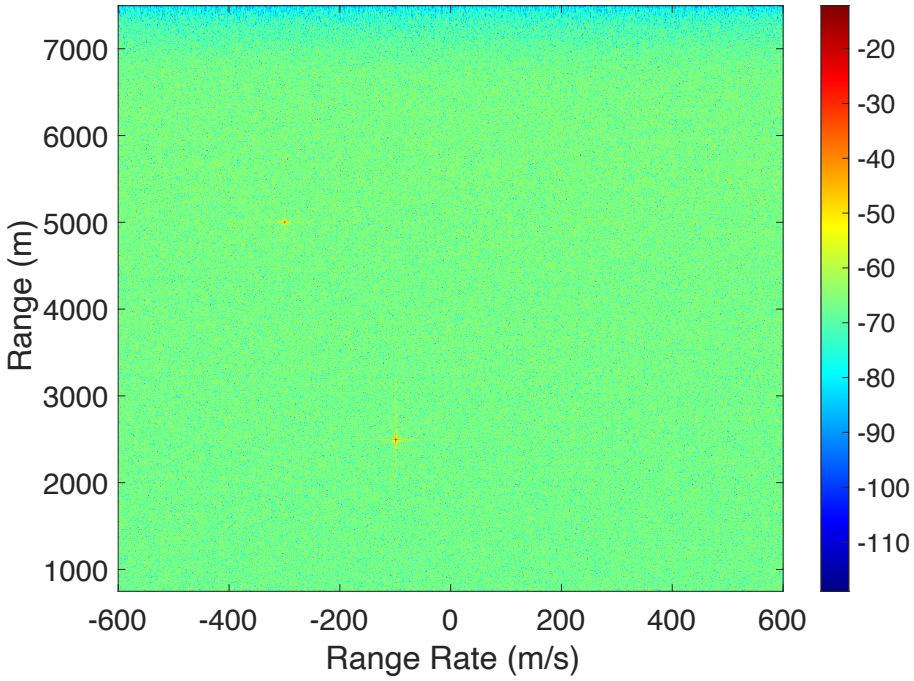

Figure 6.20: Range-Doppler map for Case 13 with interference

come equipped with formulas that enable it to calculate its own optimal threshold based on its system parameters. This alteration, however, fails to account for multiple OFDM transmitters affecting RECOIL algorithm performance.

Given that radars are often affected by the interference range of many U-NII devices, the potential of overlapping OFDM symbols becomes unavoidable. As a result, overlapping OFDM symbols could have a profound negative effect on RECOIL algorithm performance.

4G LTE and 5G NR cellular networks both utilize the U-NII bands to facilitate seamless high speed wireless connectivity to users [79, 80]. However, since single OFDMA symbols are used for 4G LTE and 5G NR downlink, they could potentially be operated on the same channel at the same time and space as radars without any possibility of overlapping OFDM symbols. This would allow them to potentially guarantee

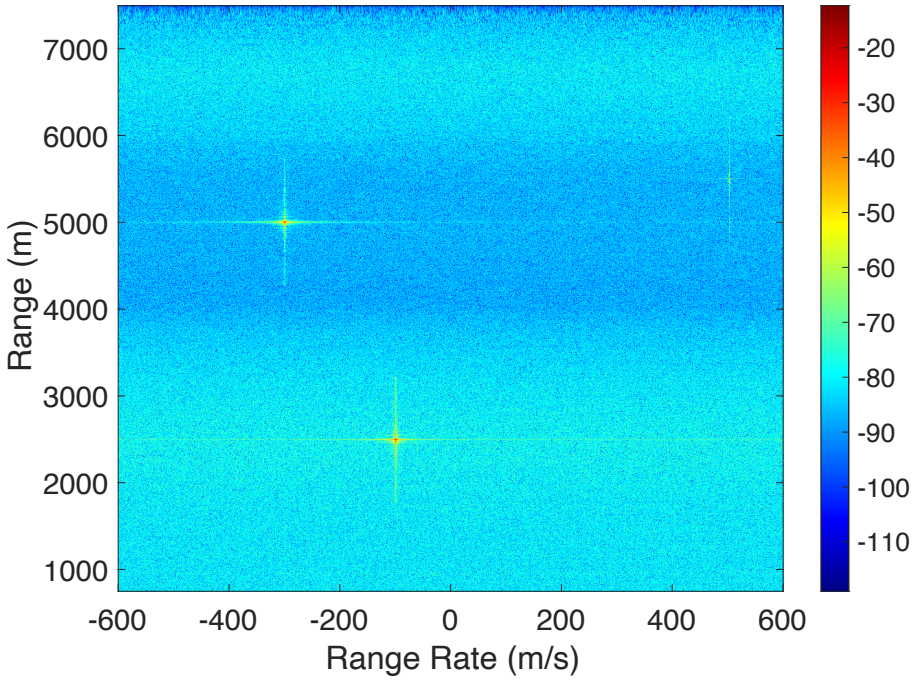

Figure 6.21: Range-Doppler map for Case 13 after interference subtraction with the RECOIL algorithm

quality of service (QoS) to their users when *best-effort* is typically employed.

The development of a standardized coordination protocol between U-NII devices and radar, where U-NII devices could relay their operating parameters, such as FFT size, constellation type/modulation order, and cyclic prefix length, could help eliminate the guesswork that goes into OFDM parameter estimation and ensure good RECOIL algorithm performance.

The implementation of such a protocol would likely be driven primarily by industry stakeholders who stand to benefit the most from its widespread adoption. With the FCC overseeing the U-NII band, it is likely that they would support and promote the protocol's adaptation, given their mission to foster the development of more efficient and effective spectrum technologies. In contrast, the NTIA would likely adopt a more

cautious stance, rigorously verifying that the proposed protocol does not adversely impact radar systems before endorsing deployment. This potential dynamic between the FCC, NTIA, and industry stakeholders embodies the principle of multistakeholder governance explored in Section 2.5.2. This underscores the importance of collaboration and consensus-building in advancing innovative solutions.

6.4.2 Redefining CBRS Regulations

The CBRS band, as discussed in Section 2.7, features a tiered access system and a cloud-based SAS to organize spectrum usage. Incumbent users, like the DoD radars in this band, have the highest priority access and other users are required to yield to them. As in the U-NII bands, equipping incumbent radar systems in this band with the RECOIL algorithm could limit the severity of instances of harmful interference without changing any existing operational regulations.

However, from a policy perspective, modifying their estimating SAS framework to help orchestrate multiple users within a shared band based on their OFDM system parameters (FFT size, constellation type/modulation order, and so on) and the analysis provided in Section 6.3 could provide a vehicle for the real-world implementation of the RECOIL algorithm. This could allow lower priority users more transmit time.

The adaptation of the RECOIL algorithm in the CBRS band, much like in the U-NII band, would likely be an industry-led endeavor. However, unlike U-NII devices, current CBRS devices would not require any modification since the SAS simply instructs them on when to transmit and at which frequencies. The implementation of the RECOIL algorithm on the consumer device side would only necessitate a software update from the SAS, potentially facilitating more rapid deployment of the RECOIL algorithm compared to the U-NII band. The FCC would once again be a probable advocate for

the implementation of this technology, while the NTIA would likely maintain a more conservative stance to preserve radar operations and avoid any unnecessary radar upgrades.

Chapter 7

Concluding Remarks and Future Research

This thesis proposes a novel interference mitigation algorithm called RECOIL, which utilizes the known structure of OFDM symbols to build a higher resolution replica of the interfering signal and then subtracts it from receiver IQ data. Simulations of the algorithm showed promising results, that are used to inform new spectrum management regulations. Although the RECOIL algorithm was framed within the context of pulse-Doppler radar, it could be extended to other applications, such as interference between multiple communication systems.

7.1 Future Research

Future research could extend in multiple directions. Analyzing RECOIL algorithm performance for multiple overlapping OFDM symbols is of primary importance. Results from this could potentially inform regulations where many communication devices operate at the same frequency as a radar without inflicting harmful interference. Also rigorizing current simulations to account for a more real-world environment could give important insight. Things like multipath and clutter modeling, CFO, and timing synchronization could be added to make the simulations more practical.

Exploring adaptive techniques for timing the transmission of radar pulses can be

promising in minimizing lost samples of periodically occurring OFDM symbols. However adjusting these radar parameters could severely impact radar system performance, which may be unacceptable.

Another potential area for further improvement is looking into techniques that identify when the RECOIL algorithm is worsening interference levels so that it can be disabled. In some cases seen in Chapter 6, like when the OFDM SNR is very low, the RECOIL algorithm can increase interference. Identifying these situations could be an important step in the real-world implementation of the RECOIL algorithm.

Finally, further research should be done in implementing blind channel, constellation, or power estimation. Since multiple interfering waveforms from the same system is a likely situation to occur, looking into techniques that utilize the fact that multiple symbols are available to provide more data in approximating these estimations may prove fruitful. Moreover, the constellation estimation work provided in Section 5.3.2.2 could potentially be improved by using machine learning techniques to predict the transmitted constellation based the received IQ points.

References

[1] Institute of Electrical and Electronics Engineers (IEEE), "IEEE standard for telecommunications and information exchange between systems - LAN/MAN specific requirements - part 11: Wireless medium access control (MAC) and physical layer (PHY) specifications: High speed physical layer in the 5 GHz band," *IEEE Std 802.11a-1999*, pp. 1–102, 1999.

[2] M. A. Richards, *Fundamentals of Radar Signal Processing*, 2nd ed. McGraw-Hill Education - Europe, 2014.

[3] B. D. Cordill, S. A. Seguin, and L. Cohen, "Electromagnetic interference to radar receivers due to in-band OFDM communications systems," in *2013 IEEE International Symposium on Electromagnetic Compatibility (EMC)*, 2013, pp. 72–75.

[4] J. A. Stine and D. L. Portigal, *Spectrum 101: An Introduction to Spectrum Management*. The MITRE Corporation, 2004.

[5] 3rd Generation Partnership Project (3GPP). (2022, March) Release 17. [Online]. Available: https://www.3gpp.org/release-17

[6] 3GPP. (2016, September) V2X. [Online]. Available: https://www.3gpp.org/v2x

[7] International Telecommunication Union Radiocommunication Sector (ITU-R), "Terms and definitions," *WRC15*, 2015. [Online]. Available: https://life.itu.int/radioclub/rr/art1.pdf

[8] National Telecommunications and Information Administration (NTIA). (2016, January) United States frequency allocations: The radio spectrum. [Online]. Available: https://www.ntia.doc.gov/files/ntia/publications/january_2016_spectrum_wall_chart.pdf

[9] The Office of Federal Register (OFR). (2022, July) Code of federal regulations. [Online]. Available: https://www.ecfr.gov/current/title-47

[10] The Department of Transportation, Communications, and Infrastructure (TCI), "National table of frequency allocations," *Title 21, Chapter 7*. [Online]. Available: https://www.tci.gov.fm/documents/communications/regulations/fsmc-title21-ch07.pdf

[11] ITU-R, "Nomenclature of the frequency and wavelength bands used in telecommunications," *V Series, Vocabulary and related subjects*, August 2015.

[12] C. T. Lopez, "Long-range discrimination radar reshapes adversaries' calculus for attacks against U.S. homeland," *DoD News*, December 2021.

[13] C. M. Thompson, R. A. Green, J. Sauder, K. L. Purcell, R. Sweitzer, and J. Armeno, *Biology and conservation of martens, sables, and fishers: a new synthesis*. Cornell University Press, 2012, ch. The use of radio telemetry in Martes research: techniques and technologies, pp. 284–319.

[14] The Food and Drug Administration (FDA). (2018, August) About wireless medical telemetry. [Online]. Available: https://www.fda.gov/radiation-emitting-products/electromagnetic-compatibility-emc/about-wireless-medical-telemetry

[15] D. F. Miller, *Basics of Radio Astronomy for the for the Goldstone-Apple Valley Radio Telescope*, C. I. of Technology, Ed. Jet Propulsion Laboratory, April 1998.

[16] NTIA. Basic elements of spectrum management: How the spectrum is used. [Online]. Available: https://www.ntia.doc.gov/legacy/osmhome/roosa2.html

[17] The United States of America, *Radio Act of 1912*. The United States of America, 1912, ch. XII.

[18] Interdepartment Radio Advisory Committee (IRAC), "Interdepartment Radio Advisory Committee: IRAC representatives effectively coordinate federal spectrum but lack seniority to advise on contentious policy issues," September 2004.

[19] United States Congress, "Communications Act of 1934," Pub. L. No. 73-416, 48 Stat. 1064, 1934. [Online]. Available: https://transition.fcc.gov/Reports/1934new.pdf

[20] NTIA. Basic elements of spectrum management: Who regulates the spectrum. [Online]. Available: https://www.ntia.doc.gov/legacy/osmhome/roosa4.html

[21] NTIA. Basic elements of spectrum management: National Telecommunications and Information Administration. [Online]. Available: https://www.ntia.doc.gov/legacy/osmhome/roosa8.html

[22] FCC. What we do. [Online]. Available: https://www.fcc.gov/about-fcc/what-we-do

[23] NTIA. IRAC. [Online]. Available: https://www.ntia.doc.gov/category/irac

[24] NTIA. (2022, February) FCC, NTIA establish spectrum coordination initiative. [Online]. Available: https://ntia.doc.gov/press-release/2022/fcc-ntia-establish-spectrum-coordination-initiative

[25] M. J. Rossini, *The Spectrum Scarcity Doctrine: A Constitutional Anachronism*. SMU Law Review, 1985, vol. 39, no. 3.

[26] *National Broadcasting Co., Inc. et al. v. United States et al.* Library of Congress, May 1943.

[27] H. Leib, "National Broadcasting Co. v. United States (1943)," *The First Amendment Encyclopedia*.

[28] J. W. Berresford, "The scarcity rationale for regulating traditional broadcasting: An idea whose time has passed," *Media Bureau Staff Research Paper*, March 2005.

[29] R. Keohane, "Multilateralism - an agenda for research," *International Journal Canada's Journal of Global Policy Analysis*, vol. 45, no. 4, pp. 731–764, 1990.

[30] M. Raymond and L. DeNardis, "Multistakeholderism: anatomy of an inchoate global institution," *International Theory*, vol. 7, no. 3, p. 572–616, 2015.

[31] International Telecommunication Union (ITU), *WRC-23 Booklet: Agenda and Relevant Resolutions*. World Radiocommunication Conferences (WRC), 2023. [Online]. Available: https://www.itu.int/hub/publication/r-act-arr-1-2022/

[32] F. H. Sanders, E. F. Drocella, R. L. Sole, and J. E. Carroll, "Lessons learned from the development and deployment of 5 GHz unlicensed national information infrastructure (U-NII) dynamic frequency selection (DFS) devices," Tech. Rep., March 2004.

[33] FCC, "Guidelines for compliance testing of Unlicensed National Information Infrastructure (U-NII) devices part 15, subpart e," December 2017.

[34] R. Mailloux, *Phased Array Antenna Handbook, Third Edition*. Artech, 2017.

[35] D. Zhao, J. Zhang, Y. Yi, P. Gu, and N. Jiang, "5G millimeter-wave phased-array transceiver: System considerations and circuit implementations," in *2019 IEEE International Symposium on Circuits and Systems (ISCAS)*, 2019, pp. 1–4.

[36] FCC, "Revision of parts 2 and 15 of the commission's rules to permit unlicensed national information infrastructure (U-NII) devices in the 5 GHz band," November 2003. [Online]. Available: https://docs.fcc.gov/public/attachments/FCC-03-287A1.pdf

[37] F. Stremler, *Introduction to Communication Systems*, 3rd ed. Pearson, January 1990.

[38] S. M. Bowers, A. Safaripour, and A. Hajimiri, "Dynamic polarization control," *IEEE Journal of Solid-State Circuits*, vol. 50, no. 5, pp. 1224–1236, 2015.

[39] R. V. Nee and R. Prasad, *OFDM for Wireless Multimedia Communications*. Artech House Publishers, December 1999.

[40] National Telecommunications and Information Administration (NTIA), *Manual of Regulations and Procedures for Federal Radio Frequency Management*. NTIA, January 2021, ch. 4-5.

[41] P. Rysavy, "Challenges and considerations in defining spectrum efficiency," *Proceedings of the IEEE*, vol. 102, no. 3, pp. 386–392, 2014.

[42] ITU-R, *Definition of spectrum use and efficiency of a radio system*. ITU-R, September 2017.

[43] Worcester Polytechnic Institute (WPI), "Software-defined radio & cognitive radio." [Online]. Available: https://www.wpi.edu/academics/departments/electrical-computer-engineering/research/sdr-cognitive-radio

[44] Q. Wang, P. Du, T. Dou, L. Gao, and C. Li, "Cognitive passive radar system: software defined radio and deep learning approach," *IET International Radar Conference 2018*, vol. 2019, no. 21, pp. 7326–7330, September 2019.

[45] Ettus. (2022, July) USRP X410. [Online]. Available: https://www.ettus.com/all-products/usrp-x410/

[46] A. R., G. Xavier, H. V, N. Prasannan, R. Peter, and S. K.P, "GNU Radio based control system," *2012 International Conference on Advances in Computing and Communications*, vol. 259-262, 2012.

[47] L. Chettri and R. Bera, "A comprehensive survey on internet of things (iot) toward 5G wireless systems," *IEEE Internet of Things Journal*, vol. 7, no. 1, pp. 16–32, 2020.

[48] J. Berghult and A. Lesser, "Radio spectrum coexistence between military radars and radio access networks," Chalmers Unversity of Technology, Tech. Rep. E 2018:115, 2018.

[49] Department of Defense (DoD), "5G strategy implementation plan: Advancing 5G technology & applications securing 5G capabilities," Tech. Rep., December 2020.

[50] DoD, "Electromagnetic spectrum superiority strategy," Tech. Rep., October 2020.

[51] C. D'Andrea, S. Buzzi, and M. Lops, "Communications and radar coexistence in the massive MIMO regime: Uplink analysis," *IEEE Transactions on Wireless Communications*, vol. 19, no. 1, pp. 19–33, 2020.

[52] FCC, *Before the Federal Communications Commission Washington, D.C. 20554*. FCC, December 2002.

[53] T. Yilmaz, E. Fadel, and O. B. Akan, "Employing 60 GHz ISM band for 5G wireless communications," in *2014 IEEE International Black Sea Conference on Communications and Networking (BlackSeaCom)*, 2014, pp. 77–82.

[54] Z. Xu, C. Lei, Z. Yue, F. Yan, and W. Dandan, "Research on the frequency coexistence of 24 GHz millimeter wave radar and 5G communication," in *2021 IEEE International Conference on Electrical Engineering and Mechatronics Technology (ICEEMT)*, 2021, pp. 656–660.

[55] G. Locke, *An Assessment of the Near-Term Viability of Accommodating Wireless Broadband Systems in the 1675-1710 MHz, 1755-1780 MHz, 3500-3650 MHz, and 4200-4220 MHz, 4380-4400 MHz Bands*. DoC, October 010.

[56] *Before the Federal Communications Commission Washington, D.C. 20554*, FCC 12-148 ed. Federal Communications Commission, December 2012.

[57] FCC, *Before the Federal Communications Commission Washington, D.C. 20554*, FCC 15-47 ed. Federal Communications Commission, April 2015.

[58] FCC. (2022, July) 3.5 GHz band overview. [Online]. Available: https://www.fcc.gov/wireless/bureau-divisions/mobility-division/35-ghz-band/35-ghz-band-overview

[59] C. Sulhoff, "FCC authorizes full commercial deployment in 3.5 GHz band, advocating american 5G leadership," January 2020. [Online]. Available: https://docs.fcc.gov/public/attachments/DOC-362108A1.pdf

[60] C. Pai, "Chairman pai statement on FCC authorization of first 6 GHz WI-FI device," December 2020. [Online]. Available: https://docs.fcc.gov/public/attachments/DOC-368593A1.pdf

[61] T. Pelkey, "FCC adopts new rules for the 6 GHz band, unleashing 1,200 megahertz of spectrum for unlicensed use," April 2020. [Online]. Available: https://docs.fcc.gov/public/attachments/DOC-363945A1.pdf

[62] FCC, "Unlicensed use of the 6 GHz band report and order and further notice of proposed rulemaking ET docket no. 18-295; GN docket no. 17-183," April 2020. [Online]. Available: https://www.fcc.gov/document/fcc-opens-6-ghz-band-wi-fi-and-other-unlicensed-uses

[63] B. Cai, W. Xie, and H. Guo, "Analysis and field trial on interference coexistence of 5G NR and 4G LTE dynamic spectrum sharing," in *2021 International Wireless Communications and Mobile Computing (IWCMC)*, 2021, pp. 1281–1285.

[64] FCC. America's 5G future. [Online]. Available: https://www.fcc.gov/5G

[65] FCC. (2021, October) Plan ahead for phase out of 3G cellular networks and service. [Online]. Available: https://www.fcc.gov/consumers/guides/plan-ahead-phase-out-3g-cellular-networks-and-service

[66] N. LaSorte, W. J. Barnes, and H. H. Refai, "The history of orthogonal frequency division multiplexing," in *IEEE GLOBECOM 2008 - 2008 IEEE Global Telecommunications Conference*, 2008, pp. 1–5.

[67] O. Liberg, M. Sundberg, Y.-P. E. Wang, J. Bergman, and J. Sachs, *Cellular Internet of Things*, 1st ed. 125 London Wall, London EC2Y 5AS, United Kingdom: Elsevier Academic Press, September 2017.

[68] "IEEE standard for information technology–telecommunications and information exchange between systems local and metropolitan area networks–specific requirements part 11: Wireless lan medium access control (MAC) and physical layer (PHY) specifications amendment 1: Enhancements for high-efficiency WLAN," *IEEE Std 802.11ax-2021 (Amendment to IEEE Std 802.11-2020)*, pp. 1–767, 2021.

[69] 3GPP, "LTE; evolved universal terrestrial radio access (E-UTRA); physical channels and modulation," 3GPP, Technical Specification TS 36.211, April 2017. [Online]. Available: https://www.etsi.org/deliver/etsi_ts/136200_136299/136211/14.02.00_60/ts_136211v140200p.pdf

[70] P. Moose, "A technique for orthogonal frequency division multiplexing frequency offset correction," *IEEE Transactions on Communications*, vol. 42, no. 10, pp. 2908–2914, 1994.

[71] S. Mohanty and S. Das, "A comparative study of pulse shaping functions for ICI power reduction in OFDM system," in *2008 Annual IEEE India Conference*, vol. 2, 2008, pp. 312–316.

[72] M.-J. Hao and C.-P. Liaw, "A companding technique for papr reduction of OFDM systems," in *2006 International Symposium on Intelligent Signal Processing and Communications*, 2006, pp. 634–637.

[73] Y. Rahmatallah and S. Mohan, "Peak-to-average power ratio reduction in OFDM systems: A survey and taxonomy," *IEEE Communications Surveys & Tutorials*, vol. 15, no. 4, pp. 1567–1592, 2013.

[74] F. C. Vilar, "Implementation of zero forcing and MMSE equalization techniques in OFDM," Master's thesis, Universidade De Fortaleza, Av. Washington Soares, 1321 - Edson Queiroz, Fortaleza - CE, 60811-905, Brazil, December 2014.

[75] FCC. (2019) U-NII and TDWR interference enforcement. [Online]. Available: https://www.fcc.gov/general/u-nii-and-tdwr-interference-enforcement

[76] D. McCarthy, "Coexistence of LTE and radar system: Methodology and assessment of radar receivers," in *2018 United States National Committee of URSI National Radio Science Meeting (USNC-URSI NRSM)*, 2018, pp. 1–2.

[77] MathWorks, "Density-based spatial clustering of applications with noise (DBSCAN)," https://www.mathworks.com/help/stats/dbscan.html, (accessed Feb. 24, 2023).

[78] F. Pingjiang and G. Lindong, "Adaptive DBSCAN-based algorithm for constellation reconstruction and modulation identification," in *2004 Asia-Pacific Radio Science Conference, 2004. Proceedings.*, 2004, pp. 177–180.

[79] G. Naik, J. Liu, and J.-M. J. Park, "Coexistence of wireless technologies in the 5 GHz bands: A survey of existing solutions and a roadmap for future research," *IEEE Communications Surveys & Tutorials*, vol. 20, no. 3, pp. 1777–1798, 2018.

[80] Qualcomm. (2020, June) 5G-NR. [Online]. Available: https://www.qualcomm.com/research/5g/5g-unlicensed-shared-spectrum